Coagulation, fouling and mixing during VDF emulsion polymerization

Estela Gelinski

N°d'ordre NNT : 2022LYO10011

THESE de DOCTORAT DE
l'Université Claude Bernard Lyon 1

Ecole Doctorale N° 206
École Doctorale de Chimie

Spécialité de doctorat : Génie de Procédés

Soutenue publiquement le 07/09/2022, par :
Estela Kamile GELINSKI

Coagulation, Fouling and Mixing during VDF Emulsion Polymerization

---

Devant le jury composé de :

LE SAUZE, Nathalie	Professeure (Univ. de Toulouse)	Présidente
MEIMAROGLOU, Dimitrios	Maître de Conférences – HDR (Univ. de Lorraine)	Rapporteur
ANDRIOLETTI, Florence	Directrice R&D (Arkema)	Examinatrice
EDOUARD, David	Maître de Conférences – HDR (Univ. Lyon 1)	Examinateur
MCKENNA, Timothy F. L.	Directeur de Recherche (CNRS Lyon)	Directeur de thèse
SHEIBAT-OTHMAN, Nida	Directrice de Recherche (CNRS Lyon)	Co-directrice de thèse

UNIVERSITE CLAUDE BERNARD – LYON 1

Président de l'Université	M. Frédéric FLEURY
Président du Conseil Académique	M. Hamda BEN HADID
Vice-président du Conseil d'Administration	M. Didier REVEL
Vice-président de la Commission Formation	Mme. Céline BROCHIER
Vice-président de la Commission Recherche	M. Petru MIRONESCU
Directreur Général des Services	M. Pierre ROLLAND

COMPOSANTES SANTE

Faculté de Médecine Lyon Est – Claude Bernard	Directeur : M. Gilles RODE
Faculté de Médecine et de Maïeutique Lyon Sud – Charles Mérieux	Directeur : M. Philippe PAPAREL
Faculté d'Odontologie	Directeur : M. Jean-Christophe MAURIN
Institut des Sciences Pharmaceutiques et Biologiques (ISPB)	Directeur : M. Claude DUSSART
Institut des Sciences et Techniques de Réadaptation (ISTR)	Directeur : M. Jacques LUAUTE
Comité de Coordination des Études Médicales	Directrice : Mme. Carole BURILLON

COMPOSANTES SECTEUR SCIENCES & TECHNOLOGIE

UFR Biosciences	Directrice : Mme. Kathrin GIESELER
UFR Faculté des Sciences	Directeur : M. Bruno ANDRIOLETTI
Département Génie Électrique et des procédés (GEP)	Administratrice provisoire : Mme. Rosaria FERRIGNO
Département Informatique	Administrateur provisoire : M. Behzad SHARIAT
Département Mécanique	Administrateur provisoire : M. Marc BUFFAT
UFR des Sciences et Techniques des Activités Physiques et Sportives (STAPS)	Directeur : M. Guillaume BODET
Institut Universitaire de Technologie Lyon 1 (IUT)	Directeur : M. Michel MASSENZIO
Polytech Lyon	Directeur : M. Emmanuel PERRIN
Observatoire de Lyon	Directeur : M. Bruno GUIDERDONI
Institut de Science Financiére et Assurances (ISFA)	Directeur : M. Nicolas LEBOISNE
Institut National Supérieure du Professorat et de l'Éducation (INSPé)	Directeur : M. Pierre CHAREYRON

ACKNOWLEDGMENTS

First and foremost, I would like to thank the president of the jury Mme. Nathalie Le Sauze and M. Dimitrios Meimaroglou for accepting being the reviewers of this work and also thanks to Mme. Andrioletti and M. Edouard.

I am very grateful to my supervisors Timothy McKenna and Nida Sheibat-Othman for accepting me in your group and for all the advices, patience and scientific support during these years of work. Thanks also to professor Alexandre Ferreira Santos who referred me to the PhD with my supervisors.

I also want to thank Arkema for the material supply and the insightful comments and suggestions during our meetings, so, Salima Boutti, Anthony Bonnet, Samuel Devisme, Gaelle Fiorio and Camille Scherpereel, my special thanks! I thank the ANR-CLEANPOLY project for the financial support (ANR-18-CE06-0023).

Je voudrais remercier Sébastien Norsic pour son aide avec l'unité de polymerisation. Saint Sébastien a été toujours très efficace et il m'a sauvé beaucoup pendant ces années de doctorat. También me gustaría agradecer a Edgar Espinoza Rodriguez por su disponibilidad y atención en el laboratorio. You two are amazing!

Je tiens à adresser mes sincères remerciements à Pierre-Yves Dugas, Manel Taam, Olivier Boyron et Franck Collas pour son aide avec l'operation des equipments et les analyses. Je dois remercier aussi Nathalie Jouglart pour sa disponibilité, son aide avec les sujets administratifs et pour les petites discussions sur la vie.

These more than three years of work learning different things, facing some problems and improving me professionally, would be much difficult without the group of friends we have at the laboratory. Being around people from different countries and cultures made me grow personally and I am very thankful to them. Thanks Yashmin and Fabiana for helping me when I arrived, thanks Igor for the discussion about our subject and life in general. I also want to thank Niyi and Amin for being so gentle and nice friends here, Mariana and Thibaut for the conversations and for sharing the laboratory.

A special thanks to Roberta – eu não sei o que seria de mim aqui em Lyon sem você para me fazer rir, dividir as alegrias e preocupações durante esses anos, to Rahman – it is so good to have someone like you here, we had great discussions and good times and also to Felipe – danado demais, também dei muita risada e fiz muito rolê aleatório com você. You guys are amazing, I am grateful for having you in my life and you are part of my family here!

Apart from my family of friends here, I want to thank my family that I left in Brazil. Mãe, pai e Leo, eu amo vocês acima de tudo e eu nunca deixei de pensar e me preocupar com vocês. Obrigada pelo suporte que me dão sempre e por terem entendido e apoiado a decisão de vir para um outro país. Je voudrais aussi remercier mon copain, Anthony, qui est devenu ma famille ici. Merci pour ton soutien et merci d'être à côté de moi en tous les moments.

ABSTRACT

The multiphase system found in emulsion polymerization processes requires adequate amounts of chemicals in the recipe to provide stability to the polymer particles, and a proper mixing to guarantee the concentration of monomer in the aqueous phase and good heat transfer. During polymerization the latex can lose its stability forming coagulum, due to physico-chemical or process related factors, and also undesirable deposits can be found on the reactor wall or the surface of internal equipment. Such out of specification material can reduce the heat transfer efficiency of the reactor, and cause degradation of product quality. This may can also increase production costs due to unprogrammed shutdowns to clean the plant, and the need to dispose safely of waste material. This work presents an experimental study on the coagulation and fouling of PVDF latex, in the presence and absence of reaction, as well as the effects of mixing during the emulsion polymerization. The results suggested that the coagulation is mainly affected by the solids content, and it is related to fouling. Both phenomena can be minimized by working with a high concentration of surfactant, the use of wax as antifouling agent and a surface treatment like electropolishing. During the experiments related to coagulation and fouling, we discovered that there were mass transfer limitations in the reactor. With the improvements in the agitation set-up it was possible to increase the mass transfer coefficients in 20 %, and a model of particle growth during the emulsion polymerization was adapted to take into account this effect during the reaction. The results showed the importance of a model considering that the monomer in water is not in equilibrium with the gas concentration, mainly for polymerizations performed at low agitation speed.

RESUME

Le système multiphase rencontré dans les procédés de polymérisation en émulsion nécessite des quantités adéquates de produits chimiques dans la formulation pour assurer la stabilité des particules de polymère, et un mélange adéquat pour garantir la concentration du monomère dans la phase aqueuse et un bon transfert de chaleur. Au cours de la polymérisation, le latex peut perdre sa stabilité en formant un coagulum, en raison de facteurs physico-chimiques ou liés au processus, et des dépôts indésirables peuvent également se former sur la paroi du réacteur ou la surface de l'équipement interne. Ces matériaux hors spécifications peuvent réduire l'efficacité du transfert de chaleur du réacteur et entraîner une dégradation de la qualité du produit. Cela peut également augmenter les coûts de production en raison des arrêts non programmés pour nettoyer l'usine, et de la nécessité d'éliminer les déchets en toute sécurité. Ce travail présente une étude expérimentale sur la coagulation et l'encrassement du latex PVDF, en présence et en l'absence de réaction, ainsi que sur les effets du mélange pendant la polymérisation en émulsion. Les résultats suggèrent que la coagulation est principalement affectée par la teneur en solides, et qu'elle est liée à l'encrassement. Les deux phénomènes peuvent être minimisés en travaillant avec une concentration élevée de surfactant, l'utilisation de cire comme agent anti-encrassement et un traitement de surface comme l'électropolissage. Au cours des expériences liées à la coagulation et à l'encrassement, nous avons découvert que le transfert de masse était limité dans le réacteur. Grâce aux améliorations apportées au système d'agitation, il a été possible d'augmenter les coefficients de transfert de masse de 20 %, et un modèle de croissance des particules pendant la polymérisation en émulsion a été adapté pour prendre en compte cet effet pendant la réaction. Les résultats ont montré l'importance d'un modèle considérant que le monomère dans l'eau n'est pas en équilibre avec la concentration de gaz, principalement pour les polymérisations réalisées à faible vitesse d'agitation.

TABLE OF CONTENTS

CHAPTER 1. INTRODUCTION

Since the discovery of fluoropolymers in the 1930s, this group of polymers has received special attention due to the its remarquable characteristics provided by the strong C-F bond present on its structure. Some of the properties enhanced by these polymers are [1]:

- High service temperature and low flammability;
- Low surface energy and coefficient of friction;
- Self-lubricating effects and low solubility in hydrocarbons;
- Low refractive index and
- Strong piezoelectric properties.

In 2019 the global market for fluoropolymers was valued at $7.7 billion and is projected to reach $11.7 billion in 2027. The most lucrative segments by type of polymer are dominated by PTFE (Polytetrafluoroethylene) followed by PVDF (Polyvinilydene Fluoride). [2]

PVDF is produced by the polymerization of VDF (Vinylidene Fluoride) by different methods, however the aqueous emulsion and suspension polymerization are the most commonly ways to produce it commercially [1,3] and the present work deals with the emulsion polymerization method.

Emulsion polymerization is one of the most common ways of producing polymer latexes [4]. The recipe generally is composed by water, surfactant, a low water solubility monomer and a water-soluble initiator [5]. Due to the heterogeneous nature of emulsion systems, several different areas of chemistry and engineering are involved, for example, colloidal and free-radical chemistry as well as transport phenomena in multiphase systems and multiphase thermodynamic equilibria [6].

The presence of a supercritical gas, liquid and solid phases in the system makes the mixing, mass transfer and monomer partitioning important, as they affect the particle formation and growth process [7,8]. At the same time the mixing can improve the reaction performance, it can lead to out of specification products.

The final product of an emulsion polymerization is a polymer colloid, called latex, in which polymer particles of few nanometers are dispersed in a continuous aqueous phase. The stability of a colloidal system can be due to the surface charges coming for example from surfactant, it can be due to steric interactions

caused by chains around the particle surface or electrosteric, having both effects [4].

Some process and chemically related factors can lead to the destabilization of the latex, and for the purposes of this thesis, we will define coagulation as the combination of desirable particles to form undesirable, free-flowing bodies (large particles, lumps, chunks…). The deposition of material on the reactor's surface, known as fouling, is also a problem during latex production and it is also associated to the loss of stability.

Both coagulation and fouling are problems faced during the emulsion polymerization of PVDF, leading to out of specification products and process shut down. So, one of the objectives of this thesis is the elimination of these problems, to keep the reactor as clean, efficient and waste free as possible.

An overview of the polymerization unit is presented in Chapter 2, as well as the two techniques used for the polymerization, the analytical methods employed for characterization of the final product, and how the polymerization is monitored and the data are treated to obtain the polymerization rate by pressure and calorimetric calculations.

The coagulation of latex during the reaction and on its absence is explored in Chapter 3. Different techniques inducing to coagulation of pre-formed latex, as shearing and salt addition, are presented and discussed.

The Chapter 4 is dedicated to the fouling of latex in the absence and presence of reaction. Different factors as surfactant and CTA concentrations, solid contents, time and reaction volume are investigated, as well as the properties of the deposited material.

The mixing in the reactor, that consequently will affect the reaction rate and latex properties is discussed in Chapter 5, presenting the limitations of the reactor used as well as proposed and tested solutions to it. The gas-liquid mass transfer in the reactor is calculated and it was used to improve the already known VDF polymerization models found in the literature, showing the importance of a non-equilibrium model.

REFERENCES

[1] Ameduri B, Sawada H, editors. Fluorinated Polymers Volume 2: Applications. Royal Society of Chemistry; 2017.

[2] Mohite S, Danekar R, Prasad E. Allied Market Research. Fluoropolymers Mark by Prod Type (PTFE, FEP, PVDF, Fluoroelastomer, PVF, PFA, ETFE, Others), Appl (Film, Tube, Sheet, Pipe, Membr Sealant, Roofing, Addit Others), End-Use Ind (Transportation Equipment, Electr El 2020. https://www.alliedmarketresearch.com/fluoropolymers-market (accessed August 24, 2021).

[3] Ameduri B. From Vinylidene Fluoride (VDF) to the Applications of VDF-Containing Polymers and Copolymers: Recent Developments and Future Trends. Chem Rev 2009;109:6632–86. doi:10.1002/chin.201017230.

[4] Thickett SC, Gilbert RG. Emulsion polymerization: State of the art in kinetics and mechanisms. Polymer (Guildf) 2007;48:6965–91. doi:10.1016/j.polymer.2007.09.031.

[5] Gilbert RG. Emulsion Polymerization. A Mechanistic Approach. London: Academic Press Limited; 1995.

[6] Pladis P, Alexopoulos AH, Kiparissides C. Mathematical Modeling and Simulation of Vinylidene Fluoride Emulsion Polymerization. Ind Eng Chem Res 2014;53:7352–64. doi:10.1021/ie403548m.

[7] Mendez Ecoscia AC, Sheibat-Othman N, McKenna TFL. Reaction engineering of the emulsion homopolymerization of vinylidene fluoride: Progress and challenges. Can J Chem Eng 2018:1–10. doi:10.1002/cjce.23308.

[8] Ecoscia ACM, Sheibat-Othman N, McKenna TFL. Emulsion polymerization of vinylidene fluoride: Effects of mixing and reaction conditions on the initial rate of polymerization. Can J Chem Eng 2022;100:654–65. doi:10.1002/cjce.24145.

CHAPTER 2. MATERIALS AND METHODS

2.1
2.1 Reaction Unit

The reaction unit represented in the Figure 2.1 was built in 2014 and is composed of different sections as the one dedicated to cool down the monomer to guarantee its liquid state while pumped to the reactor, a thermal bath to heat up or cool down the reactor, a syringe pump to introduce chemicals, the nitrogen line to purge the content of the reactor or the solutions and the vent section to remove the gases or purge the lines. The feed line of the monomer is cooled using a heat exchanger where a heat transfer fluid circulates counter currently and the monomer is added to the reactor by a diaphragm pump, having the total mass monitored by a Coriolis mass-flowmeter.

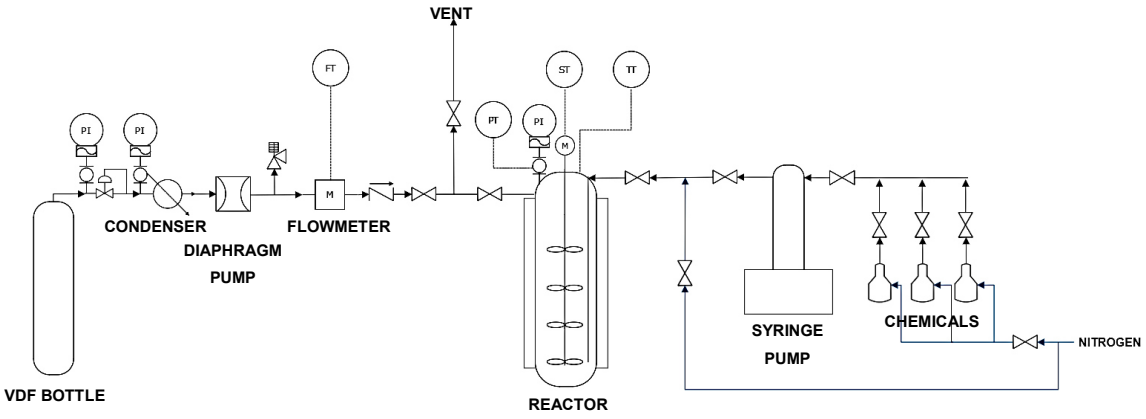

Figure 2.1 PVDF polymerization unit.

The high pressure reactor is a 3.8 L stainless steel 316 jacketed reactor with three 6-bladed 45° impellers of 5 cm diameter and one hydrofoil of 9.1 cm diameter, a dip tube and a thermocouple located 5 mm from the reactor's wall. The reactor's geometry and internals disposition are shown in Figure 2.2

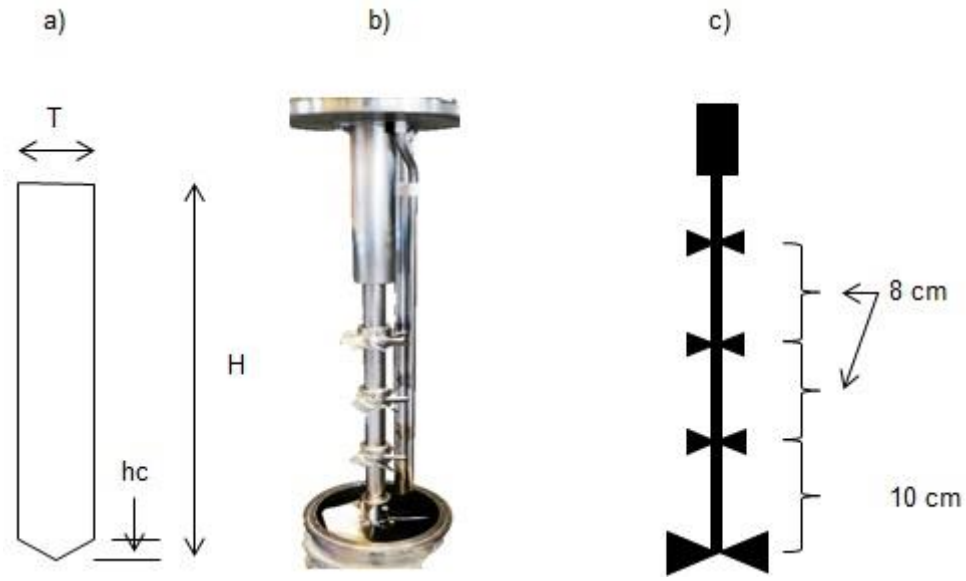

Figure 2.2 a) reactor's geometry, b) reactor's internals showing the thermocouple and dip tube and c) Set-up 2/2D with impellers spacing.

The reactor has height over tank diameter (H/T) of 5 and the height of the conical section (hc) is 3 cm. The position of the impellers in the agitation setup can be changed, and in this work two setups are used:

- Setup2: three 6-bladed 45° impellers plus hydrofoil A345
- Setup2D: three 6-bladed 45° impellers plus hydrofoil A315

A dedicated system built in Labview is recording the inlet and outlet bath oil temperatures, pressure and temperature in the reactor, the agitation speed, the monomer flowrate and the temperature on the flowmeter. This system also enables the control of the reactor temperature (by automatically manipulating the temperature set-point of the bath).

2.2 Chemicals

The vinylidene fluoride (VDF) monomer and tensioactive (TA) were kindly provided by Arkema (Pierre Bénite, France), and used without further purification.

Potassium Persulfate (KPS) (99%, Acros Organics) was used as initiator, Ethyl Acetate (CTA) (99.5%, Sigma Aldrich) was used as chain transfer agent and Sodium Acetate Anhydrous (Salt) (99%, Sigma Aldrich) was used as a buffer.

Deionized water is used as initial charge, as rinse water and to prepare the initiator + salt solution and a commercial paraffin/wax is used as antifouling agent [1–3].

2.3 Batch and Semi-Batch Reactions

The same procedure as described by Ecoscia [4] was used, which has the following steps:

1. The vinylidene fluoride monomer bottle is opened setting the outlet pressure of monomer at 30 bar by a pressure regulating valve;
2. A small amount of monomer is purged to remove any impurity present in the feed line;
3. The purge valve is closed;
4. The monomer is cooled down until -25 °C before being pumped to the reactor;
5. An initial charge of deionized water, tensioactive and wax is added to the reactor, sealing it and the agitation speed is set to the desired value while purging the initial charge in the reactor with nitrogen;
6. The reactor temperature is increased using the circulation bath until the desired temperature is reached (typically 83 °C). The reactor temperature is controlled by a cascade strategy where the master controller (reactor temperature) output is the temperature set point of the bath (slave controller);
7. The solution of initiator + salt, the chain transfer agent and the rinse water flasks are purged with nitrogen to remove oxygen;
8. Once the desired reactor temperature was reached, the remaining nitrogen in the reactor is purged, its feed valve is closed and around 5 bar of monomer is charged to the reactor and then removed;

9. When the reactor pressure is at 69 bar, the monomer feeding is stopped and the chain transfer agent is injected, followed by rinse water to ensure that all the CTA was added. The monomer feeding is restarted until the reactor pressure achieves 88 bar;
10. Once the reactor is charged with monomer, the initiator + salt solution is injected (start of reaction), followed by rinse water. All of these liquids are introduced by the syringe pump;
11. When working on batch mode, the reaction is left to proceed without subsequent monomer feed, while when working on semi-batch mode, monomer is fed to the reactor to keep the pressure constant;
12. At the end of the polymerization the agitation speed is slowed down to 150 rpm, the reactor is cooled down, and the remaining VDF is degassed;
13. The reactor content is purged with nitrogen, and then the polymer is recovered from the reactor via a bottom valve, when the reactor temperature is at 30 °C.

The reactions are performed following the reference recipe presented in the Table 2.1, with the concentrations based in the volume of water. When a different concentration of a chemical is used, it will be mentioned.

Table 2.1 Reference recipe.

	TA	**Wax**	**CTA**	**KPS**	**Salt**
g/L	1.5	1.1	15.3	0.09	0.06

2.4 Product Characterization

2.4.1 Solid Content

The solid content of produced latex was determined using gravimetric analysis by comparing wet and dried latex. Three samples of latex were placed in aluminum pans inside an oven kept at 100 °C during 2 hours.

The solid content (%) is calculated as follows,

$$SC = \left(\frac{m_{\text{latex}}^{\text{dry}}}{m_{\text{latex}}^{\text{wet}}}\right) 100 \tag{2.1}$$

where $m_{\text{latex}}^{\text{dry}}$ is the mass of latex dried and $m_{\text{latex}}^{\text{wet}}$ is the mass of latex measured before the water evaporation in the oven.

This solid content must be corrected to exclude the mass of solids used in the recipe,

$$SC_{\text{c}} = \left(SC - \frac{m_{\text{TA}} + m_{\text{KPS}} + m_{\text{Salt}}}{m_{\text{Latex}}} 100\right) \tag{2.2}$$

where the index TA states for the tensioactive, KPS is the initiator and m_{Latex} is the total mass of latex produced and collected in flasks at the end of reaction. The mass of wax is not considered on the correction because this material will remain in the reactor's surfaces as its melting point is around 55 °C, while the latex is recovered at 30 °C.

2.4.2 Particle Size

2.4.2.1 Dynamic Light Scattering

The dynamic light scattering (DLS) technique is based on the Brownian movement of particles, comparing the scattering produced by the sample to the one of a spherical similar particle, according to internal calibration curve.

Very diluted samples contained in a cell placed inside the Malvern Zetasizer Nano series ZS (Malvern Instruments) were measured with default detection angle of 173º. The reported particle diameter is the average of three measurements. The polydispersity index of the sample is checked, and a value lower than 0.08 means that the sample is monodisperse.

2.4.2.2 Laser Diffraction

The particle size distribution was measured with Mastersizer 3000® (Malvern Instruments) and the final distribution is an average of five measurements. The equipment has a red and blue lights and identify the changes of intensity from the laser beam. Some optical information about the sample and dispersant are used as input to the equipment's measurement file.

- Refractive index of disperse phase: 1.42;
- Refractive index of dispersant phase (water): 1.33;
- Adsorption index of the particles (PVDF): assumed as 0.001 from Malvern database for latex.

This technique will be used mainly to identify the presence of coagulum as it can be used to measure particle with the size ranging from 0.01 to 3500 μm.

2.4.3 Number of Particles

The number of particles is calculated based on the total volume of PVDF produced and the volume of a single PVDF particle.

$$N_{\mathrm{P}} = \frac{\frac{m_{\mathrm{Latex}}.SC_{\mathrm{c}}}{100.\rho_{\mathrm{PVDF}}}}{\frac{\pi}{6}D_{\mathrm{p}}^{3}} \tag{2.3}$$

where ρ_{PVDF} is the PVDF density (1800 kg/m^3) and D_{p} is the PVDF particle diameter measured by DLS technique.

In this work, the number of particles will be expressed in density of particles per volume of latex.

$$N'_{\mathrm{P}} = \frac{N_{\mathrm{P}}}{V_{\mathrm{Latex}}} = \frac{N_{\mathrm{p}}}{V_{\mathrm{PVDF}} + V_{\mathrm{W}}} \tag{2.4}$$

The volume of water is known by the total amount added to perform the reaction.

2.4.4 Monomer Conversion

The mass of monomer consumed by the polymerization is calculated from the total mass of polymer produced, by deducing other solid reactants fed to the reactor.

The mass of VDF can be found by,

$$m_{\mathrm{VDF}} = m_{\mathrm{Latex}} - (m_{\mathrm{W}} + m_{\mathrm{TA}} + m_{\mathrm{KPS}} + m_{\mathrm{Salt}} + m_{\mathrm{CTA}}) \tag{2.5}$$

The total conversion is calculated from the solids content by,

$$X = \frac{m_{\mathrm{Latex}} * SC_{\mathrm{c}}}{m_{\mathrm{VDF}}} * 100 \tag{2.6}$$

2.4.5 Surface Coverage

Ecoscia [4] assumed that all the tensioactive goes to the polymer particles if its concentration is lower than the Critical Micelle Concentration (CMC) of 10.7 g/L.

The surface coverage fraction is calculated by the ratio between the tensioactive and particles surfaces,

$$\theta = \frac{S_{\mathrm{TA}}}{S_{\mathrm{P}}} 100 = \frac{\frac{m_{\mathrm{TA}}}{MW_{\mathrm{TA}}} N_{\mathrm{A}} a_{\mathrm{TA}}}{N_{\mathrm{P}} \pi D_{\mathrm{p}}^2} \quad (2.7)$$

where MW_{TA} is the molecular weight of the tensioactive, N_{A} is the Avogadro's number and a_{TA} is the parking area of the tensioactive (25 Å²/molecule [4]).

2.4.6 Thermal Analysis

The Differential Scanning Calorimetry (DSC) was performed in the Mettler Toledo DSC 1 using 20 µL crucibles made of aluminum. The equipment was first purged with nitrogen at a flow of 20 ml/min and the analysis was performed following the ramp of 10 °C/min and holding time of 10 min as illustrated in Figure 2.3.

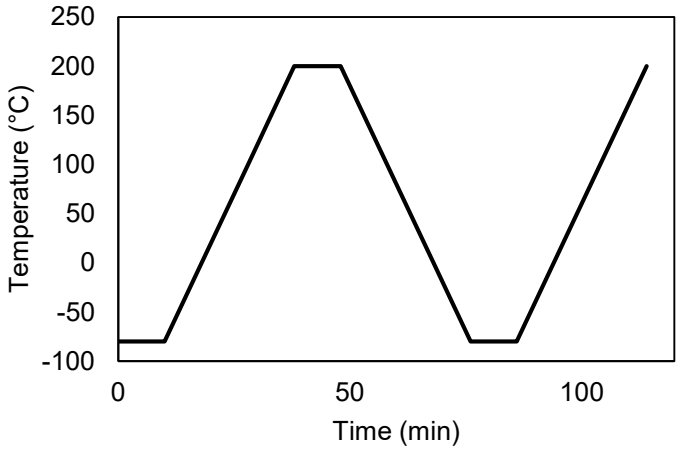

Figure 2.3 DSC analysis method for PVDF.

The crystallization temperature and crystallinity are determined from the cooling down curve and the glass transition and melting temperatures are determined from the second heating curve. The crystallinity is estimated from the enthalpy change of the sample divided by the enthalpy of pure PVDF,

$$Crystallinity = \frac{\Delta H_{\mathrm{sample}}}{\Delta H_{\mathrm{PVDF}}} 100 \quad (2.8)$$

where the specific enthalpy of 100% crystalline PVDF is equal to 104.5 J/g [5] and ΔH_{sample} is specific enthalpy of fusion (J/g) determined from the peak area.

2.4.7 Molecular Weight Distribution

The Molecular Weight Distribution (MWD) was measured using the Size Exclusion Chromatography (SEC), equipped with 3 porous columns - two columns of 1000 Å and one column of 30 Å of Polyester copolymer (Gram columns, PSS).

The solvent used is Dimethyl sulfoxide (DMSO) previously mixed with sodium nitrate ($NaNO_3$) and filtrated to remove water traces and impurities. Dried samples of the latex are solubilized in the solvent to generate solutions with a concentration around 3 mg/mL, heating the samples when necessary, to have a complete dissolution of the polymer.

Before injecting the samples in the column, the solutions were filtered using Nylon filter of 0.45 µm porous size to avoid column blocking by big chains of polymer. A PMMA calibration curve made with three standard samples with molecular weight ranging from 831 to 1,430,000 Da is used to obtain the molecular mass of the PVDF from the retention time.

2.5 Reaction Progress Monitoring

The polymerization rate is estimated in batch reactions according to the pressure decrease inside the reactor. For a semi-batch reaction, the rate can be determined by calorimetry.

2.5.1 Polymerization Rate for Batch Reactions

From the data of pressure and temperature during the reaction, it is possible to calculate the concentration of vinylidene fluoride by the Clayperon equation with a proper correction of non-ideality of the gas state.

The compressibility factor is calculated by a correlation developed by Nelson and Obert [6] as a function of pressure and temperature, but once the temperature is kept almost constant during the reaction, the calculations will be made based on pressure.

$$Z = -0.0077P_{\mathrm{r}}^{3} + 0.117P_{\mathrm{r}}^{2} - 0.4831P_{\mathrm{r}} + 1.1543 \tag{2.9}$$

where P_{r} is the reduced pressure calculated as a ratio between the pressure in the reactor and the critical pressure of VDF equal to 44.3 bar [7].

From the compressibility factor and the operational conditions, it is possible to calculate the monomer concentration,

$$c_{\mathrm{VDF}} = \frac{n_{\mathrm{VDF}}}{V_{\mathrm{HS}}} = \frac{P}{ZRT} \tag{2.10}$$

where V_{HS} is the head space volume of the reactor, a difference between the reactor empty volume (3.8 L) and the volume of latex (V_{Latex}) inside the reactor which changes as the polymer is being produced. The pressure *P* and temperature *T* during the reaction are known and monitored with the Labview system, and *R* is the gas constant.

The polymerization rate is calculated as the variation of the monomer concentration over time,

$$R_{\mathrm{p}} = -\frac{\mathrm{d}c_{\mathrm{VDF}}}{\mathrm{d}t} \tag{2.11}$$

From this, we can calculate the mass of polymer produced and consequently the solids content and the conversion.

$$m_{\mathrm{PVDF}} = (n_{\mathrm{VDF}}^{\mathrm{t0}} - n_{\mathrm{VDF}}^{\mathrm{t}})MW_{\mathrm{VDF}} \tag{2.12}$$

where $n_{\mathrm{VDF}}^{\mathrm{t0}}$ and $n_{\mathrm{VDF}}^{\mathrm{t}}$ are the number of mols of vinylidene fluoride at time zero and at the actual time t, and MW_{VDF} is the molecular weight of the VDF which is 64 g/mol [8].

The corrected solids content is given by,

$$SC_{\mathrm{c}}(\%) = \frac{m_{\mathrm{PVDF}}}{m_{\mathrm{PVDF}} + m_{\mathrm{W}}} 100 \tag{2.13}$$

Finally, the monomer conversion is calculated as,

$$X = \frac{(n_{\mathrm{VDF}}^{\mathrm{t0}} - n_{\mathrm{VDF}}^{\mathrm{t}})}{n_{\mathrm{VDF}}^{\mathrm{t0}}} 100 \tag{2.14}$$

These calculations are based on the following assumptions:

- the total volume of liquid is only affected by the latex formation;
- the mass of water as vapor in the head space is negligible;
- the pressure drop is caused by the consumption of monomer to form latex.
- The presence of monomer in the latex is neglected, since the monomer is hardly soluble in water.

2.5.2 Polymerization Rate for Semi-Batch Reactions

As the pressure in the reactor is kept constant during semi-batch reactions, it is not possible to estimate the consumption of monomer based on the pressure as described previously. So, calorimetric calculations are used to estimate the heat of reaction and then the polymerization rate.

The heat balance of the reactor is written as,

$$Q_{\mathrm{acc}} = Q_{\mathrm{feed}} + Q_{\mathrm{j}} + Q_{\mathrm{R}} + Q_{\mathrm{a}} - Q_{\mathrm{l}} \tag{2.15}$$

where Q_{acc} is the heat accumulated, Q_{feed} is the heat caused by the addition of material in the reactor, Q_{j} is the heat exchanged with the jacket, Q_{R} is the heat of reaction, Q_{a} is the heat caused by the agitation and Q_{l} is the heat loss to the environment.

The heat accumulated changes over time, as given by the following differential equation,

$$Q_{\mathrm{acc}} = \left(\sum mc_{\mathrm{p}}\right)\frac{\mathrm{d}T_{\mathrm{R}}}{\mathrm{d}t} \tag{2.16}$$

where the $\sum mc_{\mathrm{p}}$ accounts the contributions of all the chemicals added or produced in the reactor as well as its metal inserts (shaft, impellers, dip tube and thermocouple), T_{R} is the reactor temperature and $\mathrm{d}t$ is the time step.

$$\sum mc_{\mathrm{p}} = m_{\mathrm{W}}c_{\mathrm{p,W}} + m_{\mathrm{chem}}c_{\mathrm{p,chem}} + m_{\mathrm{VDF}}c_{\mathrm{p,VDF}} + m_{\mathrm{PVDF}}c_{\mathrm{p,PVDF}} + m_{\mathrm{met}}c_{\mathrm{p,met}} \tag{2.17}$$

where the index W is for water, chem is for the other chemicals added, VDF is the monomer, PVDF is the polymer and met is related to the metal parts of the reactor.

The term Q_{feed} is calculated based on the flow rate, heat capacity and temperature of the feed,

$$Q_{\mathrm{feed}} = \dot{m}_{\mathrm{feed}} c_{\mathrm{p,feed}} (T_{\mathrm{feed}} - T_{\mathrm{R}}) \tag{2.18}$$

The heat from the jacket is calculated based on the global heat exchange coefficient and the area of thermal transfer,

$$Q_{\mathrm{j}} = UA(T_{\mathrm{j}} - T_{\mathrm{R}}) \tag{2.19}$$

here the U is the global heat exchange coefficient (around 500 W/m²K), A is wetted area of the reactor wall and T_{j} is the temperature of the fluid inside the jacket. The global heat exchange coefficient is kept constant to make easier the estimation of the polymerization rate, but it is known that the U value changes with the changes in the latex properties with the progress of the reaction.

As the difference between the fluid temperature at the inlet and outlet of the bath is lower than 1 °C, in the calculations T_{j} will be represented by the outlet temperature of the bath oil.

The heat from agitation Q_{a} is negligible and the heat loss to the environment is calculate by,

$$Q_{\mathrm{l}} = b(T_{\mathrm{j}} - T_{\mathrm{amb}}) \tag{2.20}$$

where b is a heat loss coefficient and T_{amb} is the ambient temperature.

The heat of polymerization is,

$$Q_{\mathrm{R}} = R_{\mathrm{P}} V_{\mathrm{HS}} \Delta H_{\mathrm{P}} \tag{2.21}$$

The enthalpy of polymerization of vinylidene fluoride ΔH_{P} is 163 kJ/mol [7]. Once all the data to calculate the heat of reaction is available, it is possible to calculate the polymerization rate and subsequently the monomer consumption and PVDF formation allowing the calculation of solid content and monomer conversion as described previously.

NOTATION

a_{TA}	Parking area of the tensioactive, m²
A	Area of heat transfer, m²
b	Heat loss coefficient, J/K
c_{p}	Heat capacity, J/g.K
$c_{\mathrm{p,feed}}$	Heat capacity of the feed, J/g.K
$c_{\mathrm{p,met}}$	Heat capacity of metal, J/g.K
$c_{\mathrm{p,PVDF}}$	Heat capacity of PVDF, J/g.K
$c_{\mathrm{p,VDF}}$	Heat capacity of VDF, J/g.K
$c_{\mathrm{p,W}}$	Heat capacity of water, J/g.K
c_{VDF}	Concentration of VDF, mol/m³
D_{p}	Particle diameter, m
m	Mass, g
m_{chem}	Mass of chemicals (surfactant, wax, CTA and initiator), g
m_{CTA}	Mass of CTA, g
$\dot{m}_{\mathrm{feed}}$	Mass flow of feed, g/s
m_{TA}	Mass of tensioactive, g
m_{KPS}	Mass of KPS, g
$m_{\mathrm{latex}}^{\mathrm{dry}}$	Mass of latex dried, g
m_{Latex}	Total mass of latex, g
$m_{\mathrm{latex}}^{\mathrm{wet}}$	Mass of latex wet, g
m_{met}	Mass of metal inserts in the reactor, g
m_{PVDF}	Mass of PVDF, g
m_{Salt}	Mass of salt, g
m_{VDF}	Mass of VDF, g
m_{W}	Mass of water, g
m_{Wax}	Mass of wax, g
MW_{TA}	Molecular weight of tensioactive, g/mol
MW_{VDF}	Molecular weight of VDF, g/mol
N_{A}	Avogadro's number

N_{P}	Number of polymer particles
N'_{P}	Number of particles per volume, particles/m³
n_{VDF}	Number of mols of VDF, mol
P	Pressure, Pa
P_{r}	Reduced pressure
Q_{a}	Heat from agitation, J/s
Q_{acc}	Heat accumulated, J/s
Q_{feed}	Heat from the feed, J/s
Q_{j}	Heat from the jacket, J/s
Q_{l}	Heat loss, J/s
Q_{R}	Heat from reaction, J/s
R	Gas constant, Pa.mol/m³.K
$R\mathrm{p}$	Polymerization rate, mol/m³.s
S_{P}	Surface of polymer particles, m²
S_{TA}	Surface of tensioactive, m²
SC	Solid content, %
SC_{c}	Solid content corrected, %
t	Time, s
T	Temperature, K
T_{amb}	Ambient temperature, K
T_{feed}	Temperature of the feed, K
T_{j}	Temperature of the jacket, K
T_{R}	Temperature in the reactor, K
U	Overall heat capacity, J/m².K
V_{HS}	Volume of the head space, m³
V_{Latex}	Total volume of latex, m³
V_{PVDF}	Total volume of PVDF particles, m³
V_{W}	Volume of water, m³
X	Conversion, %
Z	Compressibility factor

Greek

ΔH_{P}	Heat of polymerization, J/mol
ΔH_{PVDF}	Enthalpy of PVDF, J/g
$\Delta H_{\mathrm{sample}}$	Enthalpy of a sample, J/g
θ	Surface coverage fraction
ρ_{PVDF}	Density of PVDF, g/m³

REFERENCES

[1] Amin-Sanayei R, Olmstead C. Aqueous Process for Making Fluoropolymers. US20070270534A1, 2007.

[2] Hedhli L. Polymerization of Fluoropolymers Using Polycaprolactone. EP2274345B1, 2009.

[3] Durali M, Hedhli L. Method of Producing Fluoropolymers Using Acid-Functionalized Monomers. US9434837B2, 2016.

[4] Méndez Ecoscia AC. Experimental Study of Emulsion Polymerization of Vinylidene Fluoride. University of Lyon, 2016.

[5] Sencadas V, Lanceros-Méndez S, Mano JF. Characterization of poled and non-poled _-PVDF films using thermal analysis techniques. Thermochim Acta 2004;424:201–7. doi:10.1016/j.tca.2004.06.006.

[6] Reid RC, Prausnitz JM, Poling BE. The Properties of Gases and Liquids. Fourth. New York: McGraw-Hill Inc.; 1987.

[7] Humphrey JS. Vinylidene fluoride-based thermoplastics (Overview and Commercial Aspects). Polym Mater Encycl 1996:8585–95.

[8] Arkema. GPS Safety Summaries. Vinylidene fluoride 2013. https://www.arkema.com/fr/produits/securite-des-produits/safety-summaries/ (accessed March 19, 2020).

CHAPTER 3. COAGULATION

3.1 Introduction

A colloidal system is defined as dispersion of insoluble particles, ranging in diameter from few nanometers to a few micrometers, in a continuous phase of different composition or state. We will assume that the sedimentation or creaming play only a minor role and focus on coagulation [1,2]. A colloidal system is considered stable when the particles continue to exist in the dispersed medium without forming aggregates at a considerable rate [3], but if the system loses its stability, the particles assemble forming a coagulum.

The product obtained from an emulsion polymerization is a latex comprising polymer particles with diameter around 200 nm, which is considered a polymer colloid with water as the continuous phase [4]. Therefore, studying the stability of the system and what leads to the destabilization is the key to make the process efficient and clean as possible.

For this thesis we will consider as coagulum the free-flowing bodies that can be removed from the reactor's surface by rinsing with water as well as the families of particles bigger than the common particle size of a stable latex.

3.2 Literature Review

3.2.1 Colloidal Interactions

Polymer colloids can be treated as monodisperse spheres, with smooth and uniform surfaces [5]. This is clearly not always the case, however the latex studied in the current study adheres to these criteria reasonably well.

The interaction between colloidal particles can be compared to the interaction at an atomic or molecular level, in these that they both exhibit attractive and repulsive interactions [3]. In the 1940s Derjaguin, Landau, Verwey and Overbeek developed the DLVO theory to explain the interactions between charged

particles. The theory assumes that once the particles are close enough, there may be a potential energy of interaction between them,

$$V = V_{\mathrm{A}} + V_{\mathrm{R}} \tag{3.1}$$

where V is the total interaction potential, the subscripts A refers to attraction potential, coming from van der Waals forces, and R refers to the repulsive potential due to electrostatic forces if the particles are charged (or steric forces if steric stabilization is employed).

3.2.1.1 Van der Waals attractive forces

The van der Waals forces are always attractive for particles with the same nature [6], and result from columbic interactions due to the permanent and induced dipole of the molecules [3]. The van der Waals potential of interaction between two spherical particles with radius larger than their separation distance is given by [7],

$$V_{\mathrm{A}} = -\frac{Ar_1r_2}{6d(r_1 + r_2)} \tag{3.2}$$

where A is the Hamaker constant taking into account the different permanent/induction dipole interactions, r_1 and r_2 are the radii of the interacting particles. In a monodisperse colloidal system, the particles have the same sizes, so the van der Waals potential will be reduced to,

$$V_{\mathrm{A}} = -\frac{Ar}{12d} \tag{3.3}$$

3.2.1.2 Electrostatic repulsive forces

A particle in a liquid medium will present a charge density that can be due to the dissociation of chemical functions present on its surface or coming from the adsorption of species like surfactants or ions [8]. If the medium contains electrolytes, these mobile species will form an uneven ion and counter-ion cloud

known as electrical double layer with thickness 1/κ, called the Debye length, as shown in the Figure 3.1.

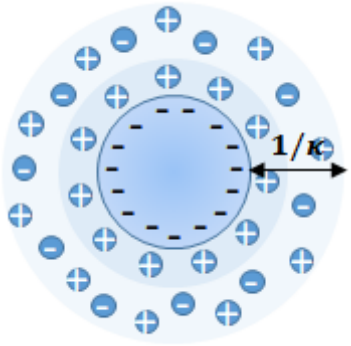

Figure 3.1 Electrical double layer around a negatively charged sphere.

The layer of counter-ions around the particle is strongly bound to the particle surface and is expected to move when the particle moves, this layer is called Stern layer. Far from the Stern layer, the surface potential falls gradually due to the diffused distribution of ions until reaching the distance $1/\kappa$ from the particle surface [3]. The Debye-Hückel parameter κ is given by,

$$\kappa = \sqrt{\frac{e^2 N_{\mathrm{A}}}{\varepsilon_0 \varepsilon_{\mathrm{r}} k_{\mathrm{B}} T} \sum_{\mathrm{i}} z_{\mathrm{i}}^2 M_{\mathrm{i}}} \qquad 3.4$$

where e is the elementary charge on a particle, N_{A} is the Avogadro's number, ε_0 is the permittivity of free space, ε_r is the relative permittivity, k_{B} is the Boltzmann constant, T is the temperature, z is the valency of the ions and M is the concentration. The thickness of the double layer can be modified by manipulating the parameters of the equation 3.4, for example, the addition of electrolytes in the medium increases the ionic strength and κ, consequently decreasing the thickness to the double layer [3].

The charged surface of a particle is characterized by a surface potential ψ_0. One way to determine experimentally the stability of a charge-stabilized colloid and estimate the surface charge density is by measuring the zeta potential, that is the potential measured at the plane exactly at the Stern layer. The signal of the zeta

potential is the same of the charged particle, and the higher its absolute value, higher the surface charge and more stable the dispersion.

When two particles approach in a distance less than the Debye length, there is an electrostatic interaction between them, due to the overlapping of the double layers, generating a repulsive force. The potential repulsive energy for a system stabilized electrostatically containing charges of any surface potential and symmetric electrolyte of valence z is [7],

$$V_{\mathrm{R}} = 32\pi\varepsilon_0\varepsilon_r r\left(\frac{k_{\mathrm{B}}T}{ze}\right)^2 \tanh^2\left(\frac{\psi_0 ez}{4k_{\mathrm{B}}T}\right)\exp(-\kappa d) \qquad 3.5$$

where ψ_0 is the surface potential. It can be noted that the potential of repulsion decreases exponentially with the separation distance, and that this potential can be manipulated by temperature, dielectric constant, electrolyte concentration, valence of ions and particle properties [3].

3.2.1.3 Steric interactions

Not only ions can be present on a particle surface to provide a repulsion potential, long chain molecules can also be anchored on a particle surface creating an envelope. Once this layer around the particle exceeds few nanometers, the van der Waals forces are overcome and the colloid is sterically stabilized. As the system studied in the current thesis is not sterically stabilized, this kind of interactions is not explained in more details.

3.2.2 Stability and Destabilization of Colloidal Dispersions

As mentioned in the previous section, the DLVO theory proposes that there exists a total energy potential between particles resulting from attractive and repulsive forces. An example of the potential curves is shown in the Figure 3.2.

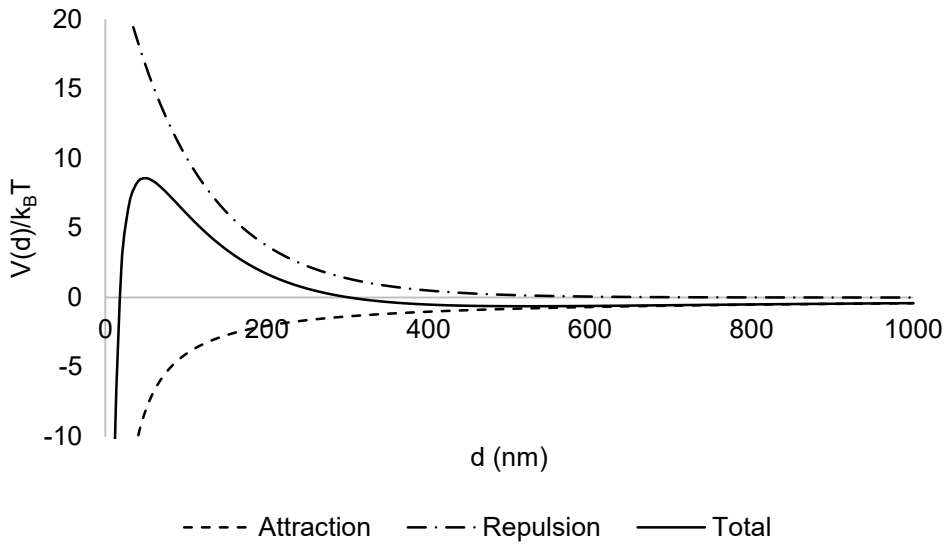

Figure 3.2 Representation of potential curves of attraction, repulsion and total potential, for a particle with R = 1000 nm, A = 2.0x10^{-20} J, κ = 1.0x10^{-2} nm and ψ_0 = 5.0x10^{-3} V.

As the attraction potential falls as an inverse power of the separation distance between particles and the repulsion potential falls as an exponential function of the distance, the total potential will present a primary minimum, a maximum and a secondary minimum when plotted as function of distance [6,9]. The stability of a colloidal dispersion can be predicted from the DLVO theory by comparing the maximum of the potential curve and the thermal energy of particles and normally a dispersion is considered stable when the maximum potential is higher than $15k_{\mathrm{B}}T$ [8,9].

The repulsion potential is very sensitive to the electrolyte content in the medium. The increase in ionic strength shifts the potential barrier for small interparticle distances and in some cases the maximum potential can be suppressed. The charge of the ions in the medium can be so strong that the double layer is compressed, having at the end only the attractive van der Waals force [10]. The point in which there is the complete vanish of the repulsive forces caused by electrolytes is known as the critical coagulation concentration (CCC).

The CCC is determined by the charge number of the counter-ions; the higher the charge, the lower the concentration of counter-ions needed to coagulate the particles. Increasing the electrolyte concentration decreases the double layer

thickness and decreases the range of the electrostatic repulsion until the complete disappearance of the potential barrier reaching the CCC [2].

Another way that leads to the coagulation of particles, but without decreasing the potential barrier is providing enough energy to the particles to surmount the maximum potential at small distances, for instance by agitation.

3.2.3 Coagulation of Particles

The colloidal stability can be provided by electrostatic or steric stabilization mechanisms. During emulsion polymerization, the chemicals used in the recipe as surfactant, initiator and salts as buffer agents, take part into the stabilization of the latex. Independently from the stabilization mechanism, coagulation can occur when the potential energy barrier of two approaching particles is overcome. The destabilization can be accelerated by the use of chemicals which will decrease the energy barrier, or by increasing the kinetic energy of the particles. Both forms of destabilization can be manipulated by the recipe or by the process while performing emulsion polymerization.

During the coagulation the small primary particles will lead to the formation of larger particles, so a population balance can be written, and in 1916 von Smoluchowski developed the theory of coagulation rate, deriving a general dynamic population balance equation in the form [11],

$$\frac{\mathrm{d}n_{\mathrm{k}}}{\mathrm{d}t} = \frac{1}{2}\sum_{\mathrm{i+j=k}} \alpha\beta\left(r_{\mathrm{i}}, r_j\right) n_{\mathrm{i}} n_{\mathrm{j}} - n_{\mathrm{k}} \sum_{\mathrm{l=1}}^{\infty} \alpha\beta(r_l, r_k) n_l \qquad 3.6$$

where n is the number concentration of particles, r is the particle radius, α is a collision efficiency, t is the time, $\mathrm{i}, \mathrm{j}, \mathrm{k}$ and l are related to the particle size class indices and $\beta(r, r)$ is the collision frequency, a function of particle size and the coagulation mechanism that can be perkinetic or orthokinetic.

Perikinetic coagulation

The perikinetic mechanism is also called Brownian coagulation due to the Brownian motion, that is the natural motion of particles caused by the thermal energy. For a colloidal system composed of spherical particles, the collision frequency function derived by Smoluchowski is,

$$\beta(r_\mathrm{i} + r_j) = \frac{2k_\mathrm{B}T}{3\mu}\left(\frac{1}{r_\mathrm{i}} + \frac{1}{r_j}\right)(r_\mathrm{i} + r_j) \qquad 3.7$$

where μ is the dynamic viscosity. This equation considers only binary collisions without the interaction of surrounding particles and it is valid for a completely destabilized system in which all the collisions will lead to coagulation.

The Smoluchowski's theory was improved with the introduction of the stability ratio W by Fuchs [12], leading to the equation,

$$\beta(r_\mathrm{i} + r_j) = \frac{2k_\mathrm{B}T}{3\mu W_\mathrm{ij}}\left(\frac{1}{r_\mathrm{i}} + \frac{1}{r_j}\right)(r_\mathrm{i} + r_j) \qquad 3.8$$

This stability ratio can be determined by the relation between the coagulation rate in fast and slow regime, which means, in the absence or presence of repulsive forces,

$$W = \frac{k_\mathrm{c}^{\mathrm{fast}}}{k_\mathrm{c}^{\mathrm{slow}}} \qquad 3.9$$

The fast and slow regimes, also called diffusion limited aggregation (DLA) and reaction limited aggregation (RLA), are determined by the ionic strength and the collision mechanisms [13]. In the DLA, every collision will result in a coagulum and the coagulation rate is limited by the time the particles take to diffuse towards one another. In the RLA, only a fraction of particles colliding will lead to a coagulum, and in this case the coagulation rate is limited by the time it takes to form it [5].

Normally the DLA is induced experimentally adding electrolyte to the system above the CCC [14–16], that is the minimum concentration of electrolyte to destabilize the dispersion [17,18]. The increase of electrolytes destabilizes the system by the compression of the double layer thickness, as shown in the equation 3.4. Hsu et al. [18] showed by mathematical manipulation that the DLVO theory presents a deviation about 15 %, comparing the cases in which the electrical double layer is considered much smaller than the particle radius and when this consideration cannot be assumed. Simulated total potentials of interaction between particles with different diameters showed that smaller the particle, the higher the CCC for particles with diameter of 100, 500 and 1000 nm, and only when the particles are larger than 1000 nm the CCC will be independent of the particle size.

Orthokinetic coagulation

The orthokinetic mechanism is caused by the fluid velocity gradients that transport the particles and this gradient in a fluid generates a shear. An equation for the orthokinetic collision frequency function was proposed by Lowry et al. [19,20] while studying the agitation-induced coagulation,

$$\beta\left(r_{\mathrm{i}} + r_j\right) = \frac{4\dot{\gamma}\phi}{\pi W} \qquad 3.10$$

where $\dot{\gamma}$ is the shear rate and ϕ is the volume fraction. The increase in the velocity when a fluid is under shearing can increase the force of collision between the particles. Also, the frequency of collision is increased with the increase in the volume fraction of particles [19].

To model the coagulation, it is possible to consider only perikinetic coagulation under certain conditions (e.g. laminar flow, low Re) [8,21,22]. But, when working at high shear, it is required to model the orthokinetic coagulation. In this case, a combined kernel is more adapted, in order to better account for the stability ratio of particles. [23–27]. The equations presented in this section give a simplified overview in order to understand the important mechanisms of coagulation and the experiments that will be presented in the second half of this chapter. More

details about the coagulation modelling can be found in Cheng et al. [27] and in the references within.

3.2.4 Coagulation Studies

As discussed above, there are different mechanisms for the destabilization of colloidal dispersions. In this sections, the studies will be divided in two parts: the influence of chemicals in the coagulation (as surfactant concentration and ionic strength), and the other studies are process - related, normally a consequence of the shearing.

3.2.4.1 Compositional factors

In addition to the principal and functional monomers, a common emulsion polymerization recipe has additives that are electrolytes like the initiator, emulsifier and pH buffer dissolved into water [28]. From the previous section, it was shown that the increase in the electrolyte concentration decreases the energy barrier against particle attraction, which leads to coagulation. The low surface charge density of the particles is also a cause of coagulation. But, this value depends on the particle diameter.

Effect of emulsifier

During emulsion polymerization, new particles can be formed if the amount of surfactant present in the system exceeds the amount required to cover the particles until they stop its adsorption, being in equilibrium with the amount of surfactant in the aqueous phase and if there is a tendency toward homogeneous nucleation. The particles covered by surfactant then will grow, thus increasing the total particle surface area, and consequently decreasing the fractional surface coverage to a critical value, resulting in the coagulation of the system to reduce its total are and reach once again the critical surface coverage [29–31].

So, there are two borderlines in terms of surface coverage, a critical value below which the particles are unstable and coagulate, and a surface coverage ratio above which the primary particles created during nucleation become stable and

a secondary nucleation occurs [30,32]. One way to overcome this is by feeding emulsifier after nucleation period at a level high enough to keep the surface coverage between these two critical values [29].

Large latex particles have surfaces flatter than the surface of very small particles, so the surfactant will be more strongly attached to the big particles, and they will be more stable than small particles having the same surface coverage. This leads to the conclusion that small particles are more susceptible to coagulation than large particles [30].

Effect of initiator

The initiator added to perform a polymerization may also be a source of ions in the system (if salt initiators are used), that can help to improve stability or increase the ionic strength, leading to destabilization. Snuparek and Tutalkova [33] showed the importance of the surface group concentration in stability in emulsion polymerization of acrylic monomers. It was observed that the sulfate end groups coming from the persulfate used as initiator, improve the stability of the latex, even under conditions of insufficient covering of particles by emulsifier. This was also observed by Chern et al. [34]. However, Fortuny et al. [35] when comparing the stabilization of PBA/PMMA provided by different species as sulfate end group, SDS and TA surfactants, observed that the stability provided by the sulfate was negligible when compared to the anionic surfactants, so it is expected that the contribution of initiator end groups to particle stabilization will only be important as we approach the lower limit of colloidal stability.

Liu et al. [36] studied the emulsion polymerization of styrene with different initiators (KPS, AIBN and AIBA) to observe their effects on particle coagulation. The increase in anionic KPS increased the particle coagulation, producing larger, narrowly distributed particles. The positive charges of AIBA initiator neutralized the surfactant charges, increasing the coagulation and advancing the time it starts during reaction, during the nucleation period. The oil-soluble AIBN initiator led to a polymerization similar to the one performed with KPS, showing that the sulfate groups from KPS are not important in the stabilization. The authors consider that the manipulation of the initiator system is an alternative to control the final particle size and distribution.

Even if the charges coming from the initiator can be responsible by part of the stability of particles, sometimes this stability is undesired. Boutti et al. [26] studied the production of a high solid content latex from MMA, BA and MAA by an unseeded emulsion polymerization testing ammonium persulfate (APS) as initiator and a redox initiator system. The goal was synthesizing a monomodal PSD latex controlling the secondary nucleation, which was obtained by using an electrically neutral initiator system with a stabilization provided by a system rich in non-ionic surfactant. The authors pointed that the charges coming from the APS initiator make difficult to control the global stability of the system, so in some processes it is interesting to use uncharged initiators.

Effect of electrolyte and alcohols

Liu et al.[38] studied the effect of electrolyte and alcohols in one-step emulsion polymerization of styrene in the presence of SDS. The addition of alcohols to the system changes the continuous phase polarity and the increase in the number of carbons of the alcohol decreases its dielectric constant. As the thickness of the double layer is dependent on the dielectric constant, a thinner electrical double layer is observed in the particles, making the system more unstable as noticed by the increase in the final particle size. This increase in particle size by coagulation was worsen when electrolytes were also added (again decreasing the thickness of the electrical double layer). As the coagulation proceeds during the polymerization, the reduction in the number of particles decreases the polymerizations rate as also observed, and the nucleation period lasted longer in specially when propanol was used. The authors consider that the use of alcohols is a way to produce large particles in a controlled way.

Ito et al. [39] studied the effect of electrolytes on coagulation during emulsion polymerization of an anionic seed of MA-MMA and a mixture of styrene and cationic dimethyl-aminoethyl methacrylate using APS as initiator. For polymers produced with the same solid content, an increase in the concentration of NaCl led to a decrease in the zeta potential of the particles, but it did not change the size of the particles in the range of concentrations tested. The addition of Na_2SO_4 as electrolyte in the same concentrations of the first salt, decreased even more the zeta potential because the double of Na+ is liberated, and around 1% of coagulum was found in the seed. While comparing the results of both salts, the

authors didn't observe a difference between them, and concluded that the extension of compression of the electrical double layer is mainly governed by the quaternary amino ions coming from the dimethyl-aminoethyl methacrylate.

A big number of works also used this methodology of performing the coagulation by the addition of an electrolyte in order to identify the coagulation parameters (such as the Hamaker constant) (see for instance Fortuny et al. [35], Melis et al. [40]).

3.2.4.2 Coagulation related to the process

The factors related to the process that can affect the coagulation are the technique used to run the polymerization (batch, semicontinuous, continuous), the heat removal and the agitation used (type of impeller, speed) [41].

In the previous section it was mentioned the existence of a critical surface coverage below which coagulation is triggered. In a similar vein, Van de Ven and Mason [42] observed the existence of a critical shear rate beyond which coagulation starts, which is logical because the same potential barrier needs to be overcome regardless of the source of the energy that leads to coagulation.

Oles [13] studied the coagulation of surfactant-free polystyrene latex in a Couette-flow system by adding salt solution to work on the DLA regime at different shear rates. The author observed a time-dependent coagulation behavior followed by a slowdown of coagulation reaching a stable final particle size. The final equilibrium size was found to be function of the volume fraction of particles. A similar induction time dependence after shearing on the aggregation of particles induced by electrolyte was observed by Guery et al. [43] while studying suspensions of non-Brownian solid particles in a rheometer with cone-plate geometry. This was also observed by the group of Morbidelli [44,45] while studying a charge-stabilized colloidal system in a strain-controlled advanced rheometric system rheometer. Both found that after an induction time there is an explosion in viscosity from a self-accelerating aggregation kinetics.

Matejicek et al. [41] investigated the influence of the agitation speed and reactor scale on coagulum formation for the emulsion polymerization of

Styrene/BA/Acrylic acid in a reactor geometrically similar to an industrial one. The amount of coagulum as a function of Reynolds number presented a V-shaped curve. At low Re number the coagulum is created from the nonuniform polymerization, as also observed by Zubitur and Asua while studying the coagulation during styrene/BA emulsion polymerization [46]. An increase in Re number decreases the coagulum due to the uniform temperature and concentration profiles, a result of a better mixing. However, the subsequent increase in the amount of coagulum is due to the increase of energy provided to the particles due to the agitation speed. The industrial and laboratory scale reactors produced the same percentage of coagulum for the same specific power input, leading to the conclusion that it is possible to scale up the coagulation behavior for the same power input, implying that it should be possible to extend improvements found in laboratory scale reactors to the industrial ones.

The effect of impeller type (one radial and two axial) on the aggregate size and structure of polystyrene in shear-induced aggregation was studied by Spicer et al. [47]. As axial impellers have lower circulation time when compared to radial impellers, it was observed that the steady state aggregate size was reached first for the axial impellers, because the frequency of exposition of the particles to the high shear area in these types of impeller is higher. The radial Rushton impeller produced the larger aggregates and an increase in agitation speed decreases the size of the final steady state aggregates. The results show the importance of choosing the agitation system when the particles in the process can suffer aggregation.

Kemmere et al., [28] studied the coagulation of polystyrene and polyvinyl acetate in stirred reactors with different scales, but keeping the same mean energy dissipation. The latex was swollen with monomers and salt was used to keep the same ionic strength before the experiments as the one found during polymerization due to the initiator. Coagulation was evaluated by the particle size distribution and the change in the number of particles compared to the seed, and taking samples after each addition of an electrolytic solution. With the increase of ionic strength, a light coagulation was observed and after several additions, an uncontrolled coagulation. There was no influence of the process conditions on

the coagulation, like reactor scale, impeller type or diameter meaning that the ionic strength dominates the coagulation mechanism in this case.

Surface coagulation was also studied by Lowry et al. [20]. They investigated the coagulation of an industrial latex in a stirred tank and in capped bottles rotated end-over-end to generate surface coagulation. Avoiding the air-liquid interface in the reactor, reduced the amount of coagulation, so the orthokinetic coagulation was related to the shearing and to the surface coagulation. The increase in agitation speed and electrolyte concentration increased the percentage of coagulation. The authors found that the initial stage of coagulation is important, because once an aggregate is formed, it can coagulate quickly with primary particles acting as a seed to form more coagulum, as also pointed by Kroupa et al. [48] while modeling the mechanism of coagulation in dispersions.

Regarding the aggregate size, it was found to depend on the formulation as well as process parameters. Oles, 1992 [13] found that the size of aggregates increases at higher concentration of particles. Several works found that a higher shear produces the smaller aggregates (Spicer et al., 1996 [44], Flesch et al., 1999 [49], Selomulya et al., 2001 [50], Kostansek, 2004 [15], Selomulya et al., 2002 [51]). Spicer et al. found that a radial impeller produces the largest aggregate for the same shear. Kostansek, 2004 [15] found that increasing the temperature above the T_g increases the aggregate size.

Table 3.1 presents some of the results of the studies about coagulation found in the literature.

Table 3.1 Results from coagulation studies found in the literature.

Reference	System		Results
Lowry et al., 1984 [19]	Emulsion polymerization	STR: Low Re: styrene High Re: vinyl chloride-ethyl acrylate	Higher the SC, lower the critical shear required to start coagulation
Lowry et al., 1985 [20]	A modified industrial latex	STR with a flat-blade impeller	Avoiding the air-liquid interface decreased the air-liquid interface coagulation Coagulation increases with speed and time.
		Capped bottles rotated end over end	Coagulation increases with the latex destabilization and reaches a plateau.
Matejicek et al., 1988 [41]	Emulsion polymerization	STR: Styrene-BA-acrylic acid	Coagulum can be formed by poor mixing at low speed, reaching a minimum with the increase of speed and then increasing again. The percentage of coagulum is independent of reactor scale for the same power input.
Oles, 1992 [13]	Surfactant-free polystyrene	Couette flow	High shear leads to an increase in aggregation rate and a decrease of the stable size. High concentration of particles produced a larger aggregate size.
Chern and Kuo, 1996 [34]	Emulsion polymerization	STR: MMA/BA 50/50	Coagulum increases with SC, low surface coverage and ionic strength with an acceleration above 50 % of SC.
Spicer et al., 1996 [47]	Polystyrene	STR: One radial flow and two axial flow impellers	High shearing produces the smaller aggregates. Radial impeller produces the largest aggregate for the same shearing.
Chern and Chen, 1997 [52]	Emulsion polymerization	STR: BA	Coagulation increases with the low surface coverage, ionic strength and agitation speed.
Kusters et al., 1997 [53]	Polystyrene	STR	Coagulation increases with ionic strength, SC and impeller speed.
Kemmere et al., 1998 [28]	Emulsion polymerization and swelling experiments	STR: Styrene at 50 °C Vinyl acetate 35 °C	Coagulation increases with ionic strength. PVAc-lattices appear to be more sensitive to ionic strength than PS-lattices. No influence of impeller speed on the coagulation rate of PS and PVAc-lattices was observed for the reactor scales investigated
Flesch et al., 1999 [49]	Polystyrene	STR	Higher shear rates lower the aggregates size.
Kemmere et al., 1999 [54]	Emulsion polymerization and swelling experiments	STR Reaction: PS lattices Swelling and reaction: PVAc latices	Higher the solid content, more sensitive to ionic strength. Operating conditions don't affect the colloidal stability of PS.

Reference	System	Results
		Swelling: the emulsifier and ionic strength have considerable influence on the colloidal stability, whereas SC and operating conditions have no influence. The ab initio experiments with vinyl acetate showed no clear dependency of colloidal stability on operating conditions
Hanus et al., 2001 [55]	BA/MMA with 1% methacrylic acid	Salt addition monitored by Dynamic Light Scattering	Coagulation increases with ionic strength.
Selomulya et al., 2001 [50]	Monodisperse latex	STR	Coagulation increases with shearing. Smaller aggregate size is produced with high shear.
Zubitur and Asua, 2001 [46]	Emulsion polymerization	STR Styrene/BA, Ab initio: thermal initiator Seeded: redox	Coagulation formed on the surface by poor mixing.
Ito et al., 2002 [56]	Seeded emulsion polymerization	Styrene, MA and MMA PMMA-MA anionic seed latex	Average particle size decreases with speed with broadening of PSD. Coagulation increases with agitation, and when decreasing pH.
Selomulya et al., 2002 [51]	Surfactant-free polystyrene	Couette flow Particles with different sizes	Aggregate size increases with SC. The maximum aggregate size decreases with shear rate. The aggregates of smaller particle size have greater overall strength than those of larger particles, for flocs of comparable sizes.
Kostansek, 2004 [15]	Emulsion polymerization under starved conditions	PBA/PMMA Reaction Limited Aggregation coagulation in a beaker stirred	Aggregate size decreases with agitation. Increase in temperature above Tg increases aggregate size.
Pourmehr and Navarchian, 2008 [57]	Emulsion polymerization	STR PVC	Coagulation increases with temperature.
Fukasawa and Adachi, 2010 [58]	Polystyrene	Reaction Limited Aggregation	The obtained rate of coagulation in the regime of reaction - limited coagulation was constant regardless of the progress of coagulation
Liu et al., 2013 [31]	Emulsion polymerization	STR BA	Coagulation increases with low surface coverage and ionic strength. Probability of coagulative nucleation increased with increasing monomer/water ratios.
Liu et al., 2014 [59]	Emulsion polymerization	STR Styrene	Coagulation increases with ionic strength and with the addition of methanol.

Reference	System		Results
Sugimoto et al., 2014 [60]	Carboxylated polystyrene	Rotation end-over-end	Coagulation decreases with pH.
Oktaviani and Adachi, 2018 [61]	Surfactant-free Polystyrene	STR	Coagulation increases with agitation. Weak dependence of the coagulation rate on the particle diameter.

3.3 Results

3.3.1 Orthokinetic Coagulation during Semi-Batch Emulsion Polymerization

The procedure is described in chapter 2 and the concentration of chemicals is presented in Table 3.2, unless otherwise mentioned.

Table 3.2 Reference recipe for batch reactions.

TA (g/L)	Wax (g/L)	CTA (g/L)	KPS (g/L)	Buffer (g/L)
1.50	1.1	15.3	0.09	0.06

The semi-batch reactions were performed at 400 rpm and 1.6 L of water.

- The main technique employed to detect the presence of coagulated particles in the product is laser diffraction using the Mastersizer 3000®. All the samples were dispersed in deionized water, measured using the same protocol and with similar obscurations.
- For a more quantitative comparison, in some experiments, the reactor was rinsed with water and the material was weighed to evaluate the amount of latex on the reactor's surfaces (that can be due to coagulation or fouling).

Among the semi-batch reactions performed to study the coagulation and fouling in the reactor, changing mainly the amount of surfactant and CTA in the recipes, only five reactions showed visible aggregates at the end with two families of particles observed by laser diffraction analysis.

Figure 3.3 presents the particle size distributions for the semi-batch reactions that generated visible aggregation. The presence of a second population of particles of bigger size can clearly be seen on the figures. Normally the particle size of the latex produced during the semi-batch reactions with the reference recipe and the solids content about 40 wt% is in the range of 230 nm (zeta-average). Surprisingly, when a second family of particles is detected, it is always in the range of 5 to 30 μm, as already noted in the previous work of the group [62].

However, as the distribution becomes very wide, it is difficult to define a unique mean size. We will discuss this point in more detail in the next sections.

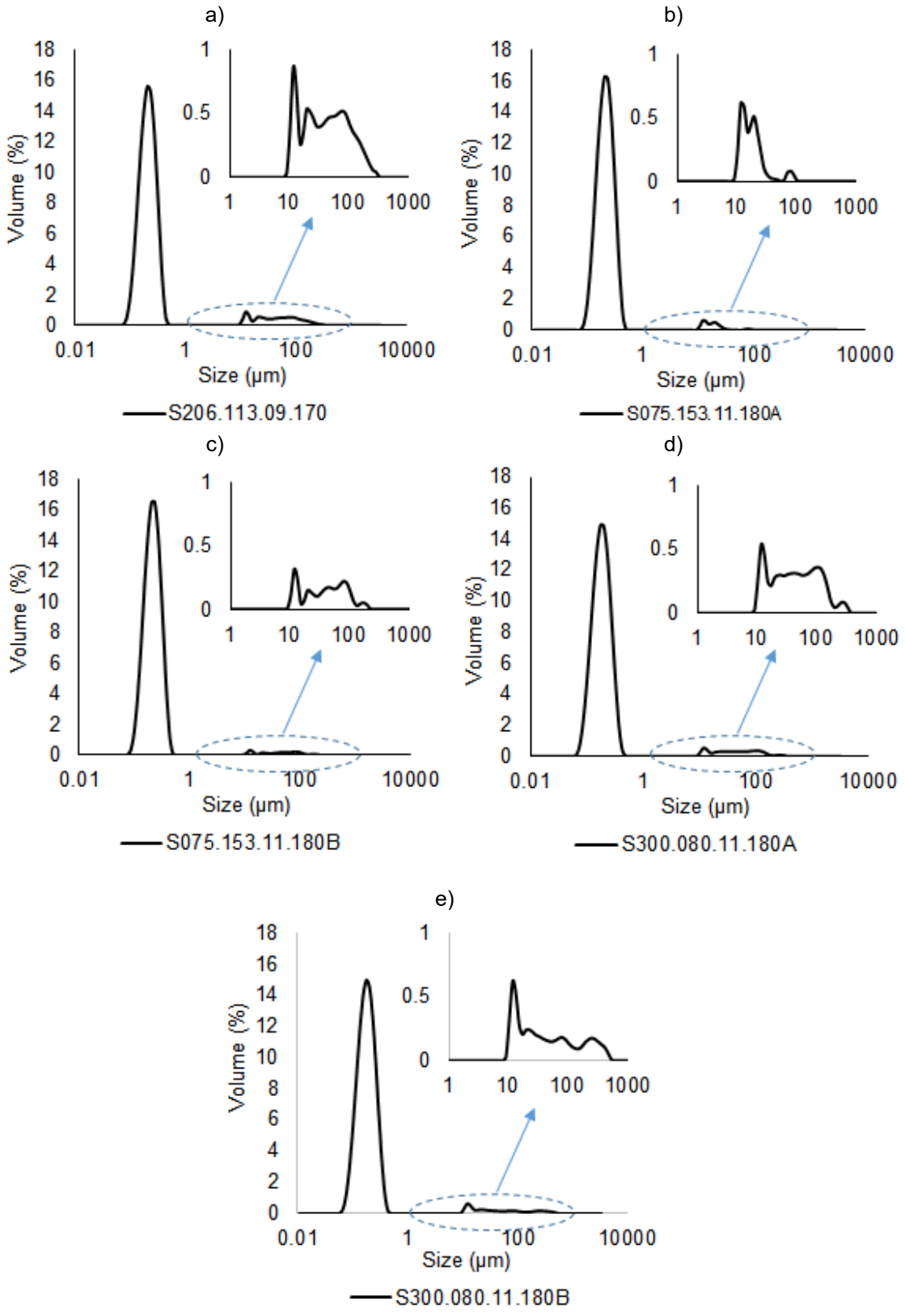

Figure 3.3 Particle size distribution of semi-batch latexes presenting coagulated/aggregated particles.

In the cases in which material observed on the agitator (which can be due to the formation of coagulation or fouling on the shaft, or to the formation of foam during depressurization), it was collected, weighed, and the percentage of PVDF is presented in the Table 3.3 together with the ratio of second population to the first one in the Mastersizer analysis and the results from the performed reactions. Unfortunately, the material was not recovered for the reactions S206.113.09.170 and S075.153.11.180A.

Table 3.3 Semi-batch reactions that presented some coagulum.

Reaction	S206.113.09.170	S075.153.11.180A	S075.153.11.180B	S300.080.11.180A	S300.080.11.180B
TA (g/L_{water})	2.05	0.75	0.75	3.00	3.00
CTA (g/L_{water})	11.3	15.3	15.3	0.8	0.8
KPS (g/Lwater)	0.25 (50 % t=0/ 50 % t=92 min)	0.09	0.09	0.09	0.09
Wax (g/L_{water})	0.9	1.1	1.1	1.1	1.1
Reaction time (min)	170	180	180	180	180
SC (%)	50.5	34.6	36.2	49.6	46.5
Dp (nm)	240	266	262	230	218
PdI	0.04	0.01	0.04	0.02	0.01
$Npx10^{-19}$ ($1/m^3$)	5.4	2.5	2.8	6.3	6.5
θ (%)	6.8	4.3	4.1	9.5	9.9
Mw (kDa)	702	370	432	1,034*	1,127*
PDI	3.39	2.67	2.94	1.19 3.25	1.20 3.52
Ratio of the 2nd population to the 1st one	0.098	0.033	0.028	0.065	0.053
PVDF lost on the reactor %	Not measured	Not measured	1.2	0.4	0.3

* Samples presenting more than one peak for MW distribution, out of the calibration curve. Only the peak in the range of the calibration data is presented.

Visible coagulum was first observed during the reaction S206.113.09.170, and one of the main factors is the higher solids content, as for the first time 50 wt% was reached, and the second factor is due to the addition of two shots of initiator. So, the destabilization may be caused by the presence of more particles, also observed in the reactions S300.080.11.180A/B, and by the higher ionic strength due to the higher amount of initiator.

The reactions S075.153.11.180A/B were performed with a lower amount of surfactant. Exactly the same recipe was used in both experiments to check reproducibility. As this recipe has a lower concentration of surfactant, it was expected that some coagulum would be produced. The material deposited on the shaft after these two reactions is shown in Figure 3.4. Probably the loss of stability was caused by the loss of surface coverage due to the growth of particles during polymerization. It can be said that the influence of surface coverage is the main factor because the reaction performed with 0.75 g/L_{water} of surfactant generated three times more material collected on the shaft when compared to the reactions performed with 3.00 g/L_{water}.

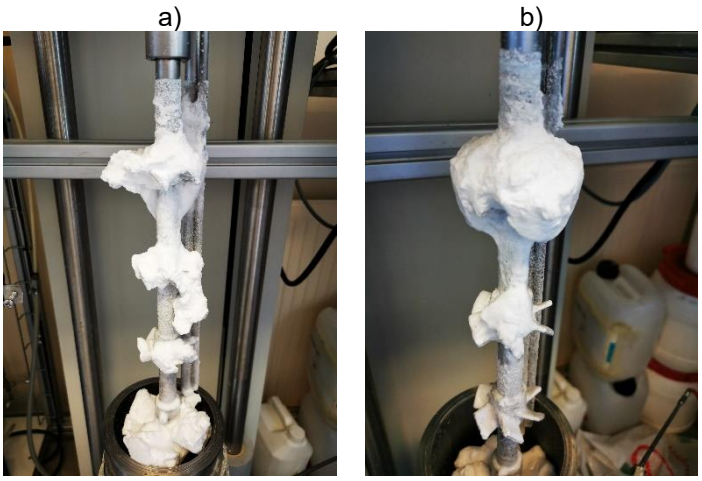

Figure 3.4 Material deposited on the shaft after the semi-batch reactions a) S075.153.11.180A and b) S075.153.11.180B.

Knowing that the coagulation of particles happens when the surface coverage is lower than a critical value [29–31], the recipe of the reactions S075.153.11.180 was repeated (S075.153.11.120), but the reaction was stopped at 120 minutes to try to follow the coagulation with time and determine what is the value of the critical surface coverage of the particles. Figure 3.5 shows that it looks like the coagulated material was just starting to be formed on the shaft. Table 3.4 shows the results of a reaction performed with the reference recipe (S150.153.11.180) and the reactions with half the amount of surfactant when coagulation was observed (S075.153.11.180B) and when it was about to start (S075.153.11.120).

Figure 3.5 Material deposited on the shaft after the semi-batch reaction S075.153.11.120.

Table 3.4 Semi-batch reactions performed with different surfactant concentration and time.

Reaction	S150.153.11.180 (Reference)	S075.153.11.180B	S075.153.11.120
TA (g/L_{water})	1.50	0.75	0.75
Time (min)	180	180	120
SC (%)	39.1	36.2	28.8
Dp (nm)	227	262	251
PdI	0.05	0.04	0.01
$Npx10^{19}$ ($1/m^3$)	4.6	2.8	2.4
θ (%)	6.4	4.1	5.1
Mw (kDa)	415	432	382
PDI	2.48	2.94	2.60
Ratio of the 2^{nd} population to the 1^{st} one	-	0.053	-
PVDF lost on the shaft %	0	6.5	0

It can be said that for the low concentration of surfactant, when reaching almost 30 wt% of solids in 120 min, the critical surface coverage of the surfactant is around 5 %. It is interesting to note that the reactions S300.080.11.180A/B performed with 3.00 g/L_{Water} of surfactant generated a deposited material in the reactor, even with a surface coverage of the free flowing latex around 9 %. This is also an effect of the number of particles in the reactions with the highest amount of surfactant, that presents around $6x10^{19}$ particles/m^3 against $3x10^{19}$ particles/m^3 for the reactions (S075.153.11.180A/B). It is important to highlight that the parking area of a surfactant is dependent on the surfactant type, temperature, electrolyte

concentration, surface of the polymer and particle size [63]. As the reactions were performed with the same surfactant, temperature, electrolyte concentration and polymer, a further investigation must be made on the surface coverage of the secondary family of particles (5 to 30 μm). From the results of percentage of PVDF lost as on the shaft, it is noticed that even with the increase in the solids content, the additional surfactant in the recipe can provide more stabilization than working with a lower concentration, as expected.

3.3.2 Orthokinetic Coagulation of Preformed Latex (in the reactor)

The influence of the time under agitation was studied in the absence of reaction. The reactor was filled with 2.2 L of latex from previous reactions, using the agitation set-up 2 at a speed of 550 rpm during a certain amount of time, controlling the temperature.

The first experiment was performed with a 20 %wt solids content latex that was left under agitation during 20 minutes at the temperature of 25 ºC. The latex has become a foamy material deposited mainly on the impellers. As the experiments were performed in the presence of air, that is less dense than the monomer, this helps improving the foam formation and stability [64].

Figure 3.6 shows the material after the shearing test in the reactor. The 45° angle of the 6-bladed impellers doesn't allow the material to drain properly through the bottom valve, but the material created has a lower density, and probably this deposition is happening when the reactor is being emptied. This justifies the rinsing procedure before the fouling quantification, because probably the material was not there under agitation.

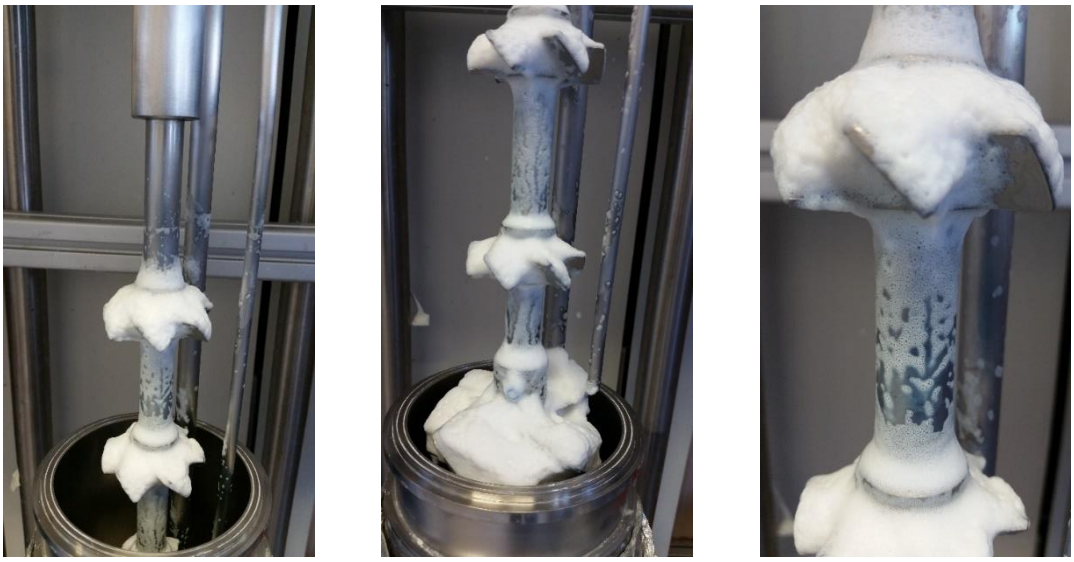

Figure 3.6 View of the material deposited on the impellers after 20 minutes at 25 ºC and 550 rpm.

For the second experiment, another latex with the same solids content was heated until 83 ºC and kept under agitation of 550 rpm during 100 min. Again the material was deposited on the shaft as can be seen in the Figure 3.7, but it can be easily removed by rinsing the surfaces with water. After rinsing, the real fouling can be seen in the Figure 3.8.

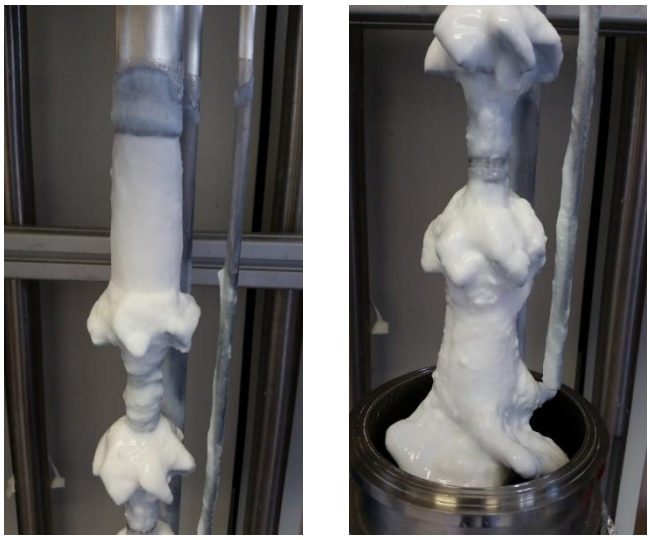

Figure 3.7 View of the material deposited on the impellers after 100 minutes at 83 ºC and 550 rpm.

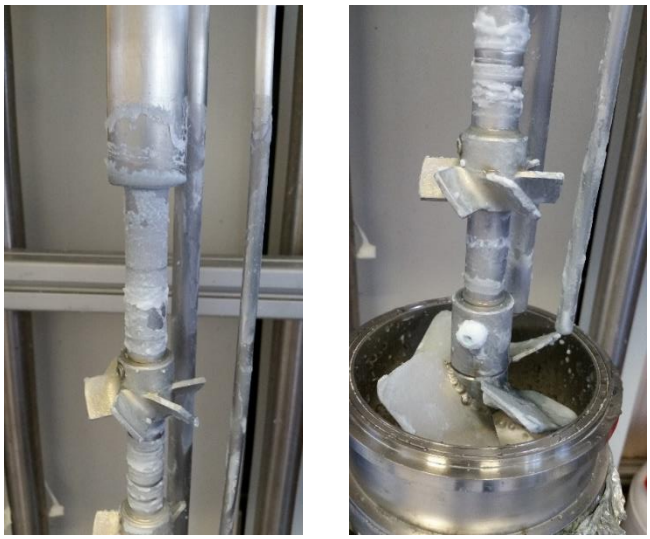

Figure 3.8 View of the material deposited on the impellers after 100 minutes at 83 ºC and 550 rpm, after rinsing with water.

The third experiment was performed with latex 20 wt% at 83 ºC kept under agitation of 550 rpm during 200 min. Again the material was deposited on the shaft but it was much thicker and denser than the previous ones, as shown by Figure 3.9. One can see the thick coagulum layer on the shaft and sedimentation, certainly produced by the flux inside the reactor.

Figure 3.9 View of the material deposited on the impellers and on the reactor after 200 minutes at 83 ºC and 550 rpm.

From the results it can be seen that the deposits are enhanced by the time under agitation, what is expected because the particles will cross the high shearing

impellers zone more times [47]. The particle size distribution of the aggregates was not measured.

3.3.3 Orthokinetic Coagulation with a Rheometer

In the previous experiments performed using the reactor, is not possible to work with a controlled shear rate, as we have different shearing in different zones of the reactor, so, to investigate *in situ* orthokinetic coagulation we also used a rheometer. The experiments were performed in a rheometer MCR 2 Anton Paar available at LAGEPP with a cone-plate CP-50. The temperature control of the sample is done only for the plate and to avoid the water evaporation during the experiments, a layer of liquid paraffin was put on the sample, which is removed before collecting the sheared material.

The viscosity data was registered during the measurement. After the end of the test, the size of the particles is measured on the Mastersizer. To perform the experiments in the rheometer, three shear rates were chosen: 50, 175 and 300 s^{-1} based in two previous studies of the group about the shearing inside the reactor [65] and shearing of latex using a couette geometry [62].

Two samples of latex with different solids contents (21.4 and 29 wt%) were left under constant shear rate for fixed times at 25 °C. Figure 3.10 shows the viscosity curve for the tests performed with two different latexes during 30 minutes. It is noticed that the coagulation happened only for the latex with the higher solid content and the shear rate of 300 s^{-1}.

The particle size distribution is shown in the Figure 3.11 and as expected, from the viscosity curves for the latex with the lower solids content, the particle size distribution is still the same after shearing in the rheometer. However, for the second latex, it is possible the see a small change on the PSD, as new populations appear around 17 μm and 100 μm. It is possible that the time was not long enough to coagulate a great amount of particles for these shear rates.

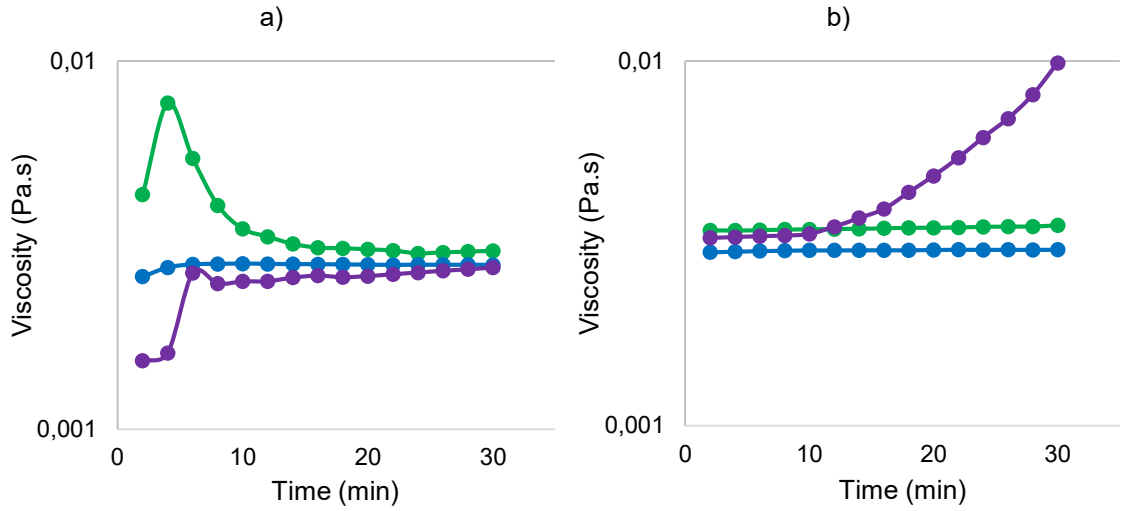

Figure 3.10 Viscosity curves measured in the rheometer under shearing for 30 min a) SC = 21.4 wt% with θ = 11.1 % and b) SC = 29 wt% with θ = 8.7 % for (-) 50 s^{-1}, (-) 175 s^{-1} and (-) 300 s^{-1}.

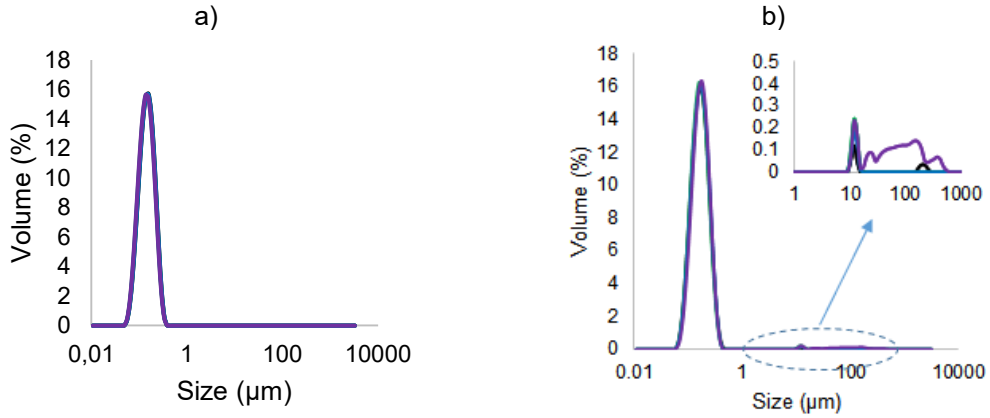

Figure 3.11 PSD for 30 min under shearing a) SC = 21.4 wt% with θ = 11.1 % and b) SC = 29 wt% with θ = 8.7 % for (-) original latex, (-) 50 s^{-1}, (-) 175 s^{-1} and (-) 300 s^{-1}.

Figure 3.12 shows the viscosity curves for the tests performed under shear rates of 50, 175 and 300 s^{-1} during 105 minutes for the same two latexes. It is possible to notice that the coagulation only happened for the latex with lower solids content under a shearing of 300 s^{-1} while for the latex with the higher solids content the coagulation happened in all cases with a sudden increase in the viscosity, like some results found in the literature [43–45].

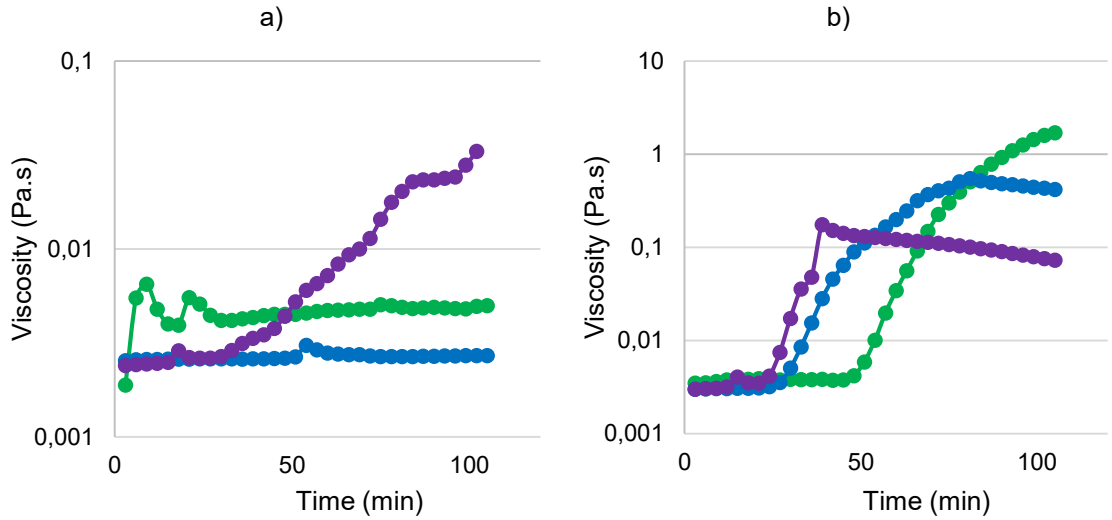

Figure 3.12 Viscosity curves for 105 min under shearing a) SC = 21.4 wt% with θ = 11.1 % and b) SC = 29 wt% with θ = 8.7 % for (-) 50 s^{-1}, (-) 175 s^{-1} and (-) 300 s^{-1}.

The particle size distribution is presented in Figure 3.13. Once again for the latex with the lower solids content, it is possible to see a small difference in the particle size distribution as a populations appear ranging between 10 and 300 µm. However, for the latex with the higher solids content only the shear rate of 50 s^{-1} was not enough to completely coagulate the primary particles. It is also possible to observe again a time dependent behavior, but also a triggering point for the coagulation that can be related to the time of contact between the particles or the coagulation efficiency.

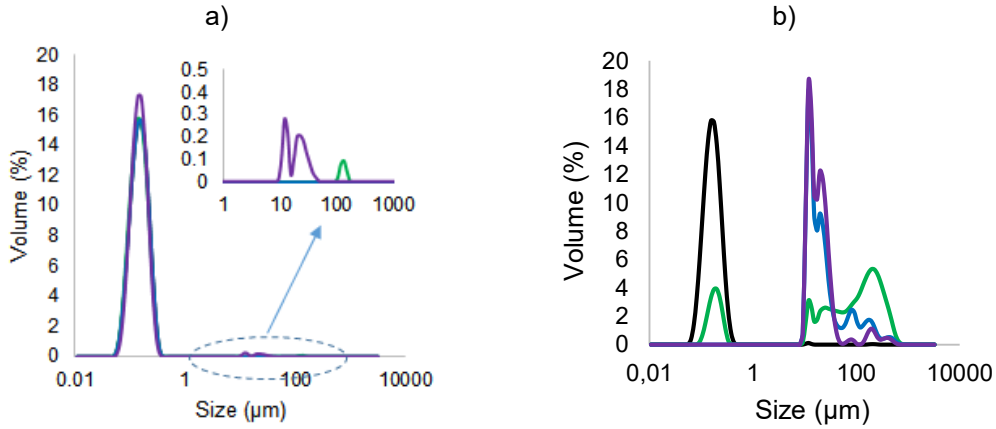

Figure 3.13 PSD for 105 min under shearing a) SC = 21.4 wt% with θ = 11.1 % and b) SC = 29 wt% with θ = 8.7 % for (-) original latex, (-) 50 s^{-1}, (-) 175 s^{-1} and (-) 300 s^{-1}.

It is interesting to notice that even if we are supposed to experience a higher average shear rate in the reactor [65] than the 300 s^{-1} tested in the rheometer,

we never had a complete coagulation of the primary family of particles after a reaction, like observed in the rheometer.

One can also notice that the second peak of coagulated particles has shoulders and with the increase of the applied shear rate, the volume percentage of the shoulder with the biggest particles decreases, probably because of breakage of aggregates. This will be discussed at the end of the next section.

3.3.4 Orthokinetic Coagulation with the Mastersizer

The Mastersizer 3000 is used to perform the measurements of particle size based on laser diffraction and it has an accessory dedicated to the dispersion of the sample on the diluent, normally water. In this work, we will also use this device in order to investigate in situ coagulation, as we can select different agitation speeds and times. Indeed, the liquid dispersion unit has a stirrer and a pump connected to the same shaft, and its speed can be changed by the user. The diluent can also be fed manually to the unit and ideally will have the same concentration of surfactant, ions or other chemical components that can be found on the dispersant of the original sample [52].

During the measurements, the obscuration of the diluted sample is around 2 – 3 %, in agreement with the recommendations for submicron particles (obscuration lower than 5 %). If the sample has particles from 1 to 10 μm, the obscuration should be in the range of 5 – 10 % and if the sample is very polydisperse, an obscuration from 10 – 20 % should be used [66]. An increase of obscuration means that more particles are dispersed and available for a possible coagulation/aggregation during the measurements, so the following measurements were performed with obscurations in the range of 5 – 7 %, which turns out to also be good for the final polydisperse distribution obtained.

The aggregation was observed following 20 consecutive measurements in the Mastersizer, which takes 7 minutes from the first to the last measurement. As when working with speeds higher than 2000 rpm the presence of bubbles can interfere on the measurements, the cell was visually checked to be sure that

bubbles are not present in the system. Both water and a solution with sodium acetate containing the same concentration of this salt as used to perform the reaction, were used as dispersants, to check how the particles behave when dispersed in water or in a salt solution, at different speeds, as presented in the Figure 3.14. A latex with 11 % of surface coverage and 186 nm is used. The first measurement is in light blue and it evolves to the purple color over time. It is possible to notice the formation of a second peak of particles for some agitation speeds. Interestingly, the second peak of particles was created in the same size region as that observed during emulsion polymerization.

When using the salt solution as dispersant (using the same speed, similar obscuration and total time of measurement), the aggregation happens only for the highest speed of the experiments and to a lesser extent than when using water as diluent. This can be due to the presence of ions with positive charge coming from the salt, that helps to increase the surfactant density in the particles and to increase the adsorption of surfactant that was probably partitioned when the latex sample is diluted in the equipment [67].

When the droplets of latex are diluted in water, the concentration of ions present in the aqueous phase will decrease, which leads to the rearrangement of the ions surrounding the particles, and this can have effects on the surfactant molecules attached to the particles. When using water as dispersant, the particles are destabilized and an increase in speed increases the volume density of the second family of particles.

The interesting point again is that there is no transition between the primary particles to the second family. This appears to agree to a certain degree with the results of Kroupa et al. [48] who observed that, while modeling the mechanism of coagulation observed, only a small number of small aggregates is formed and the fast process occurs when a large aggregate is formed. This large aggregate coagulates quickly with primary particles forming dendritic structures and maybe this process is so fast that it is not possible to be observed while performing the measurements on Mastersizer.

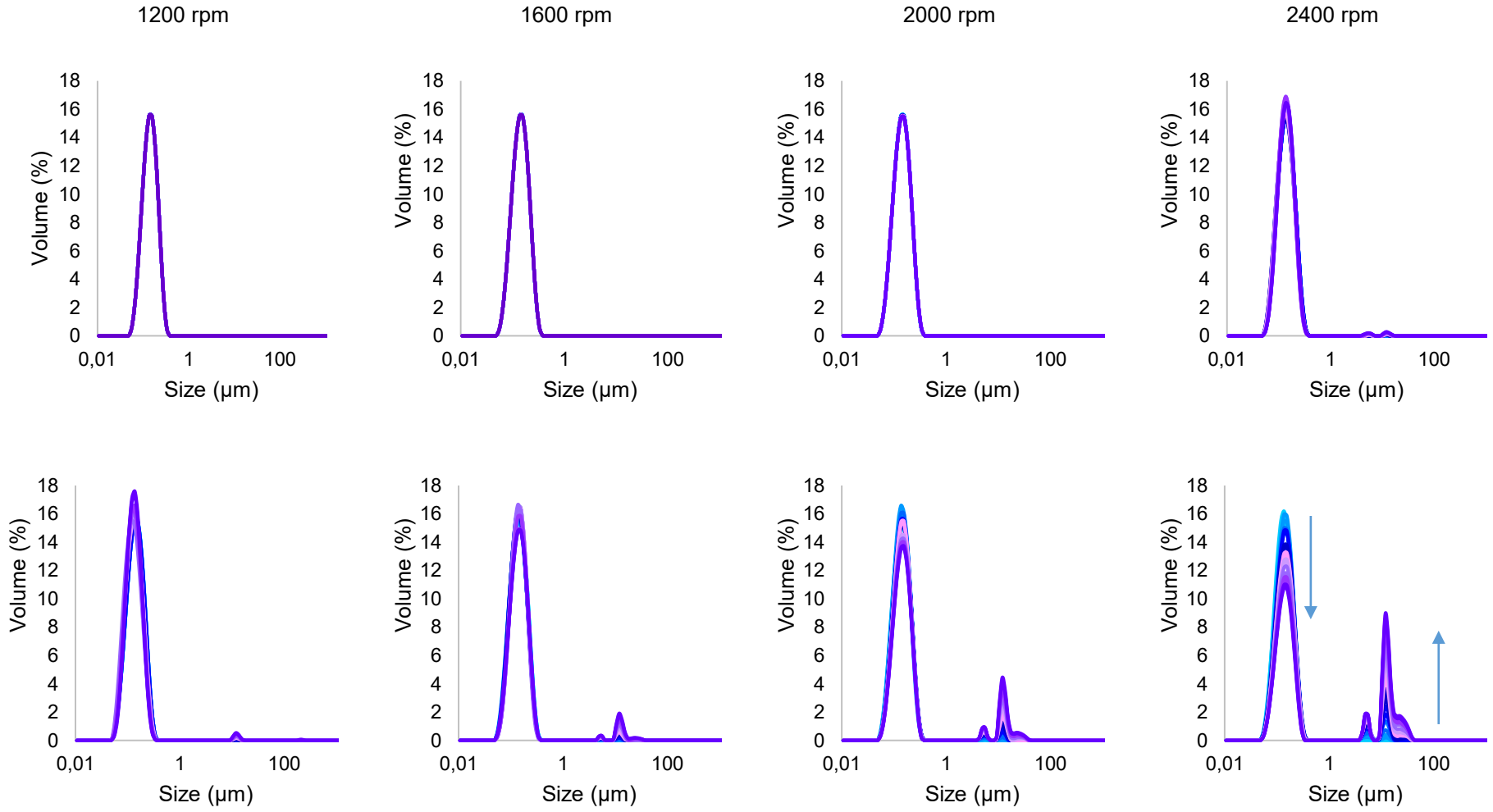

Figure 3.14 PSD evolution for different agitation speeds into the Mastersizer, when a latex with θ = 11 % is dispersed in salt solution (top) or in water (bottom). The time between each acquisition is around 23 s and the last measurement is performed 7 minutes and 20 s after the first one.

Analyzing the evolution of volume percentage for each family of particles (1st – original and 2nd - coagulum) in Figure 3.15 for the cases the latex was diluted in water, it is possible to see as expected that an increase in speed will start the coagulation of particles earlier and an increase in speed/shear will increase the aggregation rate [13].

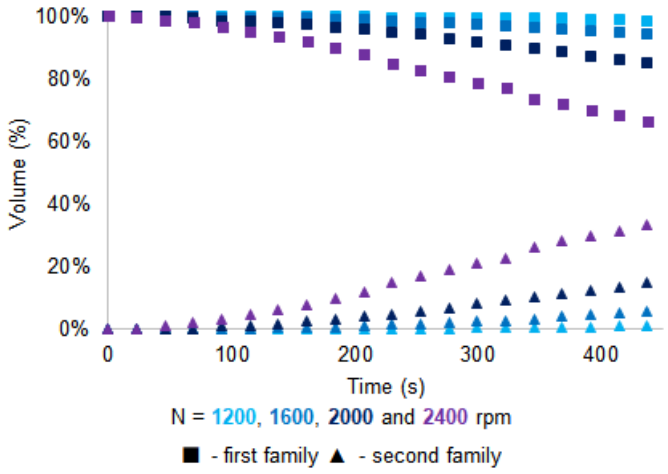

Figure 3.15 Volume of 1st and 2nd family of particle sizes as function of time for different speeds and a latex with θ = 11 % dispersed in water.

A similar behavior was observed when using a less stable latex, obtained from a reaction performed with half the concentration of surfactant. Coagulation was observed during the reaction and the free flowing latex with 262 nm was recovered, so, the surface coverage is estimated as less than 5 %. Figure 3.16 shows the results comparing a stable latex and an unstable latex. The same tendency of aggregation with speed is observed, but as the latex is less stable, when comparing to the latex with 11 % of surface coverage, it is possible to see that the volume percentage at the end of the experiments is higher for the less stable latex, which is in agreement with the theory.

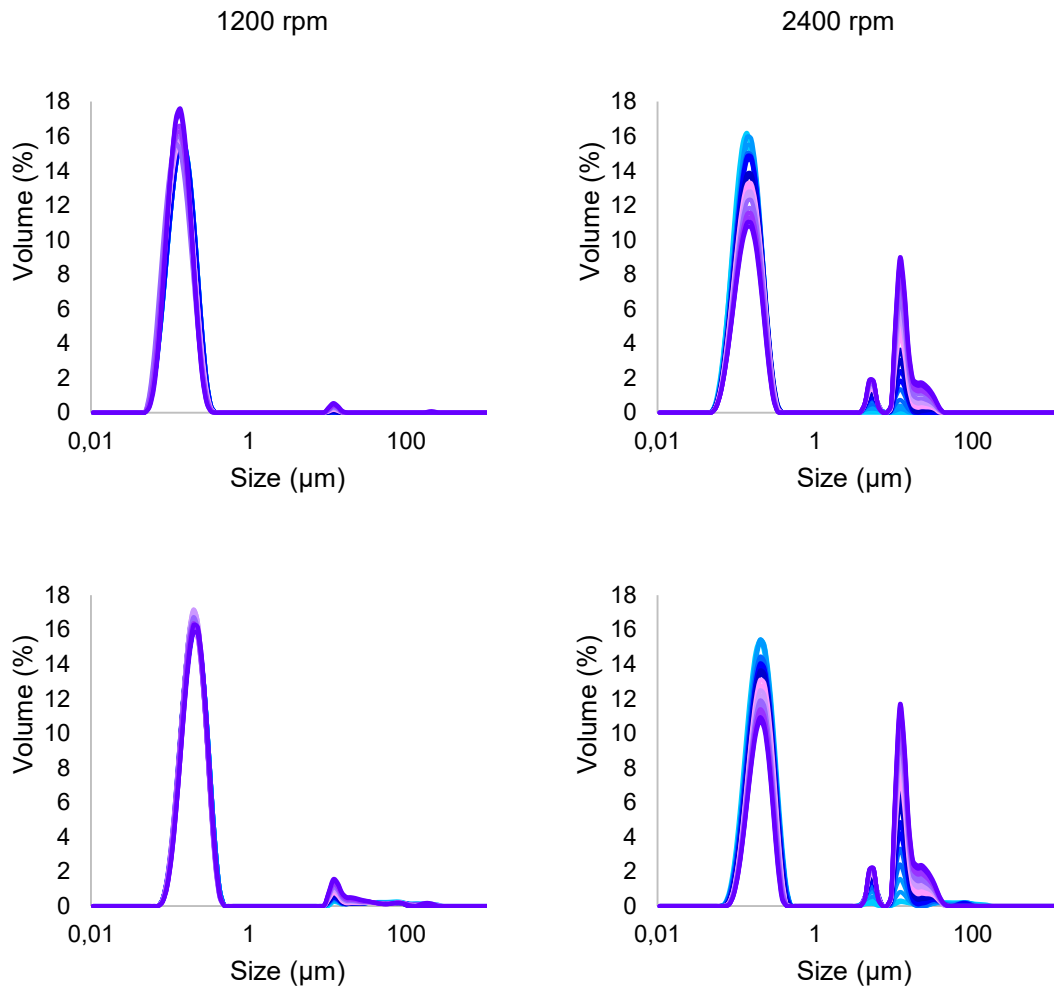

Figure 3.16 PSD evolution for different speeds in the Mastersizer when a latex with θ = 11 % (top) and a latex with θ = 4 % (bottom) are dispersed in water.

When comparing the evolution of volume percentage for each family of particles for the latexes with different stabilities diluted in water, as expected a less stable latex will produce more coagulum at the same time, and it looks like that the rate of disappearance/generation of particles slows down when the volume of primary particles is reduced to 66 %, as seen in Figure 3.17 b. This slowdown in the coagulation with the creation of big particles is reported in the literature [13], as the big particles are less prone to coagulation than small ones and that the coagulation is a mechanism found by the system to decrease the total particles area to recover the surface coverage enabling a new stability.

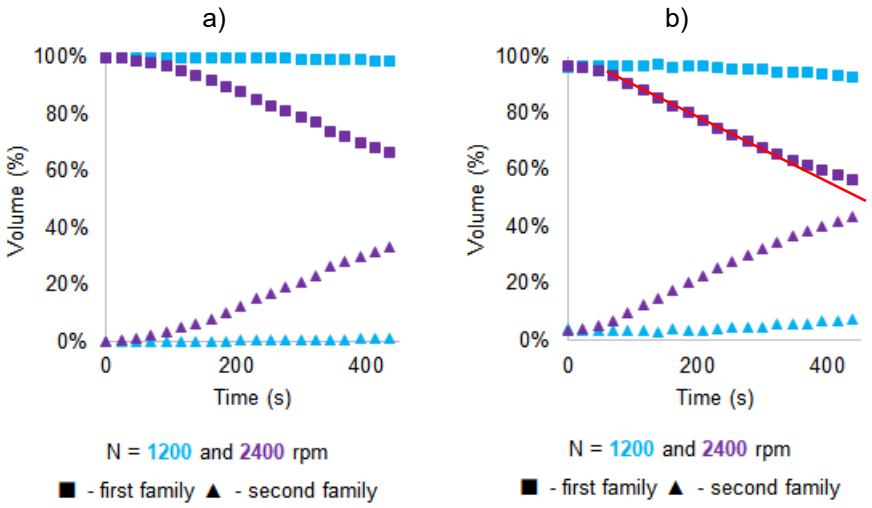

Figure 3.17 Volume of 1st and 2nd family of particle sizes as function of time for different speeds and a latex with a) θ = 11 % and b) θ = 4 % of surface coverage dispersed in water.

As the shear rate in the equipment is not uniform, it is interesting to know the range of values obtained during the experiments, considering the dispersion unit a stirred tank. The average shear rate in a stirred tank is calculated by [51],

$$\dot{\gamma}_{\mathrm{STR}} = \sqrt{\frac{\epsilon_{\mathrm{av}}}{\nu}} \qquad 3.11$$

where ν is the kinematic viscosity of the fluid and ϵ_{av} is the average energy dissipation rate calculated by [28],

$$\epsilon_{\mathrm{av}} = \frac{N_{\mathrm{P}} N^3 D^5}{v} \qquad 3.12$$

where N_{P} is the power number of the impeller, N is the impeller speed, D is the impeller diameter and v is the fluid volume in the tank. Considering the geometry of the dispersion unit that has a propeller with 3 blades (N_{P} = 0.9 [68]), D = 2x10^{-3} m and the volume of the container is equal to 1.2x10^{-4} m³.

As the agitation speed set for the analysis is between 1200 rpm and 2400 rpm, so the average shear rate in the dispersion container will be in the range of 460 to 1300 s^{-1} in agreement with the shear rate calculated by CFD from a model of the reactor developed by Ariafar et al. [65].

As there is a flux of fluid in the tube connecting the dispersion unit to the measurement cell, there will be also an average shear rate that can be calculated by [69],

$$\dot{\gamma}_{\text{tube}} = \frac{8Q}{3\pi r_{\text{tube}}^3} \quad 3.13$$

where Q is the volumetric flow in the pipe and r_{tube} is the pipe internal diameter. As the fluid velocity in the wall is zero, this is the point with the maximum shear rate, calculated by [69],

$$\dot{\gamma}_{\text{max,tube}} = \frac{4Q}{\pi r_{pipe}^3} \quad 3.14$$

According to the supplier of the Mastersizer, the flow rate in the tubes is proportional to the speed of agitation, as the impeller pumping the fluid to the cell is connected to the same axis as the propeller dispersing the sample. The maximum flow rate is 2 L/min when the speed is 3000 rpm and the pipe internal diameter is 2.4×10^{-3} m. Considering the lowest and the highest speed used for the tests, the average shear rate is in the range of 820 to 1640 s^{-1}, reaching the maximum value of 1230 s^{-1} at 1200 rpm and 2460 s^{-1} at 2400 rpm. From the values calculated, it is possible to conclude that the shearing during the coagulation in the Mastersizer is mainly caused in the tubes and it is higher than the values found from CFD simulations.

The Mastersizer also has an option of using ultrasound to break possible aggregates, and during some tests applying it for 40 seconds, it was possible to see the volume of the second peak of particles decreasing, and the volume of the first peak increasing again. Unfortunately, the curves of particle size distribution were not obtained, but the observed behavior indicates that the second family of particles is actually aggregates. The breakage of aggregates is also an explanation to the decrease of the shoulder related to big particles with the increase of shear rate when doing the experiments with the rheometer.

3.3.5 Salt-Induced Coagulation in the Turbifix

The use of turbidity measurements to estimate the stability of latex was already performed in a previous work of the group [16]. In this work, a new set-up is used that is better adapted for online measurements, the Turbifix. The device allows predicting the change in the particle size based in the multiple light scattering, by reading the transmission and backscattering values of the sample at a fixed height. Figure 3.18 shows the representation of the experiment in which a jacketed glass reactor agitated by an anchor impeller is used as a latex container. The latex is taken from the container by a peristaltic pump and sent to the measurement cell that is completely filled with the latex. So, at the same time there is a flux of latex going back to the container.

The glass container is filled with 300 mL of latex. The agitation is kept at 50 rpm and the peristaltic pump flow rate is fixed at 50 mL/min. The total volume of the inlet tube and the glass cell is 40 mL. Based on the pump flow rate, it takes around 4 minutes to renew the material in the cell. A volume of 75 µL of coagulating agent is added every 10 minutes to the latex in the glass reactor, and we monitor the kinetics by the change in backscattering. The used high pumping rate avoids the delay between the start of the induced coagulation and the measurement with TurbiFix.

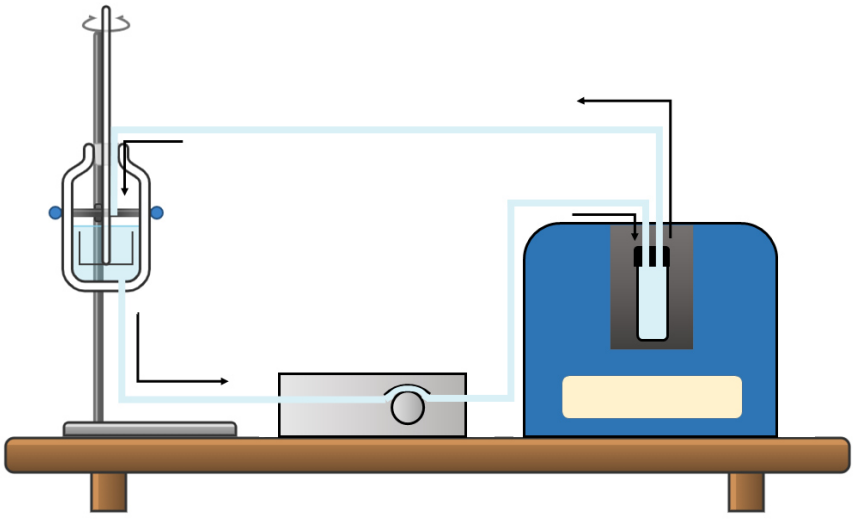

Figure 3.18 Schematic representation of the experiment by turbidity (Turbifix).

Some trials were performed with a 20 wt% solids content latex at the heights of 25 and 12 mm, with a period of 0.1 s (default parameter of the software). The changes on the

backscattering were not enough to detect the coagulation starting point. However, when the same latex was analyzed using the laser diffraction technique, it was possible to see two families of particles with different sizes (200 nm and >1 µm).

The first guess was the height chosen to perform the measurements that might not be adapted to detect the appearance of coagulation. Indeed, a test was done by making a scan of the entire height of the sample. It was possible to notice that the backscattering changes in the heights from 2 to 7 mm when coagulation occurs, as showed in the Figure 3.19. Unfortunately, the changes in the backscattering even at 5 mm were not enough to predict the changes in the particle size while analyzing the data.

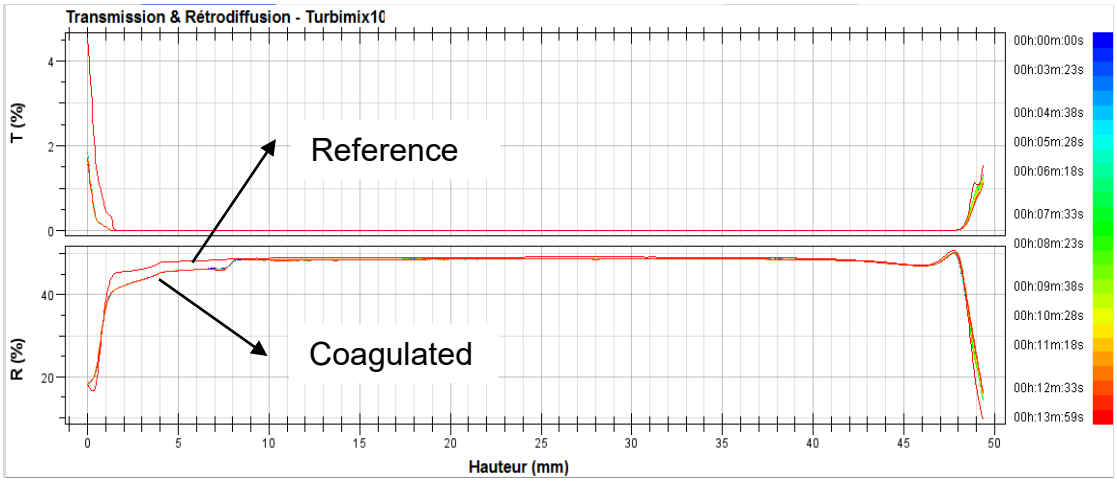

Figure 3.19 Transmission and Backscattering signals for reference and coagulated sample in the Turbifix.

Samples were taken at the start, after each salt solution (0.42 M) addition and at the end from the liquid and the foamy material present in the container, and analyzed by laser diffraction to check the particle size distribution. In Figure 3.20 the same behavior as the coagulation in the Mastersizer is observed, but with a broadening of the second family of particle sizes. Each curve is an average of 5 measurements. So, it takes less than 2 minutes to perform the measurements in the Mastersizer.

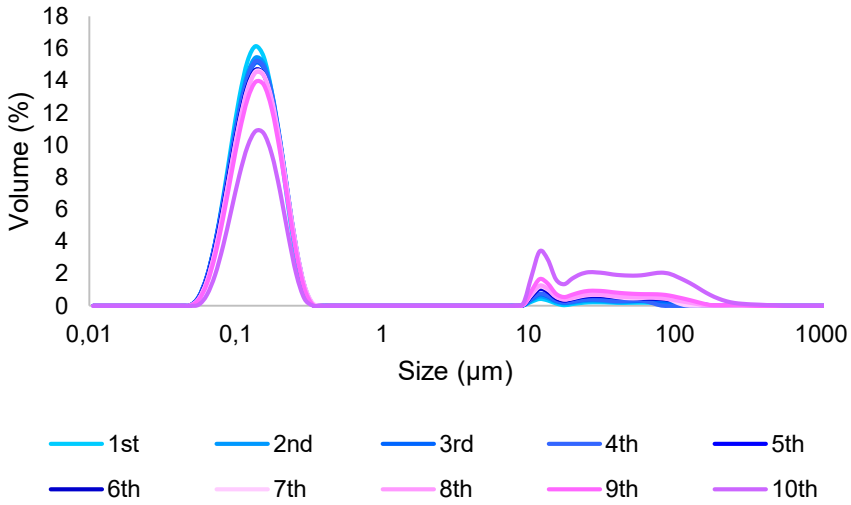

Figure 3.20 Particle size distribution after each addition of salt solution at 0.42 M in the Turbifix (10 injections of 75 µL of salt solution were realized).

Figure 3.21 shows the particle size distribution of the latex before the addition of salt solution and from the two materials found at the end, the liquid phase and the foamy material above the liquid.

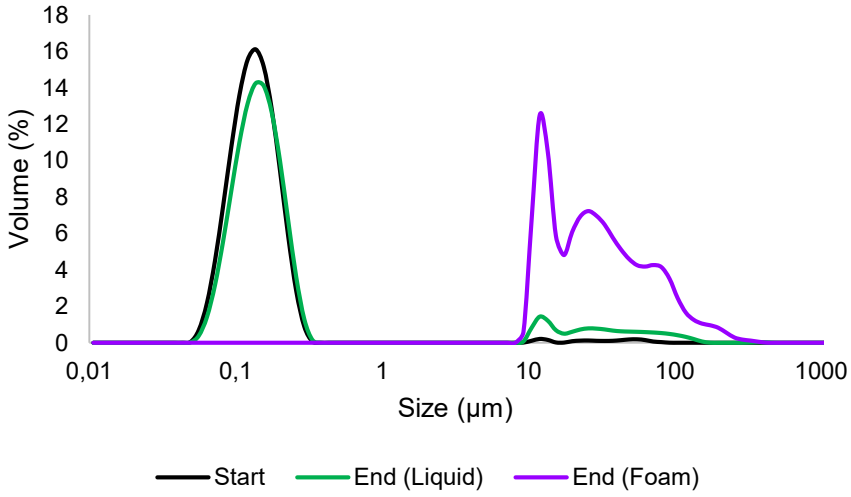

Figure 3.21 Particle size distribution at the start and at the end of the salt induced coagulation in the Turbifix.

It is observed that the particle size distribution at the end is similar to the one after the last addition of salt, so there is no difference between the liquid in the glass container and the measurement cell. But, the foamy material is completely coagulated with a

broad distribution ranging from 10 to 250 μm. As the foamy material has a lower density than the latex, probably this material is not going to the turbidity measurement cell.

3.4 Conclusions

As pointed in the literature, the low surface coverage is one of the causes of coagulation [19,31,34,52], but it can be observed that some of the reactions, even with an estimated surface coverage about 10% (for the free flowing latex) produced some coagulum and deposited material. As the creation of big particles reduced the total area to be covered by the surfactant, maybe some surfactant is released during the coagulation and it will migrate to the small particles to recover an equilibrium in surface coverage.

The effect of the surface coverage was confirmed with the coagulation performed in the Mastersizer, showing that lower the surface coverage, more coagulum is produced for the same time and agitation speed. In the case of reactions, even if some deposited material was obtained with the reactions performed with 3.00 g/L of surfactant and final solids of 48 wt%, the amount was 3 times lower than the one collected from a reaction performed with 0.75 g/L and 35 wt% of solids.

As expected, the increase in ionic strength increases the coagulation and when trying to monitor the coagulation kinetics by turbidity, it was observed that the big aggregates with no signal of original particles where floating in the latex. So, probably the coagulation observed as a foamy material is an aggregation, because the polymer density is higher than water, and big particles of polymer will go down. The hypothesis of aggregates was reinforced while observing the increase of the volume of primary particles at the same time the second peak was decreasing while using ultrasound in the Mastersizer.

The effect of shearing in the coagulation was observed by the experiments performed in the reactor, in the mastersizer and in the rheometer. An increase of shearing or time leads to an increase of the coagulation as observed by many authors in the literature [13,19,50,52,53,56,61]. And specially for the tests with the rheometer, the explosion in

viscosity was observed in agreement with some results from literature [13,43–45] stating that there is an induction time to start the coagulation.

The tests with the rheometer showed also the influence of the solids content on the coagulation, in which the increase of solids starts earlier the process of coagulation and its extension for the same shearing, but the orthokinetic coagulation in the rheometer also led to some intriguing results. Shear rates of 175 s^{-1} and 300 s^{-1} in the rheometer, were enough to complete coagulate the first family of particles, and considering the work of Aryafar et al. with the same reactor we use at the laboratory, normally we work with shear rates higher than these (0 to 1000 s^{-1}).

The use of the Mastersizer to monitor the coagulation showed the effect of the diluent used to analyze the particle size distribution. The dilution of latex in a liquid that is not similar to the one the particles are surrounded in the latex, leads to a destabilization. These experiments also showed the increase in the coagulation rate with shearing in agreement with Oles [13] and a slowdown of the coagulation rate as expected because once the big particles are formed, they coagulate slower than the small particles and the system tries to move to a new equilibrium.

No matter the destabilization mechanism of the latex, the second family of particles is detected always in the range of 5 to 300 μm, as already noted in the previous work of the group [62], and there is no intermediate size between the original particles and the aggregates which seems to be in agreement with the literature that the coagulation happens faster when a large aggregate is formed, and it will coagulate quickly with primary particles [48].

NOTATION

A	Hamaker constant
d	Distance between particles, m
D	Impeller diameter, m
e	Elementary charge, 1.6x10^{-19} C
k_{B}	Boltzmann constant, 1.38x10^{-23} m²kg/s²K
k_{c}	Coagulation rate
M	Molar concentration, mol/m³
n	Number concentration of particles, particles/m³
N	Agitation speed, tr/s
N_{A}	Avogadro's number, 6.02x10^{23} mol^{-1}
N_{P}	Impeller power number
Q	Volumetric flow, m³/s
r	Particle radius, m
t	Time, s
T	Temperature, K
v	Volume in the tank, m³
V	Total interaction potential, J
V_{A}	Attractive potential, J
V_{R}	Repulsive potential, J
W	Stability ratio
z_{i}	Valence of an ion

Greek

α	Collision efficiency
β	Collision frequency
$\dot{\gamma}$	Shear rate, s^{-1}
ε_0	Permittivity of free space, F/m
ε_r	Relative permittivity
κ	Debye-Hückel parameter, 1/m

μ	Dynamic viscosity, Pa.s
ν	Kinematic viscosity, m²/s
ϕ	Volume fraction
ψ_0	Surface potential, V

REFERENCES

[1] McNaught AD, Wilkinson A, editors. IUPAC. Compendium of Chemical Terminology. 2nd ed. Oxford: Blackwell Scientific Publications; 1997.

[2] Theodoor J, Overbeek G. Strong and weak points in the interpretation of colloid stability. Adv Colloid Interface Sci 1982;16:17–30. doi:10.1016/0001-8686(82)85003-3.

[3] Chhabra R, Basavaraj MG, editors. Colloidal Dispersions. Coulson Richardson's Chem. Eng., vol. 2a. Sixth, Butterworth-Heinemann; 2019, p. 693–737. doi:10.1016/B978-0-08-101098-3.00014-7.

[4] Gilbert RG. Emulsion Polymerization. A Mechanistic Approach. London: Academic Press Limited; 1995.

[5] Hidalgo-Alvarez R, Martín A, Fernandez A, Bastos D, Martinez F, de las Nieves FJ. Electrokinetic properties, colloidal stability and aggregation kinetics of polymer colloids. Adv Colloid Interface Sci 1996;67:1–118. doi:10.1007/978-3-319-18041-0_5.

[6] Overbeek JTG. Recent Developments in the Understanding of Colloid Stability. J Colloid Interface Sci 1977;58:408–22. doi:10.1016/0021-9797(77)90151-5.

[7] Elimelech M, Gregory J, Jia X, Williams RA. Particle Deposition and Aggregation. Measurement, Modelling and Simulation. Elsevier; 1995. doi:10.1016/b978-0-7506-0743-8.50007-8.

[8] Lachin K, Le Sauze N, Di Miceli Raimondi N, Aubin J, Cabassud M, Gourdon C. Estimation of characteristic coagulation time based on Brownian coagulation theory and stability ratio modeling using electrokinetic measurements. Chem Eng J 2019;369:818–27. doi:10.1016/j.cej.2019.03.130.

[9] Ohshima H. Interaction of colloidal particles. Elsevier B.V.; 2014. doi:10.1016/B978-0-444-62614-1.00001-6.

[10] Verwey EJW. Theory of the stability of lyophobic colloids. J Phys Colloid Chem 1947;51:631–6. doi:10.1021/j150453a001.

[11] Kramer TA. Analytical solutions for bikinetic coagulation: Incorporation of a maximum size class. J Colloid Interface Sci 2000;227:16–23. doi:10.1006/jcis.2000.6831.

[12] Fuchs VN. Über die Stabilität und Aufladung der Aerosole. Z Phys 1934;89:736–43.

[13] Oles V. Shear-Induced Aggregation and Breakup of Polystyrene Latex Particles. J Colloid Interface Sci 1992;154:351–8. doi:10.1016/0021-9797(92)90149-G.

[14] Urbina-Villalba G, Lozsán A, Rahn K, Romero-Cano MS. Calculation of the stability ratio of suspensions using Emulsion Stability Simulations. Comput Phys Commun 2009;180:2129–39. doi:10.1016/j.cpc.2009.06.023.

[15] Kostansek E. Controlled Coagulation of Emulsion Polymers. J Coatings Technol Res 2004;1:41–4. doi:10.1007/s11998-004-0023-1.

[16] Méndez-Ecoscia AC, Prates-Pereira AF, Fonseca-Marques MB, Sheibat-Othman N, McKenna TFL. A New Methodology for Measuring the Stability of Emulsion Polymer Particles. Macromol Symp 2016;360:142–51. doi:10.1002/masy.201500097.

[17] Hsu JP, Kuo YC. The Critical Coagulation Concentration of Counterions: Spherical Particles in Asymmetric Electrolyte Solutions. J Colloid Interface Sci 1997;185:530–7. doi:10.1006/jcis.1996.4591.

[18] Hsu JP, Liu BT. Effect of Particle Size on Critical Coagulation Concentration. J Colloid Interface Sci 1998;198:186–9. doi:10.1006/jcis.1997.5275.

[19] Lowry V, El-Aasser MS, Vanderhoff JW, Klein A. Mechanical Coagulation in Emulsion Polymerizations. J Appl Polym Sci 1984;29:3925–35.

[20] Lowry V, El-Aasser MS, Vanderhoff JW, Klein A, Silebi CA. Kinetics of Agitation-Induced Coagulation of High-Solid Latexes. J Colloid Interface Sci 1986;112:521–9. doi:10.1016/0021-9797(86)90121-9.

[21] Aryafar S, Sheibat-Othman N, McKenna TFL. Coupling of CFD Simulations and Population Balance Modeling to Predict Brownian Coagulation in an Emulsion Polymerization Reactor. Macromol React Eng 2017;11:1–17. doi:10.1002/mren.201600054.

[22] Krapivsky PL, Connaughton C. Driven Brownian coagulation of polymers. J Chem Phys 2012;136:1–14. doi:10.1063/1.4718833.

[23] Adachi Y. Dynamic aspects of coagulation and flocculation. Adv Colloid Interface Sci 1995;56:1–31.

[24] Sheng-Hua X, Zhi-Wei S, Xu L, Wang JT. Coupling effect of Brownian motion and laminar shear flow on colloid coagulation: A Brownian dynamics simulation study. Chinese Phys B 2012;21:1–8. doi:10.1088/1674-1056/21/5/054702.

[25] Meyer CJ, Deglon DA. Particle collision modeling - A review. Miner Eng 2011;24:719–30. doi:10.1016/j.mineng.2011.03.015.

[26] Gambinossi F, Mylon SE, Ferri JK. Aggregation kinetics and colloidal stability of functionalized nanoparticles. Adv Colloid Interface Sci 2015;222:332–49. doi:10.1016/j.cis.2014.07.015.

[27] Cheng D, Ariafar S, Sheibat-Othman N, Pohn J, McKenna TFL. Particle Coagulation of Emulsion Polymers: A Review of Experimental and Modelling Studies. Polym Rev 2018;58:717–59. doi:10.1080/15583724.2017.1405979.

[28] Kemmere MF, Meuldijk J, Drinkenburg AAH, German AL. Aspects of coagulation during emulsion polymerization of styrene and vinyl acetate. J Appl Polym Sci 1998;69:2409–21. doi:10.1002/(SICI)1097-4628(19980919)69:12<2409::AID-APP12>3.0.CO;2-S.

[29] Mayer MJJ, Meuldijk J, Thoenes D. Dynamic Modeling of Limited Particle Coagulation in Emulsion Polymerization. J Appl Polym Sci 1996;59:83–90.

[30] Sajjadi S. Particle formation and coagulation in the seeded semibatch emulsion polymerization of butyl acrylate. J Polym Sci Part A Polym Chem 2000;38:3612–30. doi:10.1002/1099-0518(20001001)38:19<3612::AID-POLA170>3.0.CO;2-3.

[31] Liu B, Zhang M, Zhou C, Ren L, Cheng H, Ao Y, et al. Synthesis of monodisperse, large scale and high solid content latexes of poly(n-butyl acrylate) by a one-step batch emulsion polymerization. Colloid Polym Sci 2013;291:2385–98. doi:10.1007/s00396-013-2987-9.

[32] Boutti S, Graillat C, McKenna TF. High solids content emulsion polymerisation without intermediate seeds. Part I. Concentrated monomodal latices. Polymer

(Guildf) 2005;46:1189–210. doi:10.1016/j.polymer.2004.11.042.

[33] Šňupárek J, Tuťálková A. Particle coagulation at semicontinuous emulsion polymerization. II. Characterization of surface groups. J Appl Polym Sci 1979;24:915–21. doi:10.1002/app.1979.070240404.

[34] Chern C, Kuo YN. Shear-induced coagulation kinetics of semibatch seeded emulsion polymerization. Chem Eng Sci 1996;51:1079–87. doi:10.1016/0009-2509(95)00349-5.

[35] Fortuny M, Graillat C, McKenna TF. Coagulation of Anionically Stabilized Polymer Particles. Ind Eng Chem Res 2004;43:7210–9. doi:10.1021/ie0342917.

[36] Liu B, Wang Y, Zhang M, Zhang H. Initiator Systems Effect on Particle Coagulation and Particle Size Distribution in One-Step Emulsion Polymerization of Styrene. Polymers (Basel) 2016;8:1–14. doi:10.3390/polym8020055.

[37] Boutti S, Graillat C, McKenna TF. High solids content emulsion polymerisation without intermediate seeds. Part II. In situ generation of bimodal latices. Polymer (Guildf) 2005;46:1211–22. doi:10.1016/j.polymer.2004.11.044.

[38] Liu B, Jiang F, Chen J, Han Y, Bai Y, Zhang M. Aqueous phase properties on governing particle coagulation and mechanism nucleation in one-step emulsion polymerization of styrene. J Macromol Sci Part A Pure Appl Chem 2020;57:181–8. doi:10.1080/10601325.2019.1680254.

[39] Ito F, Makino K, Ohshima H, Terada H, Omi S. Salt effects on controlled coagulation in emulsion polymerization. Colloids Surfaces A Physicochem Eng Asp 2004;233:171–9. doi:10.1016/j.colsurfa.2003.11.012.

[40] Melis S, Kemmere M, Meuldijk J, Storti G, Morbidelli M. A model for the coagulation of polyvinyl acetate particles in emulsion. Chem Eng Sci 2000;55:3101–11. doi:10.1016/S0009-2509(99)00594-1.

[41] Matejicek A, Pivonkova A, Kaska J, Ditl P, Formanek L. Influence of Agitation on the Creation of Coagulum during the Emulsion Polymerization of the System Styrene-Butylacrylate- Acrylic Acid. J Appl Polym Sci 1988;35:583–91.

[42] van de Ven TGM, Mason SG. The Microrheology of Colloidal Dispersions. IV. Pairs of Interacting Spheres in Shear Flow. J Colloid Interface Sci 1976;57:505–

16. doi:10.1016/0021-9797(76)90229-0.

[43] Guery J, Bertrand E, Rouzeau C, Levitz P, Weitz DA, Bibette J. Irreversible shear-activated aggregation in non-brownian suspensions. Phys Rev Lett 2006;96:11–4. doi:10.1103/PhysRevLett.96.198301.

[44] Zaccone A, Wu H, Gentili D, Morbidelli M. Theory of activated-rate processes under shear with application to shear-induced aggregation of colloids. Phys Rev E - Stat Nonlinear, Soft Matter Phys 2009;80:1–8. doi:10.1103/PhysRevE.80.051404.

[45] Zaccone A, Gentili D, Wu H, Morbidelli M. Shear-induced reaction-limited aggregation kinetics of Brownian particles at arbitrary concentrations. J Chem Phys 2010;132:1–6. doi:10.1063/1.3361665.

[46] Zubitur M, Asua JM. Factors affecting kinetics and coagulum formation during the emulsion copolymerization of styrene/butyl acrylate. Polymer (Guildf) 2001;42:5979–85. doi:10.1016/S0032-3861(01)00039-8.

[47] Spicer PT, Keller W, Pratsinis SE. The Effect of Impeller Type on Floc Size and Structure during Shear-Induced Flocculation. J Colloid Interface Sci 1996;184:112–22. doi:10.1006/jcis.1996.0601.

[48] Kroupa M, Vonka M, Kosek J. Modeling the Mechanism of Coagulum Formation in Dispersions. Langmuir 2014;30:2693–702. doi:10.1021/la500101x.

[49] Flesch JC, Spicer PT, Pratsinis SE. Laminar and Turbulent Shear-Induced Flocculation of Fractal Aggregates. AIChE J 1999;45:1114–24. doi:10.1002/aic.690450518.

[50] Selomulya C, Amal R, Bushell G, Waite TD. Evidence of Shear Rate Dependence on Restructuring and Breakup of Latex Aggregates. J Colloid Interface Sci 2001;236:67–77. doi:10.1006/jcis.2000.7372.

[51] Selomulya C, Bushell G, Amal R, Waite TD. Aggregation Mechanisms of Latex of Different Particle Sizes in a Controlled Shear Environment. Langmuir 2002;18:1974–84. doi:10.1021/la010702h.

[52] Chern CS, Chen YC. Stability of the polymerizable surfactant stabilized latex particles during semibatch emulsion polymerization. Colloid Polym Sci

1997;275:124–30. doi:10.1007/s003960050061.

[53] Kusters KA, Wijers JG, Thoenes D. Aggregation kinetics of small particles in agitated vessels. Chem Eng Sci 1997;52:107–21. doi:10.1016/S0009-2509(96)00375-2.

[54] Kemmere MF, Meuldijk J, Drinkenburg AAH, German AL. Colloidal Stability of High-Solids Polystyrene and Polyvinyl Acetate Latices. J Appl Polym Sci 1999;74:1780–91.

[55] Hanus LH, Hartzler RU, Wagner NJ. Electrolyte-Induced Aggregation of Acrylic Latex. 1. Dilute Particle Concentrations. Langmuir 2001;17:3136–47. doi:10.1021/la000927c.

[56] Ito F, Ma G, Nagai M, Omi S. Study of particle growth by seeded emulsion polymerization accompanied by electrostatic coagulation. Colloids Surfaces A Physicochem Eng Asp 2002;201:131–42. doi:10.1016/S0927-7757(01)01030-5.

[57] Pourmehr M, Navarchian AH. Batch Emulsion Polymerization of Vinyl Chloride: Application of Experimental Design to Investigate the Effects of Operating Variables on Particle Size and Particle Size Distribution Mahdi. J Appl Polym Sci 2009;111:338–47. doi:10.1002/app.

[58] Fukasawa T, Adachi Y. Direct observation on the Brownian coagulation of PSL particles through optical microscope in the regime near critical coagulation concentration (CCC). J Colloid Interface Sci 2010;344:343–7. doi:10.1016/j.jcis.2009.12.066.

[59] Liu B, Zhang M, Yu G, Chen D, Zhang H. Effect of aqueous phase composition on particle coagulation behavior in batch emulsion polymerization of styrene. Colloids Surfaces A Physicochem Eng Asp 2014;452:159–64. doi:10.1016/j.colsurfa.2014.03.100.

[60] Sugimoto T, Kobayashi M, Adachi Y. The effect of double layer repulsion on the rate of turbulent and Brownian aggregation: Experimental consideration. Colloids Surfaces A Physicochem Eng Asp 2014;443:418–24. doi:10.1016/j.colsurfa.2013.12.002.

[61] Oktaviani O, Adachi Y. Determination of the Rate of Salt-Induced Rapid

Coagulation of Polystyrene Latex Particles in Turbulent Flow Using Small Stirred Vessel. Colloids and Interfaces 2018;3:5. doi:10.3390/colloids3010005.

[62] Méndez Ecoscia AC. Experimental Study of Emulsion Polymerization of Vinylidene Fluoride. University of Lyon, 2016.

[63] Piirma I, Chen SR. Adsorption of ionic surfactants on latex particles. J Colloid Interface Sci 1980;74:90–102. doi:10.1016/0021-9797(80)90173-3.

[64] Alooghareh MH, Kabipour A, Ghazavi M, Mohammad Mousavi Sisakht S, Razavifar M. Effects of different gases on the performance of foams stabilized by Cocamidopropyl betaine surfactant and silica nanoparticles: A comparative experimental study. Petroleum 2021. doi:10.1016/j.petlm.2021.09.002.

[65] Ariafar S. Scale-up of Emulsion Polymerization Process: Impact of changing characteristic times. Université Claude Bernard Lyon 1, 2016.

[66] Longworth-Cook S. Laser Diffraction: my top Q&A 2019. https://www.materials-talks.com/blog/2016/08/09/laser-diffraction-my-top-questions-answered/ (accessed March 7, 2020).

[67] Davis CR, Martinez CJ, Howarter JA, Erk KA. Impact of Saltwater Environments on the Coalescence of Oil-in-Water Emulsions Stabilized by an Anionic Surfactant. ACS ES&T Water 2021;1:1702–13. doi:10.1021/acsestwater.1c00066.

[68] Hall S. Blending and Agitation. Branan's Rules Thumb Chem. Eng. 5th ed., Butterworth-Heinemann; 2012, p. 257–79. doi:10.1016/b978-0-12-387785-7.00016-5.

[69] Lovell PA. Dilute Solution Viscometry. In: Allen G, Bevington JC, editors. Compr. Polym. Sci. Suppl., Pergamon; 1989, p. 173–97. doi:10.1016/b978-0-08-096701-1.00009-4.

CHAPTER 4. FOULING

4.1 Introduction

Based on estimations performed in 2020, the market demand of plastics in 2021 was evaluated at approximately 320 million tonnes [1], of which close to 20% (or 60 million tonnes) were made using a dispersed phase free radical polymerization process (i.e. emulsion and suspension) [2]. These materials are produced in the form of particles on the order of 10^2 nm for emulsion polymers, or 10^2 micrometers for suspension products. These particles must be sufficiently stabilized, or they will coagulate to form undesirable lumps in the final product, or be deposited on the reactor wall and internal equipment such as agitators or baffles in the form of lumps or films. Obviously this last situation is to be avoided as it can lead to problems of product quality, as well as to a reduction in the heat removal capacity of the reactors.

For the purposes of this thesis, we will define fouling as the deposition of material that cannot be removed by rinsing or flushing procedures, located on surfaces inside a reactor, and in particular on the reactor wall and other heat exchange surfaces, baffles, agitators, feed tubes and other internal equipment. Issues related to the mechanism and modelling of coagulation have been extensively addressed in the past [3–5], but there appears to be less discussion of the mechanisms behind fouling in these systems. Furthermore, coagulation and fouling are clearly problematic in a wide number of process unit operations; however, we will limit our discussion to fouling in the narrower case of free radical polymerization in aqueous media.

In this context, reactor fouling can lead to any number of problems. Fouling on the agitator and/or baffles can cause reductions of mixing efficiency. This can cause the poor distribution of reactive components and, thus poor control of product quality. Furthermore, a reduction in the linear speed of the reactor contents can lead to the reduction of the overall heat transfer coefficient, even in the absence of wall fouling. Wall fouling will automatically lead to a slight increase in the resistance to heat transfer through the reactor wall. Given that the systems of interest are exothermic, anything that leads to a reduction in heat transfer capacity can force one to reduce the polymerization rate at best, and at worst cause a loss of temperature control in the reactor. This in turn can lead to quality problems, or safety problems such as thermal runaway [6,7].

Detection and estimation of fouling is strategically important to generate appropriate compensating actions to ensure that the polymerization will proceed in the desired way [6]. Depending on the extent of fouling, several layers can be formed, leading to a complete clogging of confined areas or tubes, used for instance to exist a flux of fluid. This may require to shut down the plant to remove the deposited films using high pressure water jet or solvents, which generates a lot of waste and new costs.

4.2 Literature Review

4.2.1 Phenomena related to fouling

During polymerization in dispersed media, the deposition of material can be due to direct attachment of polymer particles or coagula on the surfaces, and/or by adsorption of water soluble polymer and oligomers to the internal surfaces [8]. Henry et al. [9] indicated that the polymer particles can have two types of interactions in dispersed media: particle-particle interactions (causing their agglomeration) and particle-surface interactions (i.e. with the surface of the polymerization reactor or processing equipment) (see Figure 4.1). One may also add the phenomenon of formation of skin of polymer at the water air interface that is frequently observed in dispersed media, especially around the agitator or reactor wall [8]. These interactions are present in colloidal systems, such as emulsion or suspension polymerizations. They depend on several conditions such as the colloidal stability of the dispersion, the flow patterns in the equipment and the solids content. Based on this, the authors summarized the different phenomena related to the particulate fouling: deposition, re-entrainment and clogging.

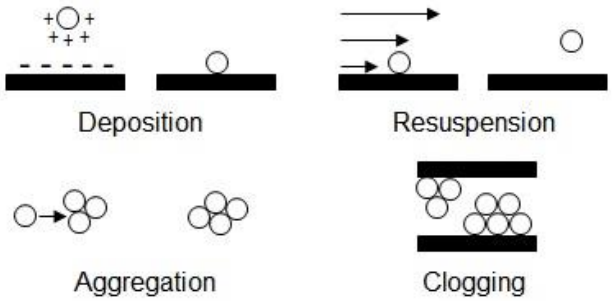

Figure 4.1 The four elementary phenomena of fouling. Adapted from [5].

The deposition of particles is governed by the physicochemical properties of the particles and the surfaces, as well as the hydrodynamic conditions of the system [10]. It consists of the transport of the particles by fluid motion from the bulk to the internal surface of an equipment, and their attachment to the material [11]. Re-entrainment of particles may occur, by resuspension of the deposited particles in the fluid. As the particles get deposited on the surface, they may act as seed for forward material accumulation. Usually, this film cannot be removed by ordinary flushing procedures. The accumulation of several layers of particles may cause clogging, (i.e. the complete blockage of a cross section), which represents the most troublesome stage of fouling.

When a particle from a colloidal system is close enough to a surface, an attractive potential is generated between the particle and the surface, due to the van der Waals force. An attractive potential can also be generated when the particles and the surface have opposite charges, for instance an electrostatic force. In both cases, the resulting attraction will generate a flux of particles toward the surface and consequently a concentration gradient with some consequences in the medium. However, the presence of particles at the surface may on the contrary avoid further deposition. Indeed, van de Ven [12] mentioned the blocking process, in which a particle free in the medium moving towards an already attached particle will move away from the surface.

As discussed above, fouling, which is caused by the interaction between the particles and the surface of the equipment, is to be distinguished from particle agglomeration / aggregation, which is caused by the particle-particle interaction. Particle aggregation, and the possible formation of coagulum, depend on the stability of the particles (i.e. the surface coverage by an emulsifier, softness of the polymer) and the frequency of collision between particles (which depends on the hydrodynamics, temperature, viscosity, concentration of particles). So, they are favored in a colloidal system that has

a low surface coverage, under high electrolyte concentration or when the particle concentration is high [10]. However, these phenomena are related, and an enhanced particle stability may reduce both of them [13]. However, the coagulation of particles will not necessarily lead to fouling, nor will avoiding coagulation by ensuring the stability of particles prevent fouling.

The conditions of the surfaces of the equipment also play an important role during fouling, as the roughness and presence of imperfections can contribute to fixing the polymer particles or radicals containing oligomeric species [10], and also the surface charge of the metal plays its role in fouling of charged particles [8]. Glass-lined reactors are less prone to fouling because of their low average roughness, that is the average absolute deviation from a mean line of a material surface in a sample length [14], of 0.03 μm [15], while that of stainless steel is in the range of 0.40 to 6.00 μm for a bored/turned surface finish and 0.10 to 0.80 for an electropolished one [16]. But, not all the reaction operational conditions enable the use of glass.

Other the factors affecting the fouling of organic fluids were pointed by Watkinson [17] as the temperature of the surface and the bulk, variations in composition and the presence of branching in the deposits, the metal as part of the surface or present as a dissolved ion, the flow velocity and the flow channel geometry.

In the presence of reaction, the fouling process involves the possible steps presented in Figure 4.2. The reaction can occur in the bulk phase or in the boundary layer, generating the precursor that will be found attached to the wall. As mentioned before, transport phenomena are involved, but another important aspect to be investigated is whether the fouling is initially formed in the bulk, in the boundary layer or on the surface.

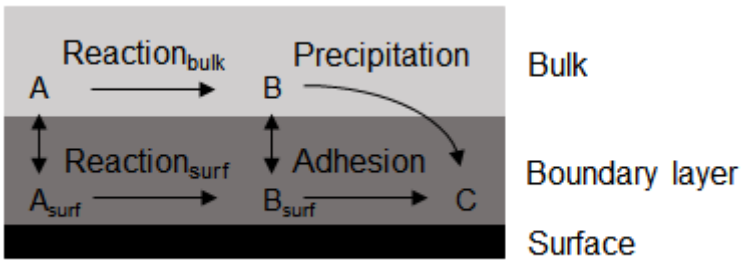

Figure 4.2 Chemical reaction fouling mechanism. Adapted from [12].

Despite this difficulty, to avoid the fouling problem, it is necessary to identify of its precursors and the kinetics of their formation. Investigation of the physicochemical or process parameters influencing the fouling, two types of studies were conducted in the literature, either with or without the reaction.

4.2.2 Fouling in the absence of reaction

Very useful information can be obtained regarding the ability of a latex or equipment for fouling in the absence of reaction. Such studies can help to isolate the phenomena by avoiding simultaneous changes in the media related to the reaction, such as the increase of the viscosity and the solids content. A wide range of temperatures, concentrations, viscosities, mixing rate and surfaces can be covered and their effects evaluated under comparable conditions.

As previously discussed, one of the factors influencing the fouling is the surface of the equipment that will be in contact with the particles. Its influence can be studied using a piece of the material used to build the equipment, and putting it in contact with the polymer under controlled conditions [8,18–20].

Urrutia et al. [8] presented one of the few works dedicated to fouling in emulsion polymerization. They studied latexes synthesized by emulsion copolymerization of butyl acrylate (BA) and methyl methacrylate (MMA) (50 / 50), with different stabilities using a mixture of ionic and nonionic surfactants, at 50 wt% solids content. They used Hastalloy 316 stainless steel as substrate, measured the fouling gravimetrically, and considered conditions of both perikinetic and orthokinetic fouling separately. Perikinetic fouling results from the natural movement of particles (Brownian movement). For these experiments, the substrate was put into the latex, which is contained in a glass bottle and placed in a thermal bath at constant temperature, without stirring. They highlighted that the amount of estimated fouling may become erroneous following the way the substrate was treated after being extracted from the latex. Indeed, the estimated amount of fouling increased with increasing the time of exposure to air, which was explained by the change in temperature when removing the substrate from the bath, as also observed by Gottschalk et al. [18]. To avoid this measurement error, it was

suggested to cool the dispersion (by dilution and cooling the bath) before extracting the substrate into air. The kinetics of perikinetic fouling were found to be faster than the production time of industrial latexes (2 - 4 h), as in 30 min the limiting amount of fouling was reached, then keeping almost the same value for longer periods of time. The authors found that the coverage of particles on the substrate was near to 80 % of a monolayer in a simple cubic arrangement. The deposition of only one layer can be explained by the change of the sign of surface's charge exposed to the latex once the particles are deposited on the substrate. Initially the surface charge is positive. For a latex with pH of 2, the negatively charged particles are attracted by the positive surface, so they deposit and create a layer of negative particles. This layer prevents forward attachment by electrostatic repulsion. As the surface charge of the stainless steel changes from positive to negative at the pH of 4.3, ammonia was added to the latex to increase its pH to overcome the isoelectric point of the metal. The change on the surface charge decreased the fouling to half. But, even with the negative charge of the surface, this was not enough to completely prevent the particles from attaching to it. Also, the fouling was found to reduce with lower solids content. So, according to the authors, there is an equilibrium correlation between the concentration of particles and the amount of fouling, but it can be also related to the total charge of the latex and the surfaces, as more particles may attach to a surface to counteract the charges of the free particles in the latex. Increasing the temperature during the perikinetic tests showed a slight increase of fouling. The authors proposed that this can be due to the decrease of the extension of the hydrophilic moiety of the nonionic surfactant in water (when increasing temperature), as the particles can be packed more closely together on the surface as their stability decreases. It is also possible that the increased mobility of particles leads to a higher frequency of collision with the substrate. Finally, this increase might be due to having softer polymer particles, because the experiments were performed above the copolymer glass transition temperature.

Urrutia et al. [8] also studied fouling under orthokinetic conditions where the latex was forced to flow, thereby increasing the frequency and the energy of collision between particles. Note however that all the parameters influencing the perikinetic fouling are also expected to affect the orthokinetic fouling (e.g. surface coverage, concentration of particles, viscosity, etc.). In this part of their study, a one-liter glass reactor with an axial flow impeller was used and the substrates were inserted as baffles. The fouling was

measured again by gravimetry. Initially, the effect of different agitation speeds was investigated. The chosen speed was 400 rpm, because at this value coagulation on the surface was observed, and above this value foam was formed. The amount of fouling was found to be much higher than under perikinetic alone. As expected the fouling was higher for the less stable latex. The fouling increased with time (while it was found to reach a plateau in perikinetic fouling at 30 min), showing an acceleration in the kinetics of deposition when comparing the less stable latex to the more stable. The fouling increased with the temperature. Fouling was found to be heterogeneous and this is a result of the different flow patterns inside the reactor. This observation became more noticeable when comparing axial and radial flow type impellers. A stronger flow causes the formation of more aggregates, but they can be also removed from the surface, so we reach an asymptotic value of fouling in zones were fluid velocity is high.

In a related study from the same group, Urrutia et Asua [20] investigated the impact of different ratios of monomer / polymer particles on the orthokinetic fouling. The experimental set-up is the same as their previous study [8]. The fouling was found to increase with the monomer concentration until 20 %, and then seemed to remain constant at higher concentrations. Variabilities of results were seen at 40 % of monomer, but this can be caused by experimental error when removing big aggregates. The authors give two possible explications for the increase of fouling with the increase of monomer ratio. One is the decrease of the polymer glass transition temperature and the second is the decrease in the surface coverage when the particles swell with the monomer and their surface area increases. An increase in the ionic strength was found to increase the fouling. From the visual observation of the attached material, it was found that more material was attached over the height of the impeller due to the radial flow and the high flux close to the impeller.

Gottschalk et al. [18] evaluated the influence of the surface roughness and temperature on fouling. A propeller with no shear was used to keep the latex uniform, so we may assume this is perikinetic fouling. They compared technically smooth and electropolished stainless steel, as well as electropolished coated ones. A resistance, with both sides covered by a piece of the material, was used to heat or cool the surfaces and was submerged in a polymer dispersion of VINNAPAS® LL 6120 (90 % vinyl acetate + 10 % ethylene). The temperature was measured on both sides of the

pieces. Knowing the heat flux applied to the resistance, it was possible to estimate the resistance generated by the layer of polymer and so the amount of fouling. They investigated the effects of the fluid temperature, solids content and heat flux. Among the studied materials, the uncoated stainless steel surfaces showed the lowest overall tendency to fouling, for the different evaluated factors. There is also a higher tendency of fouling when increasing the temperature. There is also a clear dependency on the heat flux density (so the rate of temperature change). Also, increasing the solids concentration increases the fouling, most likely because of the higher availability of particles and the increased frequency of interactions. A higher viscosity of the polymer dispersion also increases the extent of fouling, which can be explained by the fact that the renewal of the viscous boundary layer becomes less frequent. The structure of the fouling on the surfaces was studied by microscopy. The fouling layers attached to the surfaces differ significantly when the piece tested was heated or cooled. On one hand, the structures observed during the heating tests have crater structures, that can be caused by local destabilization of the dispersion, phase inversion or evaporation of wrapped water as the experiments were performed in the range from 30 to 70 °C. On the other hand, the structures formed during cooling tests were uniform and smooth. In both cases a thin polymer film is formed. The authors suggest that it is probable that the polymer adhering to the pieces dries after removal from the dispersion and not during the test (as also suggested by Urrutia et al. [8]). In this case, the formed layer what can vary according to the temperature difference between the pieces and the air. The results show that there is no optimal material for all the evaluated parameters. So, the surface and operation conditions must be chosen according to the process. If the operation conditions allow, then reducing the temperature difference between the surface and the fluid, in combination with a surface modification, can reduce the formation of fouling.

In a subsequent study, Hohlen et al. [19] studied the fouling caused by particles of a vinyl acetate / ethylene copolymer dispersion (VINNALPAS® LL6120) during heating or cooling in a flow channel upstream a reactor (so orthokinetic fouling). A stainless steel plate was located inside the flow channel with several thermocouples on it, and the flow channel containing this plate was subject to heating or cooling by fluid in countercurrent flow. It was not possible to calculate the fouling resistance from the temperature curves of the plate as in the previous work of the same group [18], due to

the changes of the dispersion properties, then a constant heat flux cannot be assumed. So, the thickness of the fouling layer and the determination of surface coverage of the plate by polymer particles were determined by digital microscopy. It was observed that the polymer covered only some part of the plate and mainly at the edge situated at the entrance of the flow channel, probably because of the low fluid velocity (i.e. fluid stagnation). In the cases of aggregates deposited on the plate, they occurred also at the low fluid velocity areas. In the areas with high velocity, the aggregates are removed or their formation is suppressed. When analyzing the structures of the deposits by microscopy, craters were found to form for the heated samples, but as the experiments were performed below the boiling point of the dispersion, the authors state that the craters are not caused by evaporation.

Table 4.1 summarizes the different observations during fouling experiments in the absence of reaction.

Table 4.1 Methods employed to study fouling of polymer dispersions on a substrate in the absence of reaction*.

Reference	Set-up	Measurement	Polymer	Effect of studied parameters
Urrutia et al., 2017 [8] **Urrutia et Asua, 2021 [20]**	<u>Perikinetic fouling:</u> Glass bottle in a thermostated bath containing a plate of the substrate.	Gravimetry	50/50 PBA/PMMA (synthesizes in emulsion polymerization)	A negative charge of stainless steel (by changing pH) reduces fouling to 1/2. Fouling ↑ with: T, ionic strength, SC and when decreasing particle stability. Stabilization after 30 min at 80 % surface coverage.
	<u>Orthokinetic fouling:</u> 1 L stirred tank containing baffles of the substrate.			Fouling ↑ with: T, t, flow intensity, swelling with monomer (up to 20 %) and when decreasing particle stability. Heterogeneous fouling.
Gottschalk et al., 2015 [18]	2 plates of substrate with a heating resistance in sandwich immerged into a slightly stirred polymer dispersion.	Heat balance Microscopy (qualitative)	VINNAPAS® LL 6120 (90/10 vinyl acetate /ethylene)	Substrate material: less fouling with stainless steel than other materials. Fouling ↑ with: T, $\dot{T}$, SC, η.
Hohlen et al., 2020 [19]	Flow channel containing a plate of substrate.	Microscopic 2D images (quantitative)		Fouling ↑: in regions with low speed (stagnation), and at the entrance of the channel.

*: T is temperature, t is time, SC is solids content, $\dot{T}$ is variation of temperature, η is viscosity

4.2.3 Fouling in the presence of reaction

During the reaction, the contents of the reactor evolve due to the creation and possible aggregation of particles, progressive consumption of monomer droplets and the increase in the solids content and the viscosity. As these factors cannot be controlled individually, the study of fouling during polymerization is more challenging. However, it can provide supplementary information compared to the studies without reaction as it considers the real reaction conditions.

Vanderhoff [21] mentioned that the fouling on surfaces in the case of emulsion polymerization can be a result of latex destabilization, polymerization in large monomer drops or in a separate monomer layer, polymerization of monomer in the head space of the reactor or surface polymerization on the surfaces which is mainly related to the wettability of the monomer-polymer phase.

Kemmere et al. [10] studied the colloidal stability and fouling of polystyrene and polyvinyl acetate lattices produced in seeded emulsion polymerizations, stabilized by anionic and steric emulsifiers, for different solids contents, electrolyte concentrations and operating conditions such as the impeller speed, type and diameter. The authors evaluated the fouling based on visual observations and deviation of estimated and calculated mean energy dissipation. They found that an increase of the solids content (from 25 to 35 %) makes the fouling more sensitive to the concentration of electrolytes. This is reasonable because, as mentioned above, the frequency of particles-surface collisions increases, then the probability of deposition will depend on the particle stability and so the concentration of electrolyte. There was no effect of the impeller speed on fouling for emulsion polymerizations up to 50 % of solids content until 60 % of conversion. But, for conversions higher than 60 % the fouling increased with the stirrer speed. At constant mean energy dissipation, radial-flow impellers were found to generate more uniform power input and could minimize fouling compared to axial impellers.

McFadden and Wu [22] patented a continuous process for the production of polymer in a heat exchanger, that can operate for emulsion, solution or suspension polymerization. They claim that the fouling can be a result of the encounter of cold

reactants with a hot surface, making the temperature a key point to control fouling. They stated that the fouling can be controlled by the amount of monomer fed to reactor. In emulsion polymerization (of BA, MMA or methacrylic acid), when the amount of monomer exceeds 75 % saturation of polymer, the reactor surfaces tend to foul with polymer. This was explained by the excess of monomer polymerizing on the surface. The authors suggested that the surface of the channel exposed to the reacting mixture may be coated with graphite or PTFE to reduce interactions.

Hohlen et al. [19] studied the fouling also during polymerization, using the same set-up used without reaction, but with different polymer (vinyl acetate/vinyl ester). The optical images showed that fouling structures formed during polymerization consist of a compact polymer film with small elevations. The increase of the temperature of the heating plate increases the roughness and the amount of fouling. The inverse profile was observed when the wall temperature was lower than the bulk temperature. This can be explained by the driving temperature.

Urrutia et Asua [20] studied orthokinetic fouling also in the presence of reaction, using the same set-up presented in the previous section for the study without reaction [8]. Different amounts of the seed latex were swollen with a mixture of BA/MMA (50/50 wt/wt) keeping the total content of the organic phase at 50 wt% without further addition of stabilizer. In the presence of reaction, fouling increases for monomer contents of 20 % and 40 % more significantly than without reaction, showing that the effect of monomer is stronger during the reaction. The highest amount of fouling was obtained for the highest ratio of monomer. This could be due to a higher level of aqueous phase polymerization, eventually resulting in precursor particles and / or water soluble oligoradicals that adsorb onto the surfaces. When increasing the monomer ratios from 20 % to 40 %, there is more initiator available to create radicals, the concentration of monomer is high and there are less particles coming from the seed, because the initial solids content was constant. Particle precursors undergo a fast increase in the surface area as they are small, so they need surfactant to stabilize, and the surfactant comes only from the remaining amount in the seed. For 40 % of monomer, there is less surfactant per surface area than with lower fractions, so the precursors are instable and can be captured by the existing particles or by the baffles. The hypothesis of fouling caused by the decrease of the glass transition temperature of the polymer due to the swelling of particles is not excluded. Increasing the amount of initiator increases

the ionic strength of the dispersion, and causes an increase in the fouling. As discussed above, the effect of the ionic strength on fouling was validated without reaction. For the different investigated factors, the extent of fouling was lower in the absence of reaction than in presence of reaction, for comparable conditions.

Böttcher et al. [23] studied the fouling in emulsion polymerization of BA, MMA and in some cases with the addition of acrylic acid to aid colloidal stability. They used a quartz crystal microbalance with dissipation monitoring (QCM-D) to detect and quantify fouling on a ring-shaped thermal pad placed in a glass container with a stirrer. During reaction, it was observed that the fouling layer of the polymers produced with acrylic acid was thinner than the ones produced without it. Knowing that acrylic acid improves the polymer stability, it was concluded that the fouling in the presence of acrylic acid is caused by the deposition of layers of single particles. This layer is called passivation layer and helps to prevent further fouling. For the polymerizations without acrylic acid, the authors state that the fouling happens by the deposition of coagulum created in the bulk showing the presence of two different mechanisms for fouling formation according to latex stability.

Table 4.2 summarizes the observations during experiments studying fouling in the presence of polymerization.

Table 4.2 Methods employed to study fouling of polymer dispersions in the presence of reaction*.

Reference	Set-up	Measurement	Polymer	Effect of studied parameters
Urrutia et Asua, 2021 [20]	1 L stirred tank containing baffles of the substrate.	Gravimetry	50/50 PBA/PMMA (synthesizes in emulsion polymerization)	Fouling ↑ with: T, ionic strength, swelling with monomer (up to 20 %) and SC
Kemmere et al., 1999 [10]	Three baffled stainless steel reactors of different size and two different impellers.	Visual observation (qualitative)	Seeded PST and ab-initio PVAc emulsion polymerization	Fouling ↑ with: ionic strength, SC and N. Large radial-flow impellers are more suitable to avoid fouling.
McFadden and Wu, 2002 [22]	Non cylindrical heat exchanger	Salt tracer study of residence time and visual observation	Example: monomer mixture (46 % BA, 53 % MMA and 1 % methacrylic acid)	Fouling ↑ if: amount of monomer in the reactor higher than 50 % of the amount that can be swollen by polymer and T_{wall}.
Hohlen et al., 2020 [19]	Flow channel containing a plate of substrate.	Microscopic 2D images (quantitative)	Vinyl acetate/vinyl ester	Fouling ↑ with: increased temperature difference between the heating surface and the bulk fluid.
Böttcher et al., 2022 [23]	Quartz Crystal Microbalance (QCM)	Gravimetry	PMMA, PBA Acrylic acid used to improve stability	Fouling ↓ when using acrylic acid (by the improvement in stability)

*: N: stirring speed, T_{wal}: temperature of the wall

4.2.4 Methods for fouling reduction

There are few generalizations that can be applied to reduce fouling in dispersed media, but each system must be studied separately and a better understanding of the polymerization system may lead to the modifications that can be performed in the recipe, polymerization technique, agitation system and reactor modification.

Coating of the reactor wall

In the patents, the use of additives or coatings is extensively explored to prevent fouling on the surface of the equipment. Such additives must be chemically inert and insoluble in any of the raw materials (except the continuous aqueous phase) employed during polymerization or post-processing steps, and must not change the color of the polymer when this characteristic is considered imperative to the final product. Among such coatings one may cite metals as salts (e.g. alkali and alkaline earth) or hydroxydes [24–30], aminic groups [26,28–31], polymeric materials [27,29,32–34] and polysaccharides [35–37]. They can be applied to ethylenically unsaturated monomers [24–30,33,35–38], PVC production [31,39–41], vinyl halides [24,42] and water soluble polymers [43].

The coating can be applied by brushing, spraying, filling the reactor followed by withdrawal or by some automatic filling methods. It can be dried by blowing hot air or applying the coating on a previously heated surface. These procedures can be followed by an optional washing of the surfaces with water and in some cases the coating can be composed of a double coating [25,27]. The coating material may also be added directly to the polymerization medium [33,36,37]. The injection of the additives in the system is preferred to be performed before the monomer feed, to be sure the surfaces will be wetted by the chemical acting as a protection [42]. Such chemicals may also have the ability to destroy the radicals adsorbed on the surface to avoid the development of polymer [31].

Not all the patents explain the reasons how the coating prevents / reduces the fouling. Some coatings are mainly effective against fouling caused by the absorption of monomers on the wall that can lead to its polymerization [32,35]. It is believed that the

key advantages of the coating are the increase of the wall hydrophobicity [36,37], lowering the surface tension of the wall [32,43], pH of the medium [29,35,40], or the reduction of roughness by electropolishing of the wall [40,43].

4.2.5 Improvement of the recipe or reactor design

Normally the reduction of fouling can be obtained by changing the recipe, polymerization technique as well as the reactor design. Some of these modifications are listed below and are summarized from the works mentioned in the previous sections, and from Vanderhoff [21]:

- Use of seeded polymerization;
- Addition of a stabilizer at an appropriate conversion;
- Control the monomer/polymer ratio;
- Work at low ionic strength;
- Rigorous temperature control;
- Continuous addition of monomer instead a charge at the beginning;
- Work with different agitation speed, but keeping a good heat and material transfer;
- Use of the appropriate material for the reactor;
- Surface modifications as polishing, use of coatings of surface charge change by overcoming the isoelectric point of the metal;
- Modification of the agitator and baffle system;
- Modification of reactor geometry;
- Monomer addition directly in the liquid phase;

Some of the methods found in patents are shown in Table 4.3.

Table 4.3 Methods employed to reduce fouling.

Reference	Polymer and Process	Actions to reduce fouling
Geddes, 1990 [32]	Emulsion, dispersion polymerization	Coating with a film of oleophobic-hydrophobic polymeric material of surface energy in the range of about 10-15 dynes/cm.

Reference	Polymer and Process	Actions to reduce fouling
Balwe et al., 1974 [39]	Suspension polymerization of polymerizates containing at least 80 % of polyvinyl chloride	Using from 0.001 % to 1 wt% based on monomer, of an unbranched dialkyl peroxy dicarbonate and 0.0001 to 0.01 wt% based on monomer, of a water soluble salt of nitrous acid.
Goetze et al., 1975 [42]	Suspension polymerization of a polymerizate containing at least 70 % polyvinyl halides	Use 10 to 300 ppm, of water soluble reducing agents (based on the water content). A reactor with surface having a roughness of at most 1 µm. Flow velocity on the surface is at least 0.3 m/s.
Collete et al., 1996 [43]	Suspension polymerization of hydrophilic/superabsorbant polymers	Applying a coating of a solution or dispersion of a fluorinated copolymer on an electropolished surface.
Fitzwater and McFadden, 2001 [44]	Continuous tubular or channel addition or condensation polymerization Example: 46 % BA, 53 % MMA and 1 % MA	Modifying the reactor geometry to avoid the generation of gas.

4.2.5.1 Process modelling to predict fouling

The works dedicated to the modelling of fouling are few in the literature and mainly concern homogeneous polymerization (solution or bulk, and in particular low density polyethylene). However, as the fouling may be due to the reactor geometry, some information can be obtained from homogeneous polymerization models, that may remain valid in heterogeneous polymerization. The models may be used to predict the conditions in which the deposition of polymer occurs and evaluate its amount. As the mechanisms leading to the fouling formation are still not clear, some models are data-based or empirical, but also computational fluid dynamic simulation can be interesting to employ.

Zhang et al. [6] used a neural network model to estimate fouling, as a step decrease in the overall heat exchange coefficient, to match the monitored real-time reactor calorimetry data of a solution polymerization of MMA, in a pilot scale reactor. Fouling is detected when the predicted behavior during the reaction deviates from the observed one, so its amount is estimated to reduce the difference between the polymerization curves. This strategy can be used when detailed mechanistic relationships are not available.

Buchelli et al. [45–47] published a sequence of papers dedicated to the study of fouling effects in a Low Density Polyethylene (LDPE) tubular polymerization reactors. The fouling thickness was again estimated from the decrease in the overall heat exchange

coefficient when polymer accumulates at the reactor wall. CFD was used to model the local effects at the wall and to predict the changes in the heat transfer coefficient and temperatures over time. Also, the decrease in reactor temperature leads to a phase change, where an equation of state is used to predict the two-phase envelope. The last improvement in the model was the simulation of reaction kinetics, including macro and micromixing, using CFDReaction and DynoChem software. They found that the fouling thickness was linear over time, and a mass transfer coefficient was estimated from data plant but the value was several orders of magnitude lower than the one calculated by correlations. So, the authors believe that not all the foulant particles transfer to the wall at the same rate, and not all the particles reaching the wall become fouling, what can be affected by the wall roughness.

One more study on fouling in LDPE production was performed by Fries et al. [48], where a large diameter reactor with low flow rate was used to produce as much fouling as possible. Three modules, axial, radial and radial compartmentalized; were considered in the Predici simulator to reproduce the experimental data. A sensitivity analysis for the polymer diffusion coefficient was made. A better fitting of experimental data was obtained using the radial compartmentalized module. The enrichment of polymer near wall (i.e. fouling) was found to lead to tailing in the molecular weight distribution.

Begall et al. [49] also used CFD simulations to optimize the geometry of a millireactor, to avoid areas of slow moving and stagnant flow which are suitable to generate fouling. With some modifications, they reduced the slow moving areas by 39 % and stagnant areas by 65 %, with almost no changes in the reactor pressure drop. This can be a starting point to decrease the occurrence of fouling and still miss an experimental validation.

4.3 Results

4.3.1 Fouling in the absence of reaction

The perikinetic tests were performed with the 6-bladed 45° pitch impellers made of stainless steel 316 left in contact in the absence of agitation with a latex 20 wt% produced according to the reference recipe. The total time of experiments are two and sixteen hours at ambient temperature, and after the test the impeller was rinsed with water and the material deposited is measured gravimetrically.

Aluminum pans were used as a container and two different configurations were tested: one with the impeller touching the bottom of the pan and the other without touching it, suspended by a claw covered with plastic.

It was observed that the deposition of particles occurred mainly at the bottom of the impeller when in contact with the aluminum pan, and this deposition also increased with time. However, when the impeller was not touching the aluminum pan, the amount of material deposited seems to be constant after two hours of experiment, as shown in Table 4.4.

Table 4.4 Amount of material deposited in SS316 impellers during perikinetic experiments.

	Mass (mg)	
Time (h)	Impeller in contact with Al	Impeller not in contact with Al
2	38.3	11.4
16	134.6	12.4

The deposition of particles when the two metals are in contact is due to the flow of electrons created when metals with different potentials are in contact in the presence of a solution containing electrolytes [50]. As long as the metals are in contact, there will be the electric flux and deposition of particles, as seen with the increase of material attached with time.

The constant amount of material deposited after two hours on the impellers when contact with aluminum may be the passivation layer [8,23]. This layer of material is created on a surface and the particles already attached will avoid further deposition of

particles with the same charge. As the reference latex has a pH between 3 and 4, and in this case the stainless steel surface is positive, the negatively charged PVDF particles will attach to the surface.

From the results it is possible to state that for a reference latex, there will be always a deposition of material on the surfaces of the reactor, that can be increased when a phenomenon like galvanic corrosion happens in the system, as also observed when changing the screws used to fix the impellers to the shaft as shown in Figure 4.3.

a) b)

Figure 4.3 Deposition on the screws of the impellers when using a) stainless steel and b) non galvanized steel.

4.3.2 Fouling in the presence of reaction

4.3.2.1 Batch reactions

The batch reactions were performed according to the procedure described in chapter 2 and the reactions were based on the concentration of chemicals presented in the Table 3.2. Whenever a concentration is changed, it will be mentioned.

Table 4.5 Reference recipe for batch reactions.

TA (g/L)	Wax (g/L)	CTA (g/L)	KPS (g/L)	Buffer (g/L)
1.50	1.1	15.3	0.09	0.06

All the batch reactions were performed with set-up 2 at 550 rpm, with a total volume of water of 2.2 L, producing a latex with approximately 20 wt% of solids. After the end of the reactions and after the removal of the latex, the reactor and its internals were rinsed with deionized water and left to dry overnight. Pictures were taken to have some qualitative comparison of the fouling produced when working with different recipes/reactions.

As in set-up 2 the hydrofoil could be easily removed without losing the attached material, the mass of fouling on it was measured, but not on the other parts of the reactor.

4.3.2.1.1 Effect of CTA concentration (batch reactions)

Reactions were performed by only changing the concentration of CTA (ethyl acetate) in the recipe and the results are presented in the Table 4.6. It can be seen that as the concentration of CTA is increased, more material is found on the hydrofoil, this tendency can be related to:

- The increase in CTA makes the polymerization rate slower [51], taking more time to produce a latex with the same solids content. Then, the latex will be in contact with the impeller, so undergoing shear, for more time;
- The presence of CTA makes the particles softer [52] thereby facilitating their attachment to the surface. Indeed, the used chain transfer agent is liquid ethyl acetate which is believed to partition between the polymer and water phases. However, its concentration remains relatively low compared to the polymer and can hardly have an effect of softening;

For the moment, it is not possible to define what is, or are the main causes for the increase in deposition while increasing the CTA concentration.

Table 4.6 Batch reactions performed with different CTA concentrations.

CTA (g/L_{water})	**2.6**	**5.1**	**12.1**	**15.3**
Time (min)	43	67	120	140
SC (%)	20.8	20.6	21.2	21.4
Dp (nm)	186	177	176	186
PdI	0.01	0.02	0.02	0.02
$Npx10^{19}$ ($1/m^3$)	4.0	4.6	4.8	4.1
θ (%)	11.1	10.7	10.3	10.8

CTA (g/L_{water})	2.6	5.1	12.1	15.3
Mw (kDa)	608*	635*	231	192
PDI	2.91	2.90	2.25	2.26
Fouling on the Hydrofoil (g)	0.2	0.2	0.6	0.8

* Samples presenting more than one peak for MW distribution, out of the calibration curve. Only the peak in the range of the calibration data is presented.

Pictures were taken for a qualitative comparison of the extent of fouling when changing the CTA concentration, as shown in the Figure 4.4 and Figure 4.5. It can be seen that the produced fouling is heterogeneous, showing the patterns of flux specially in the hydrofoil. Also, it looks like the fouling above the liquid surface (white ring in the pictures in Figure 4.5) is different from the fouling below it.

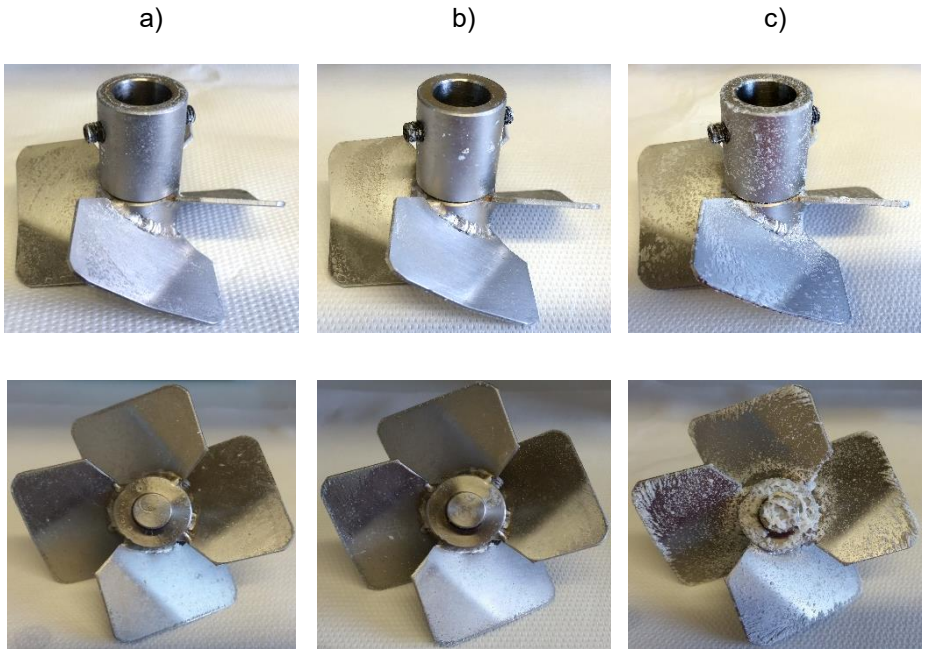

Figure 4.4 Hydrofoil views for batch reactions with different CTA concentrations a) 2.6 g/L, b) 5.1 g/L and c) 15.3 g/L.

a) b) c)

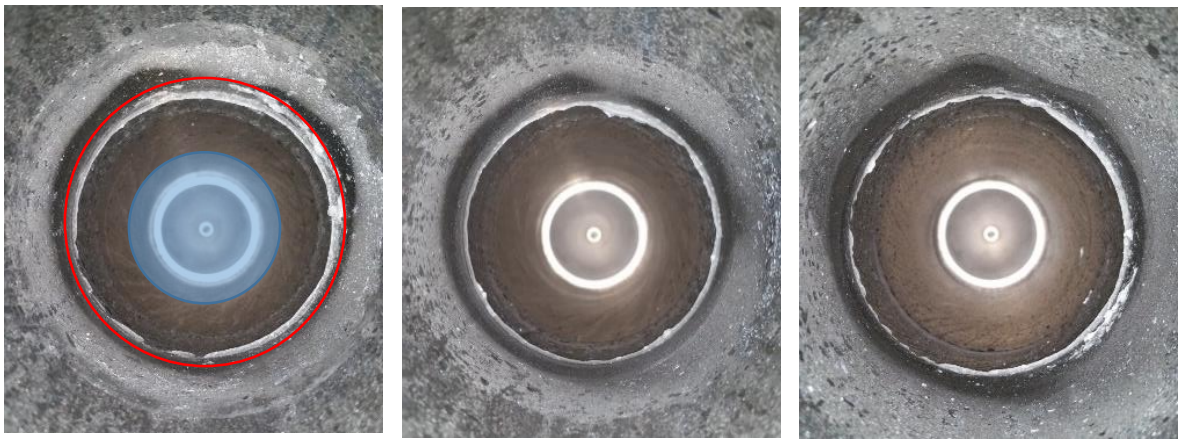

Figure 4.5 Top view of the reactor wall for batch reactions with different CTA concentrations a) 2.6 g/L, b) 5.1 g/L and c) 15.3 g/L. (Hydrofoil area in light blue and the white ring shown in red at figure a)

4.3.2.1.2 Effect of surfactant concentration and the presence of wax

To have a more quantitative estimation of fouling on all the parts of the reactor, a new strategy was developed. This time, the surfaces of all the reactor were cleaned with household sponges, after emptying and rinsing the reactor. The sponges were not rinsed so that all material removed from the reactor wall remained on the sponge. The sponges were weighed before and after cleaning to know how much of the material goes to the internals (this includes the hydrofoil, the 3 pitched 6-blade impellers, dip tube and thermocouple) and to the wall.

The concentration of CTA was kept at 15.3 g/L, because with this value it is possible to proceed with the polymerization with a good temperature control. Reactions were performed by changing only the concentration of surfactant, and in this way changing the stability of particles. Reactions without paraffin/wax were also performed because the use of wax to avoid fouling in this system is well known [53–55].

Table 4.7 Batch reactions performed with different concentrations of surfactant and wax.

TA (g/L)	**1.25**	**1.50**	**1.75**	**1.50 A**	**1.50 B**
Wax (g/L)		1.1		0	
Time (min)			150		
SC (%)	21.4	21.2	21.7	20.8	21.6
Dp (nm)	192	185	183	177	187
PdI	0.03	0.01	0.03	0.03	0.03
Npx10^{-19} (1/m^3)	3.7	4.2	4.4	4.6	4.1

TA (g/L)	1.25	1.50	1.75	1.50 A	1.50 B
θ (%)	9.4	10.8	12.3	10.6	10.8
Mw (kDa)	177	177	182	176	187
PDI	2.36	2.32	2.22	2.29	2.35
PVDF lost as fouling (%)	0.08	0.09	0.14	0.31	0.25

The height of latex reached in the reactor was measured, making it possible to calculate the total area of internals and the area of the wall covered by fouling, to indicate the values as density per m². The results are presented in the Figure 4.6.

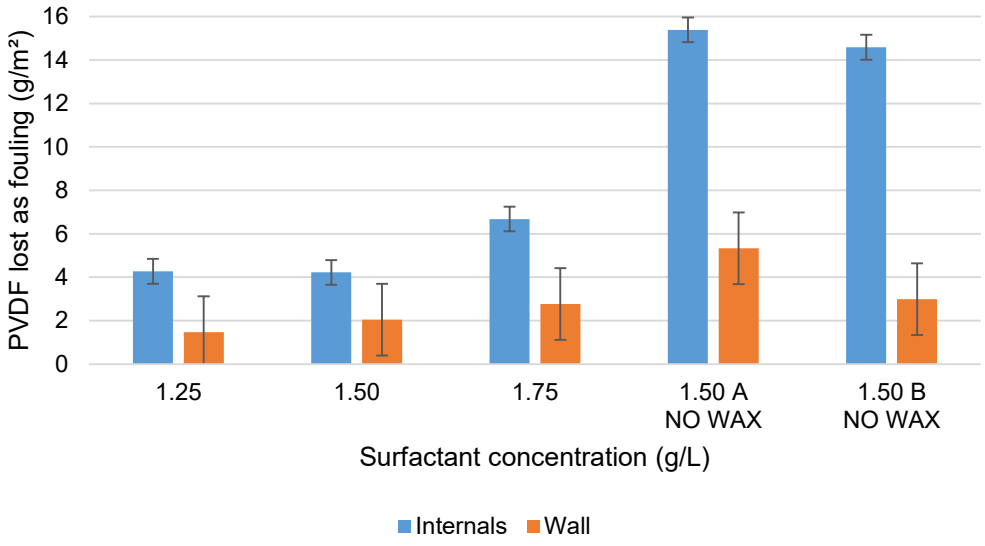

Figure 4.6 Density of PVDF lost as fouling in different areas of the reactor for batch reactions with different concentrations of surfactant and presence or absence of wax.

It was observed that the tendency of fouling increases with the increase of surfactant concentration. But, from the error of the measurements found from the reproducibility of the reaction without wax, it is possible to state that the results observed for a surfactant concentration of 1.25 and 1.50 g/L are the same, probably the difference in the surfactant was not enough to see the expected tendencies. It is possible to check the effectiveness of the wax as an anti-fouling agent, because the density of PVDF deposited in the surface increased three times.

One special point to be highlighted is that the density of fouling on the wall is always lower than on the reactor internals, even if the total area covered by deposits is in the same order of magnitude for the shaft and wall. This can be explained by the surface treatment of the reactor that is electropolished while the other parts are not treated.

The surface treatment was already cited in the literature as a way of fouling reduction [40,43].

The highest amount of PVDF lost represents a mass of 0.53 g, knowing that the density of PVDF is 1800 kg/m³, it is possible to calculate the volume of PVDF and then the thickness of a layer, assuming that the fouling is uniformly distributed on 1000 cm² of fouled surface (the visual observations show this is not always the case, so the thickness can be considered a minimum value). The calculated thickness is equal to 3 µm. This value is very low, and does not allow estimating the fouling by the reduction in the overall heat exchange coefficient, as done in some studies reported in the literature [18,45] .

Figure 4.7 and Figure 4.8 show the visual patterns of fouling produced while running the experiments in which the amount of surfactant (in the presence and absence of wax) was modified. It can be seen that the reaction performed without wax has PVDF attached on the reactor's surface, even above the commonly found visible layer of latex, which confirms its interest as an anti-fouling agent. Visually, it can be seen that the material deposits in specific areas of the hydrofoil, as the center of its axe and the borders of the blades. The reaction performed with the higher concentration of surfactant (1.75 g/L), seems to have produced a more uniform deposition of material on the hydrofoil.

a) b) c) d)

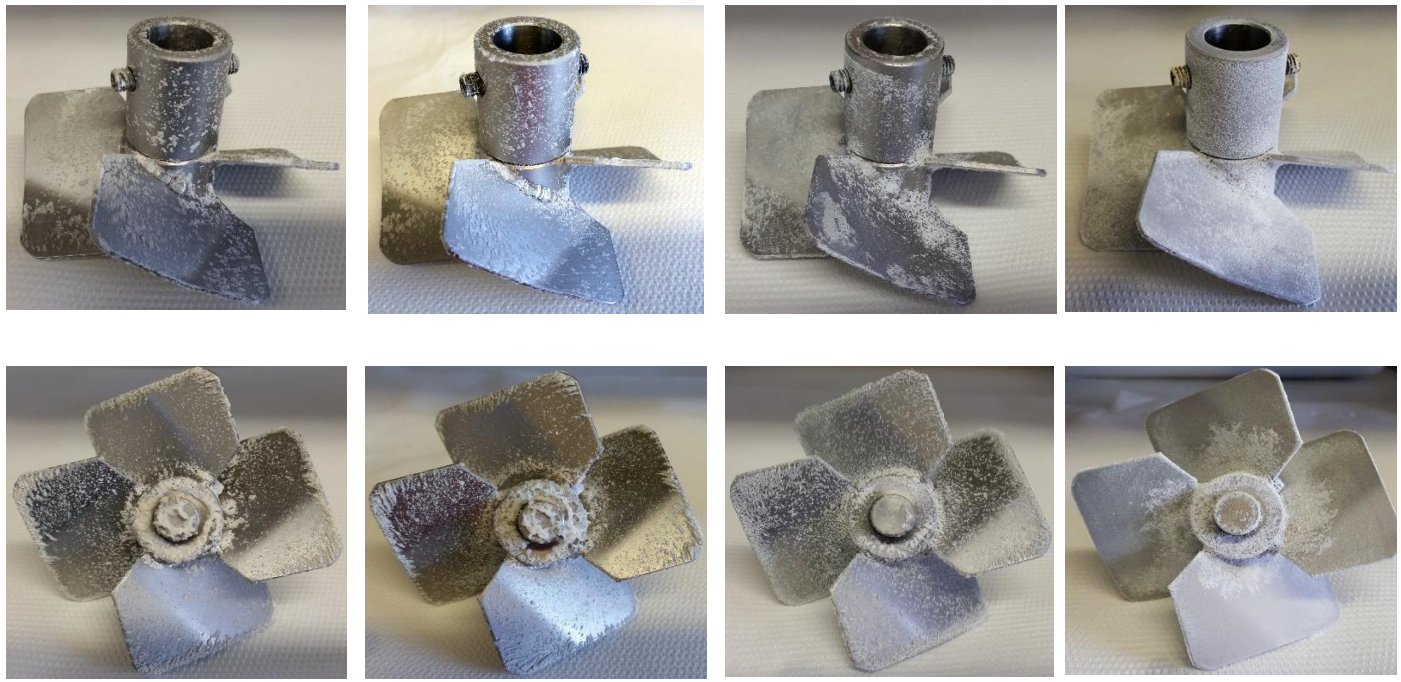

Figure 4.7 Hydrofoil views for different concentrations of surfactant and in the absence of wax a) 1.25 g/L, b) 1.50 g/L, c) 1.75 g/L and d) 1.50 g/L without wax.

a) b) c) d)

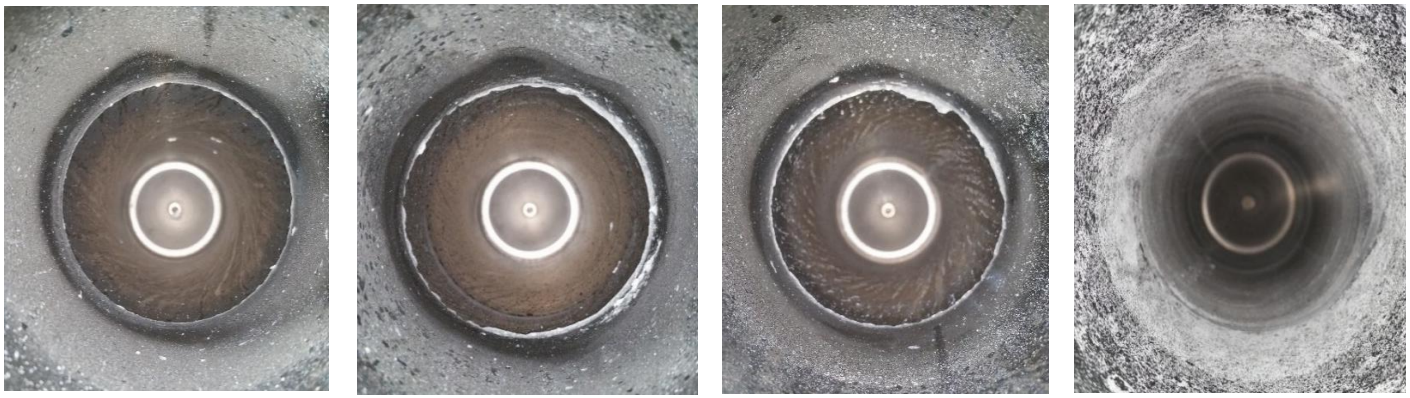

Figure 4.8 Top view of reactor wall for different concentrations of surfactant and in the absence of wax a) 1.25 g/L, b) 1.50 g/L, c) 1.75 g/L and d) 1.50 g/L without wax.

4.3.2.2 Semi-batch reactions

All the semi-batch reactions presented in this section were performed with the one shot protocol and set-up 2 at 400 rpm, keeping again the same reference concentration of chemicals presented in the Table 3.2. If a different concentration of a chemical is used, it is mentioned in the text. The amount of fouling collected after each reaction followed the same procedure as the one used for the batch reactions using a sponge.

4.3.2.2.1 Effect of the reaction volume (i.e. mixing effect)

It is interesting to compare the extent of fouling when the reactions were performed with the reference volume of water (2.2 L) and the reduced initial charge (1.6 L), as this was found to affect mass transfer and the reaction rate, and so the solids content, (will be more detailed in chapter 5).

Table 4.8 Semi-batch reactions performed with different volumes of water.

Water (L)	**2.2**	**1.6**
Time (min)	180	
SC (%)	32.0	39.1
Dp (nm)	221	227
PdI	0.05	0.05
Npx10^{-19} (1/m^3)	3.9	4.6
θ (%)	8.0	6.4
Mw (kDa)	257	415
PDI	2.30	2.48
PVDF lost as fouling (%)	0.05	0.14

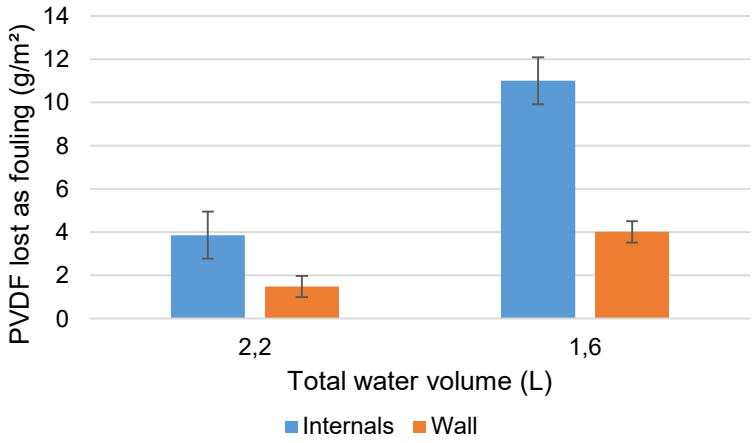

Figure 4.9 Density of PVDF lost as fouling in different areas of the reactor for semi-batch reactions performed with different volumes of water.

The increase in fouling is clear when decreasing the volume, and can be due to the increase in solids content. Also, as the concentration of surfactant was not changed, the increase in solids content reduces the surface coverage of the particles by surfactant. At the same time, more particles are found in the system, the final molecular weight is not the same and these two reactions have different mixing profiles. In Figure 4.10 and Figure 4.11, it is possible to see the fouling on the hydrofoil and reactor's wall.

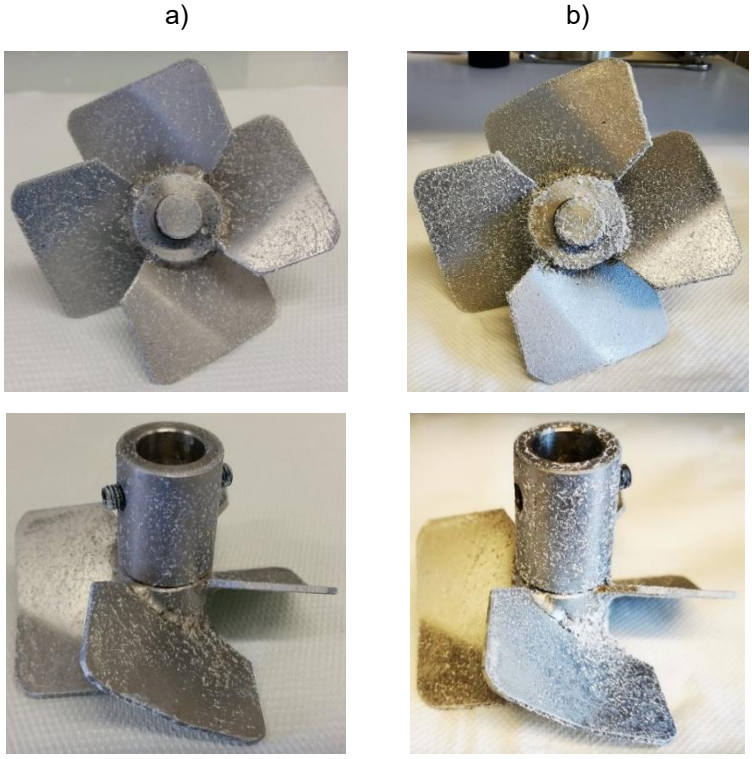

Figure 4.10 Bottom and side views of the material attached to the hydrofoil after the semi-batch reactions performed with different volumes of water a) 2.2 L and b) 1.6 L.

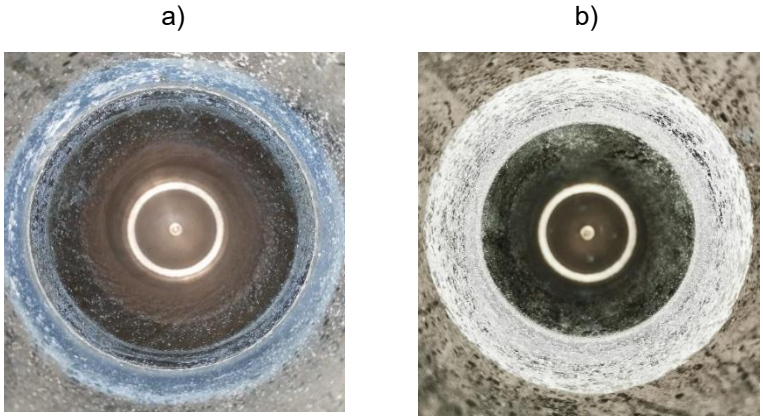

Figure 4.11 Top view from the reactor wall showing the attached material after the semi-batch reactions performed with different volumes of water a) 2.2 L and b) 1.6 L.

From the pictures of the reactor's wall, one can see again the well-defined layer of polymer, probably created by the vortex and splashing of material in the liquid. Also, the density of fouling is not the same in this area when comparing to the one covered by liquid since the beginning of the reaction.

The total amount of PVDF lost as fouling for these two reactions are 0.05 and 0.14 % for 2.2 and 1.6 liters of water, respectively. The increase in fouling of about three times seems not to correspond only to the increase in the solids content that was about 22 %. So, probably the change in mixing patterns/vortex in the reactor shown in Figure 4.12, also increases in the monomer concentration and the polymer molecular weight, taking part in the fouling results.

a) b)

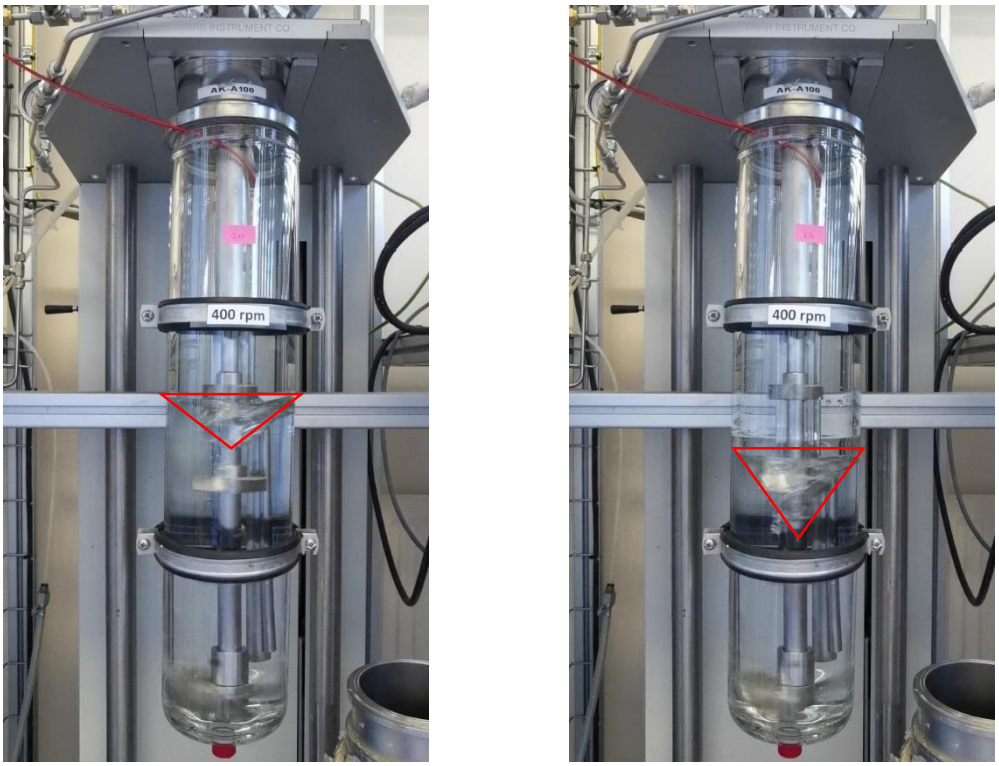

Figure 4.12 Differences in vortex with set-up 2 at 400 rpm and volumes of water of a) 2.2 L and b) 1.6 L.

4.3.2.2.2 Effect of the surfactant

To better elucidate the effect of surfactant concentration, half and double of the reference concentration were tested, keeping the amounts of other chemicals, total volume of water of 1.6 L and total polymerization time all the same. The results are presented in the Table 4.9.

Table 4.9 Semi-batch reactions performed with different concentrations of surfactant.

TA (g/L)	0.75 A	0.75 B	1.50	3.00
SC (%)	34.6	36.2	39.1	36.7
Dp (nm)	266	262	227	193
PdI	0.01	0.04	0.05	0.02
Npx10^{19} (1/m^3)	2.5	2.8	4.6	7.0
θ (%)	4.3	4.1	6.4	11.8
Mw (kDa)	370	432	415	452
PDI	2.67	2.94	2.48	2.92
PVDF lost as fouling (%)	0.21	0.16	0.14	0.03

Figure 4.13 shows the density of PVDF lost as fouling on the wall and the total amount lost on the internals and wall.

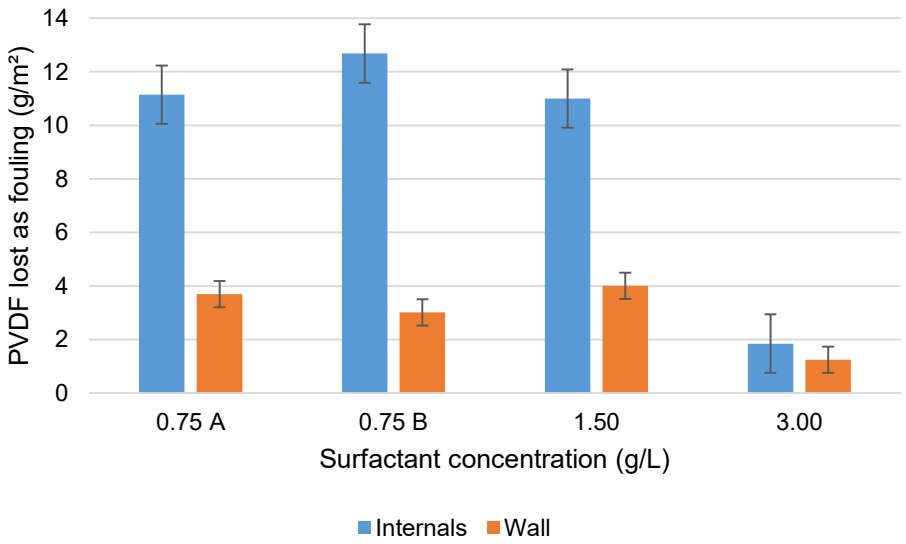

Figure 4.13 Density of PVDF lost as fouling in different areas of the reactor for different concentrations of surfactant.

As expected, it can be seen that the reaction performed with more surfactant produced the lowest amount of fouling due to the higher stability of the particles. The reactions performed with 0.75 and 1.50 g/L of surfactant seem to have produced a similar amount of fouling, but it seems that there is an optimal value for the surfactant concentration when increasing it to 3.00 g/L as the PVDF lost as fouling decreased drastically.

It is worth pointing that the reaction performed with the lowest amount of surfactant produced 150 g of destabilized latex, as shown in the previous chapter

on coagulation. Also, as the surface coverage is based on the particle size measured for the free flowing material that could be recovered from the bottom valve of the reactor, this calculation is not reliable in presence of coagulum.

Figure 4.14 and Figure 4.15 show the fouling on the hydrofoil and reactor's wall, where the influence of the surfactant is visible.

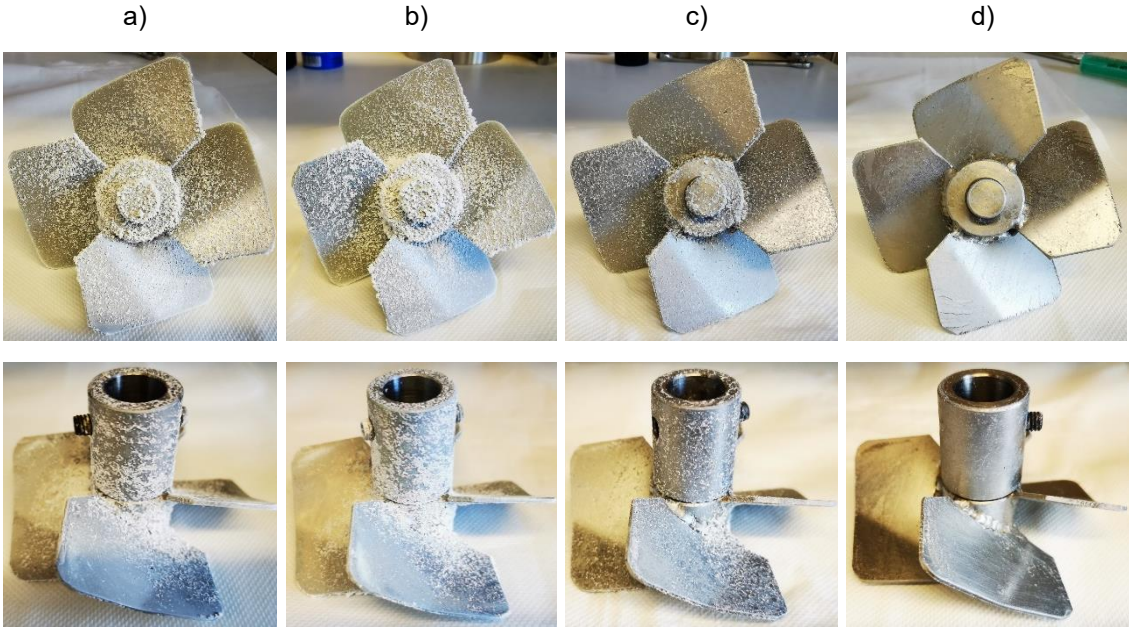

Figure 4.14 Bottom and side views of the material attached to the hydrofoil after the semi-batch reactions performed with different surfactant concentrations a) 0.75 g/L A, b) 0.75 g/L B, c) 1.50 g/L and d) 3.00 g/L.

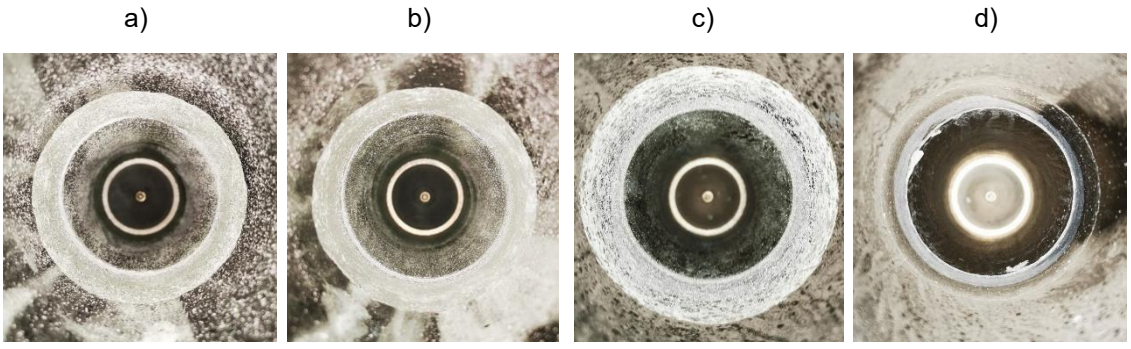

Figure 4.15 Top view from the reactor wall showing the attached material after the semi-batch reactions performed with different surfactant concentrations a) 0.75 g/L A, b) 0.75 g/L B, c) 1.50 g/L and d) 3.00 g/L.

For the reactions with surfactant concentration of 0.75 and 1.50 g/L, the percentage of PVDF lost as fouling is equal to 0.18 % and 0.14 % respectively. But, for the reaction performed with 3.00 g/L the value falls to 0.03 %, five times

lower, showing that the improvement in the stability of particles by adding more surfactant is effective in decreasing the fouling.

4.3.2.2.3 Effect of reaction time

The same recipe of the reactions with 0.75 g/L of surfactant was repeated, but the reaction was stopped at 120 minutes to study the effect of duration of the reaction (i.e. detect the starting point of the latex destabilization and try to find the critical surface coverage of the latex). The results are presented in the Table 4.10.

Table 4.10 Semi-batch reactions stopped at different times.

Time (min)	**180 A**	**180 B**	**120**
SC (%)	34.6	36.2	28.8
Dp (nm)	266	262	251
PdI	0.01	0.04	0.01
Npx10^{-19} (1/m^3)	2.5	2.8	2.4
θ (%)	4.3	4.1	5.1
Mw (kDa)	370	432	382
PDI	2.67	2.94	2.60
PVDF lost as fouling (%)	0.21	0.16	0.06

The fouling results are shown in the Figure 4.16. It can be seen that when the reaction was stopped at 120 minutes, the density of PVDF lost as fouling on the wall is around 50 % of the final density found at 180 minutes of a similar reaction. The density of fouling on the internals is around 30 % of the expected final value. It can be suggested that the stability of particles decreases when increasing the solids content, which then may lead to more fouling, but the effect of time under shearing cannot be neglected.

Comparing the percentage of material lost at 120 and 180 minutes, the amount of PVDF lost as fouling represents 0.06 % at 120 minutes while the value increased to 0.16 % at 180 minutes, almost three times.

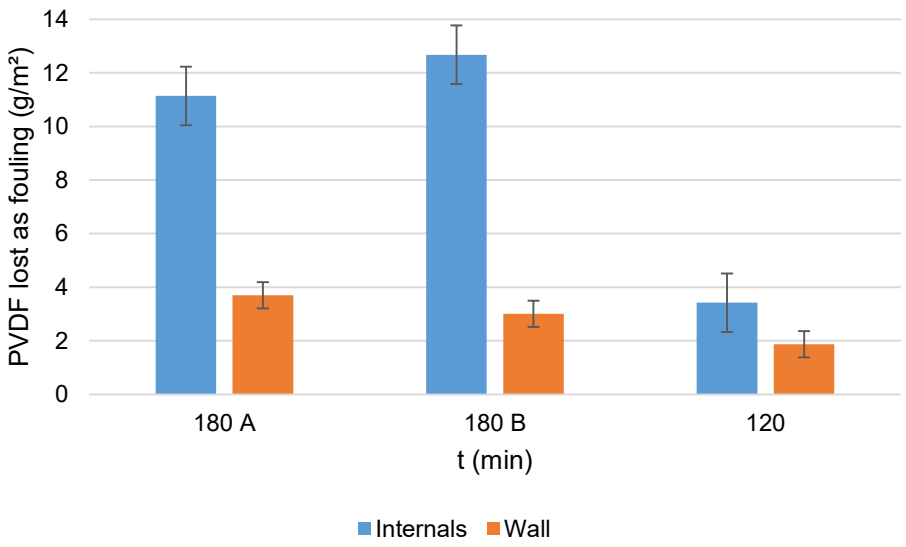

Figure 4.16 Density of PVDF lost as fouling in different areas of the reactor for different polymerization times in which 180 minutes the system is destabilized.

Figure 4.17 and Figure 4.18 show a big difference on fouling when changing the reaction time. As expected, the thick layer of fouling that normally is found on the wall at 180 min, is reduced for the reaction stopped at 120 minutes, as less solids content is produced.

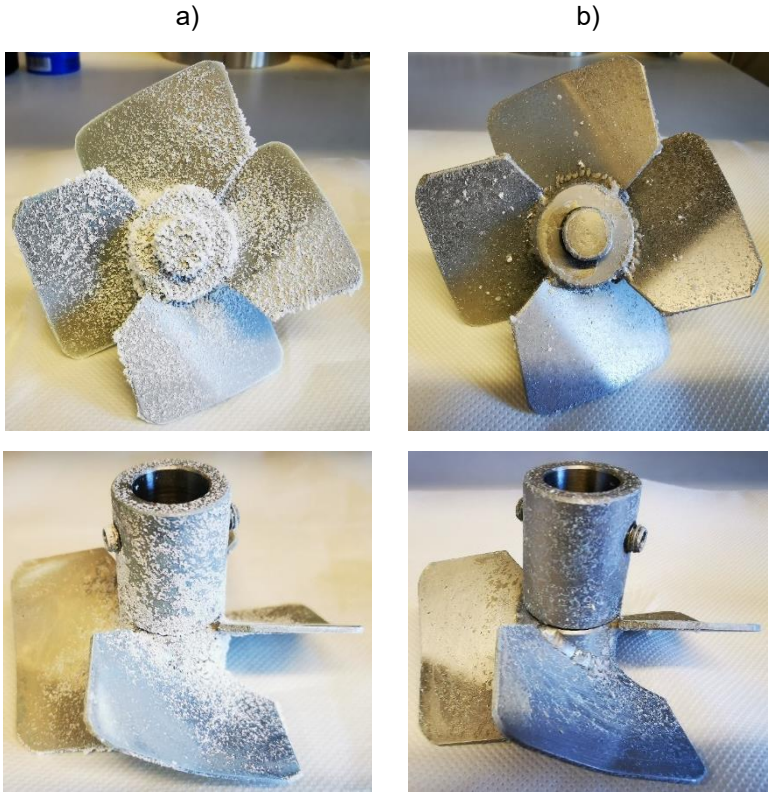

Figure 4.17 Bottom and side views of the material attached to the hydrofoil after the semi-batch reactions stopped at different times a) 180 min and b) 120 min.

a) b)

Figure 4.18 Top view from the reactor wall showing the attached material after semi-batch reactions stopped at different times a) 180 min and b) 120 min.

4.3.2.2.4 Effect of time and polymer Mw – by changing the CTA concentration

As mentioned in the section 4.3.2.1 for batch reactions, an increase in the amount of CTA slows down the reaction. So, the concentration of CTA was decreased in a way that a latex with the same solids content was produced (as that obtained at 180 minutes) but taking 120 minutes instead of 180. The results are presented in the Table 4.11. This allows to study the influence of the polymer molecular weight and reaction time at similar solids content.

Table 4.11 Semi-batch reactions performed with different concentrations of CTA (TA = 1.5 g/L).

CTA (g/L)	**15.3**	**7.9**
Time (min)	180	120
SC (%)	39.1	37.9
Dp (nm)	227	224
PdI	0.05	0.02
Npx10^{-19} (1/m^3)	4.6	4.7
θ (%)	6.4	6.6
Mw (kDa)	415	910
PDI	2.48	3.72
PVDF lost as fouling (%)	0.14	0.12

From the results it can be confirmed that the solids content produced is similar as well as the particle size, but the main difference as expected was the increase in the molecular weight with the decrease of the CTA concentration.

In Figure 4.19, it can be seen that the density of PVDF lost as fouling on the wall is virtually the same for the two reactions. The amount on internals is higher for the latex with a higher concentration of CTA in the recipe (so taking more time to be produced, and leading to shorter polymer chains). First, it is known that the CTA is a solvent to the PVDF, but during the polymerization it is partitioned between particles and water and its concentration is comparatively low regarding to polymer concentration, so it can hardly have an effect of softening of particles.

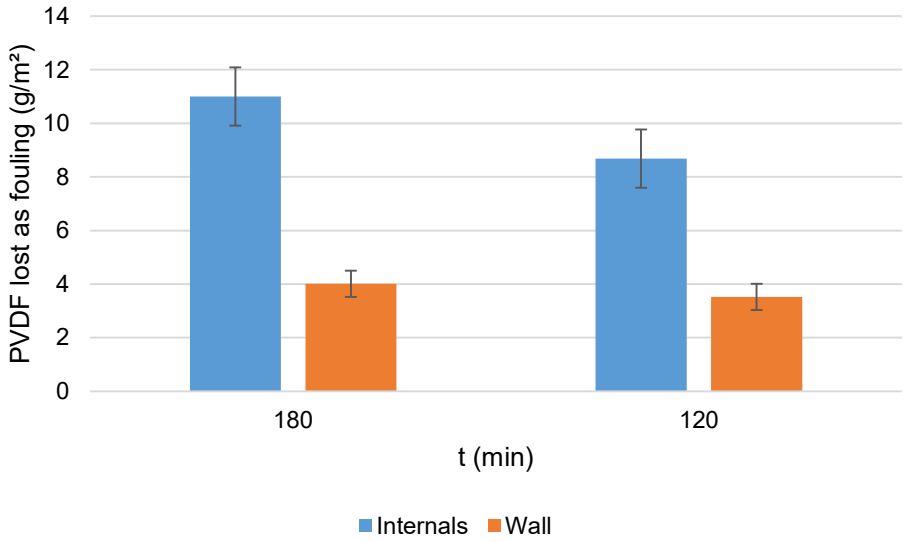

Figure 4.19 Density of PVDF lost as fouling in different areas of the reactor for different polymerization times producing a latex with the same solid content.

Second, the time particles are under shearing in the reactor is not the same, and an increase of time can increase fouling. Third, two polymers with a very different molecular weight were produced.

For the reaction performed at 180 min the PVDF lost as fouling represents 0.14 % and for the reaction producing the same solid content but in 120 minutes, the PVDF lost as fouling is equal to 0.12 %. Both reactions produced virtually the same amount of fouling for the same solids content, the only difference is found in its distribution inside the reactor. It can therefore be concluded that the solids content has a more important effect on fouling than the reaction time and the polymer molecular weight.

The amount of fouling on the hydrofoil and reactor wall are presented in Figure 4.20 and Figure 4.21. It seems that the fouling for both reactions (producing a

latex with the same solids content but in different times and polymer Mw) is almost the same.

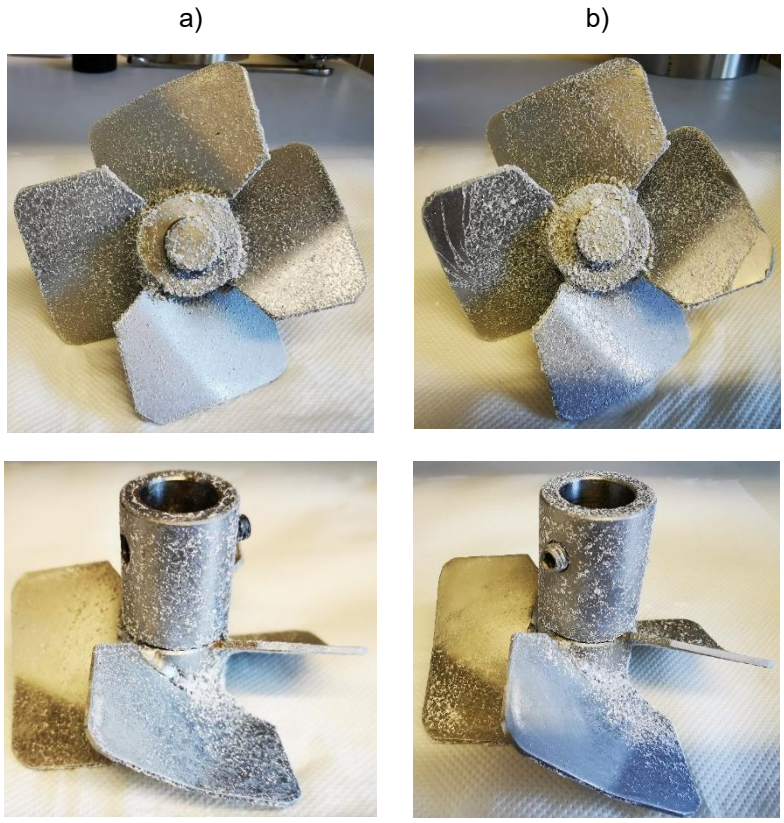

Figure 4.20 Bottom and side views of the material attached to the hydrofoil after the semi-batch reactions producing the same solid content in different times a) 180 min and b) 120 min.

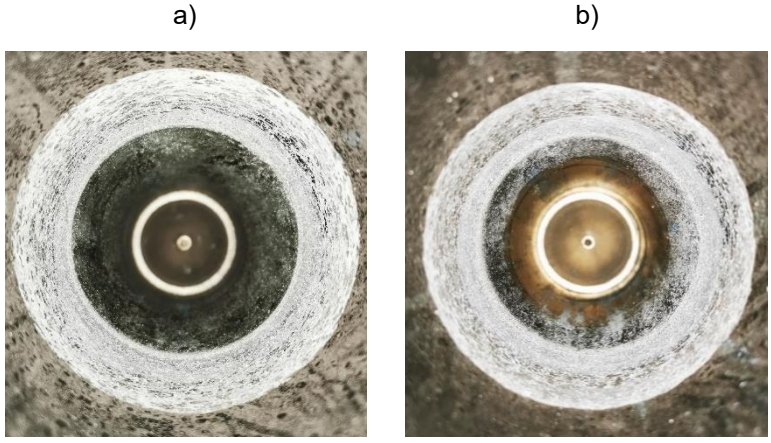

Figure 4.21 Top view from the reactor wall showing the attached material after the semi-batch reactions producing the same solid content in different times a) 180 min and b) 120 min.

4.3.2.2.5 Effect of solids content - by changing the CTA concentration

As the decrease of the concentration of CTA leads to higher polymerization rates and consequently, higher solids content for the same time, the effect of the solids content on fouling was investigated by changing the CTA concentration. Taking

as reference the reaction that produced the lowest amount of fouling (TA = 3.00 g/L and 180 min), together with a lower concentration of CTA, a latex with a higher solids content for the same polymerization time was produced. The results are presented in the Table 4.12.

Table 4.12 Semi-batch reactions performed with different concentrations of CTA (TA = 3.0 g/L).

CTA (g/L)	**15.3**	**7.8 A**	**7.8 B**
SC (%)	36.7	49.6	46.5
Dp (nm)	193	230	218
PdI	0.02	0.02	0.01
Npx10^{-19} (1/m³)	7.0	6.3	6.5
θ (%)	11.8	9.5	9.9
Mw (kDa)	452	1,034*	1,127*
PDI	2.92	3.25	3.52
PVDF lost as fouling (%)	0.03	0.19	0.34

* Samples presenting more than one peak for MW distribution, out of the calibration curve. Only the peak in the range of the calibration data is presented.

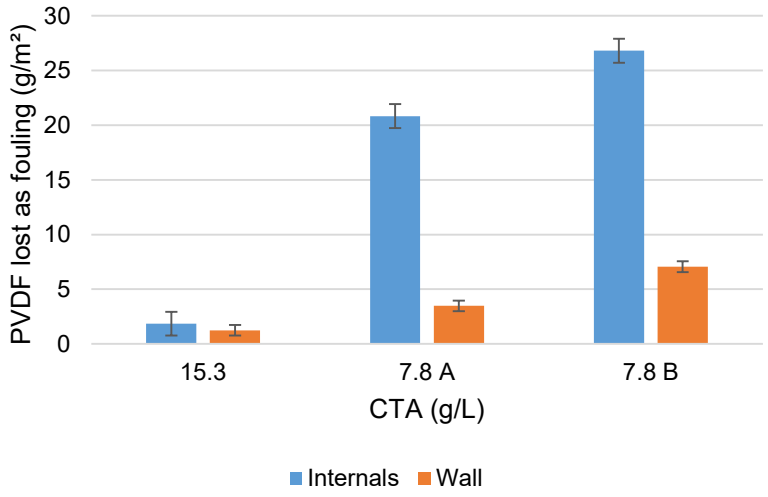

Figure 4.22 shows the increase in the PVDF lost as fouling on the wall when the solids content goes from 37 to 50 %. But, the increase was more important for the reaction 7.8 B.

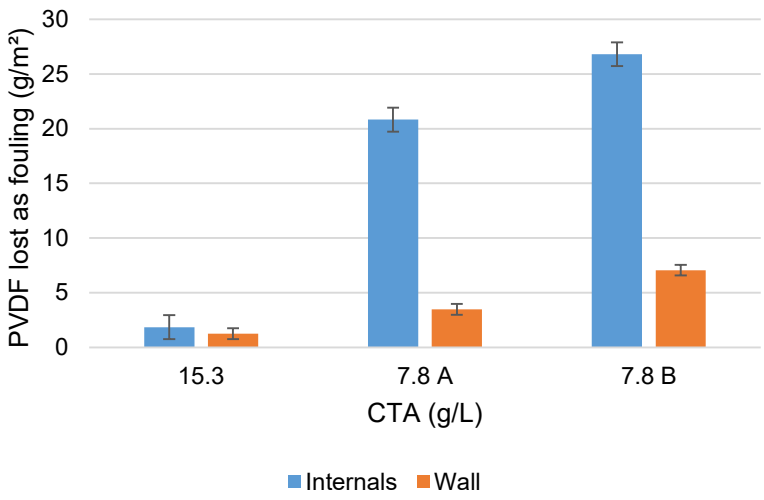

Figure 4.22 Density of PVDF lost as fouling in different areas of the reactor for different CTA concentrations (TA = 3.0 g/L).

Reactions A and B were similar except the depressurization/pressurization process used to collect samples during the reaction. As at the moment a system to collect samples at high pressure was not part of the reactor, it was necessary to depressurize the reactor, and then pressurize again to continue with the polymerization. The estimated total delay between the pressurization after sample collection and the resume between reaction A and B was about 30 minutes. As a result of increasing the solids content to 50 wt%, the reactions 7.8 A and 7.8 B produced respectively 88 and 62 g of destabilized latex (i.e. mass of coagulation). Also, we observed the increase of the molecular weight of the polymer in these reactions as well as the presence of tailing in the distribution, as shown in Figure 4.23.

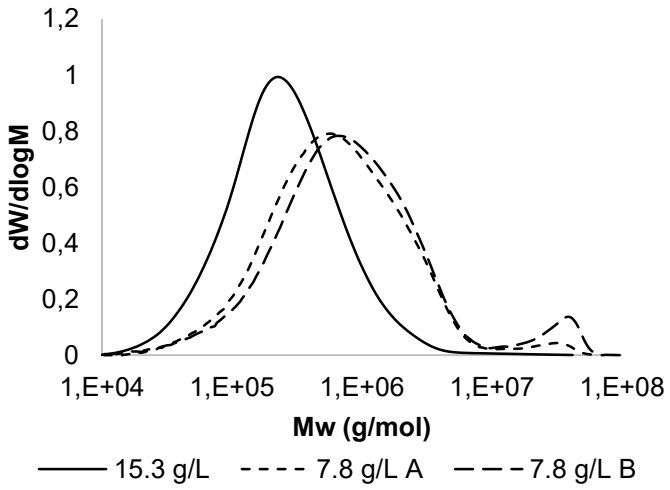

Figure 4.23 Molecular weight distribution for the semi-batch reactions performed with different CTA concentrations. * Molecular weight values above 1 million are out of the calibration curve.

As the surfactant concentration was not changed, this increase in the solids content led to a decrease in the surface coverage, but the value is still high compared to reactions that produced a destabilized latex. Even in these conditions the latex destabilization was observed as mentioned in the coagulation chapter. As noticed before, the destabilization of latex increases the fouling mainly in the internals of the reactor as opposed to the wall.

The pictures showing the fouling on the hydrofoil and reactor wall are presented in Figure 4.24 and Figure 4.25 from the most clean condition to the most dirty one regarding the fouling on the reactor after the polymerization. Unfortunately, the picture from the wall after the reaction 7.8 A was not taken. The presence of two “rings” of fouling on the wall for the reaction 7.8 B is due to the depressurization and pressurization procedure used to collect samples during the reaction, and the total mass of PVDF lost as fouling for this reaction is 4.11 g.

The percentage of PVDF lost as fouling for the reaction performed with 15.3 g/L of CTA is 0.03 %, while the reaction 7.8 g/L A is 0.19 % and the reaction 7.8 g/L B is 0.34%. It can be noticed that the depressurization/pressurization process generated the double of the amount of fouling.

a) b) c)

Figure 4.24 Bottom and side views of the material attached to the hydrofoil after the semi-batch reactions at different CTA concentrations a) 15.3 g/L, b) 7.8 g/L A and c) 7.8 g/L B.

a) b)

Figure 4.25 Top view from the reactor wall showing the attached material after the semi-batch reactions at different CTA concentrations a) 15.3 g/L and b) 7.8 g/L B.

4.3.2.2.6 Effect of depressurization rate

At the end of polymerization, the remaining amount of gas in the reactor is purged, and from the previous results it seems that the rate this depressurization is performed can affect the fouling in the reactor as the release of gas under pressure is a method for foam generation [56]. To check this effect, two different depressurization rates were tested at the end of a polymerization performed with the same recipe and conditions. The fast depressurization rate is equal to 8 bars/min and the low depressurization rate is equal to 2 bars/min.

Figure 4.26 shows the pictures taken from the reactor head after the two different depressurization rates performed.

a) b)

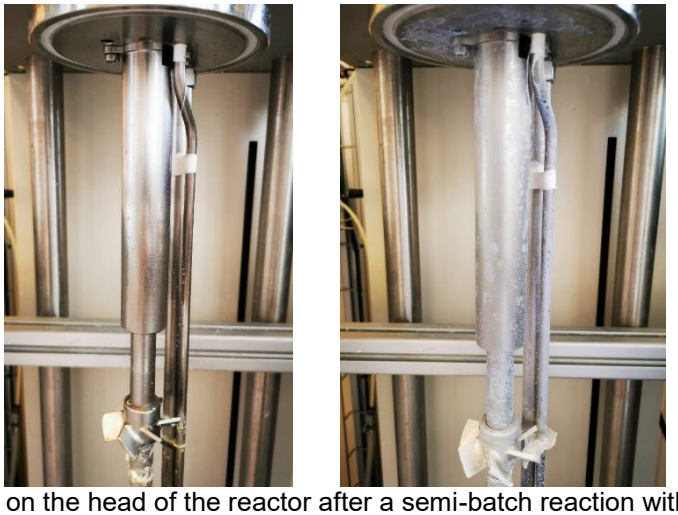

Figure 4.26 Fouling on the head of the reactor after a semi-batch reaction with depressurization rate of a) 8 bars/min and b) 2 bars/min.

It can be seen that the low depressurization rate produced a deposition of particles reaching the top of the reactor, which is not observed when the fast depressurization is performed. So, it is preferable to perform a fast depressurization of the reactor to avoid this additional fouling at the end.

As the foaming formation phenomena are not the subject of this thesis, future studies about it must be realized to investigate the causes and ways to avoid it, has an impact on fouling creation.

4.3.3 Properties of polymer deposits

After the end of some reactions, the material attached to the reactor's wall was collected and analyzed by DSC and SEC to check any difference could be detected between it and the PVDF in the free-flowing latex.

As the reactor is cooled down to 30 ºC at the end of the reaction, the wax will go back to its solid state and as its density is lower than the density of water, during the cooling down of the reactor, the wax will move to the liquid interface but it can also be found on the surfaces of the reactor. So, in some cases the material on the wall was collected above the interfacial layer of wax (called W1), in the

interface (called WI) and below it (called W2), as showed in the Figure 4.27. The DSC and molecular weight results are presented in the following sections.

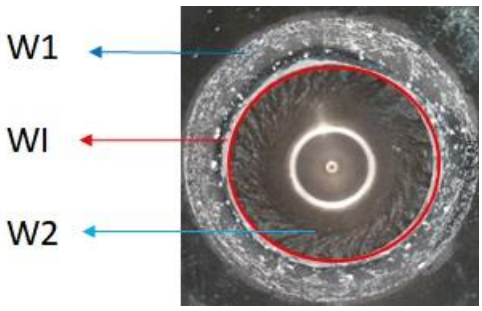

Figure 4.27 Areas of the reactor wall from which the material was collect for analysis.

4.3.3.1 Differential Scanning Calorimetry

The analysis was performed following the DSC procedure described in chapter 2. From Figure 4.28, is possible to notice that when comparing to the main PVDF latex (curve EKG_SB03, 10,2100 mg), the samples from the attached materials do not show a significant difference in the crystallization temperature. But, it can be seen that the crystallinity is lower, most likely because wax is present in the wall material. The peaks found around 30 and 50 ºC are related to the wax.

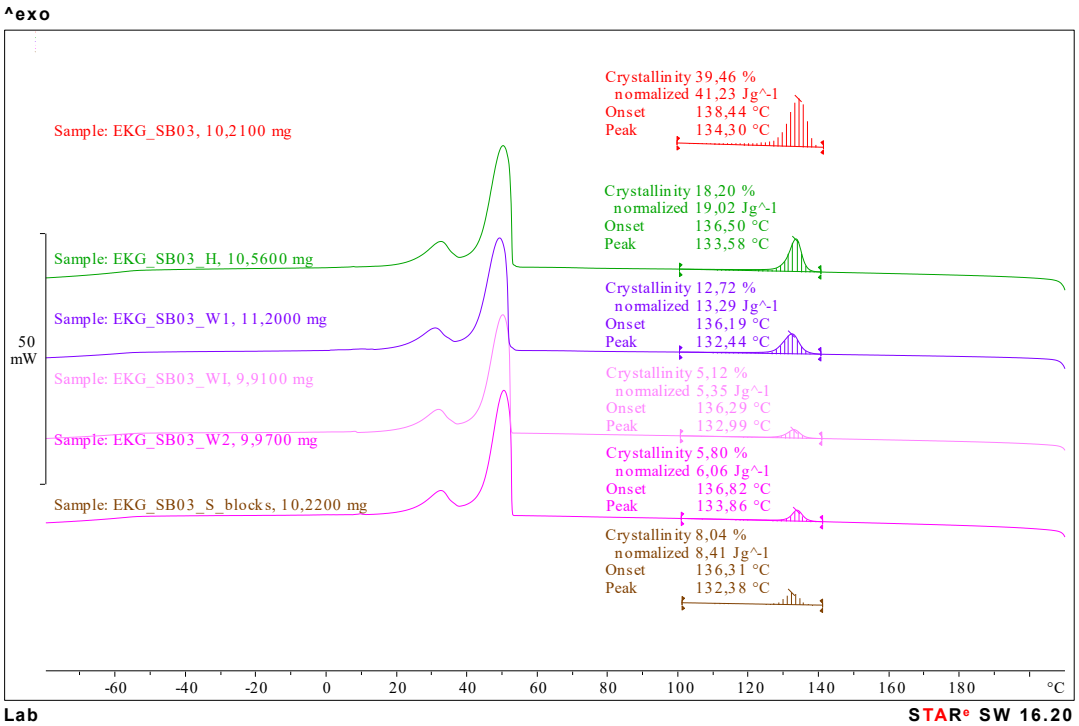

Figure 4.28 Example of DSC cooling curve for latex and the material collected from the reactor.

Figure 4.29 shows that there is no significant difference in the melting temperature of the attached materials, and as the amount of PVDF in the sample is small, it makes it difficult to determine the glass transition temperature. Once again it is possible to see the peaks related to the wax around 30 and 50 ºC.

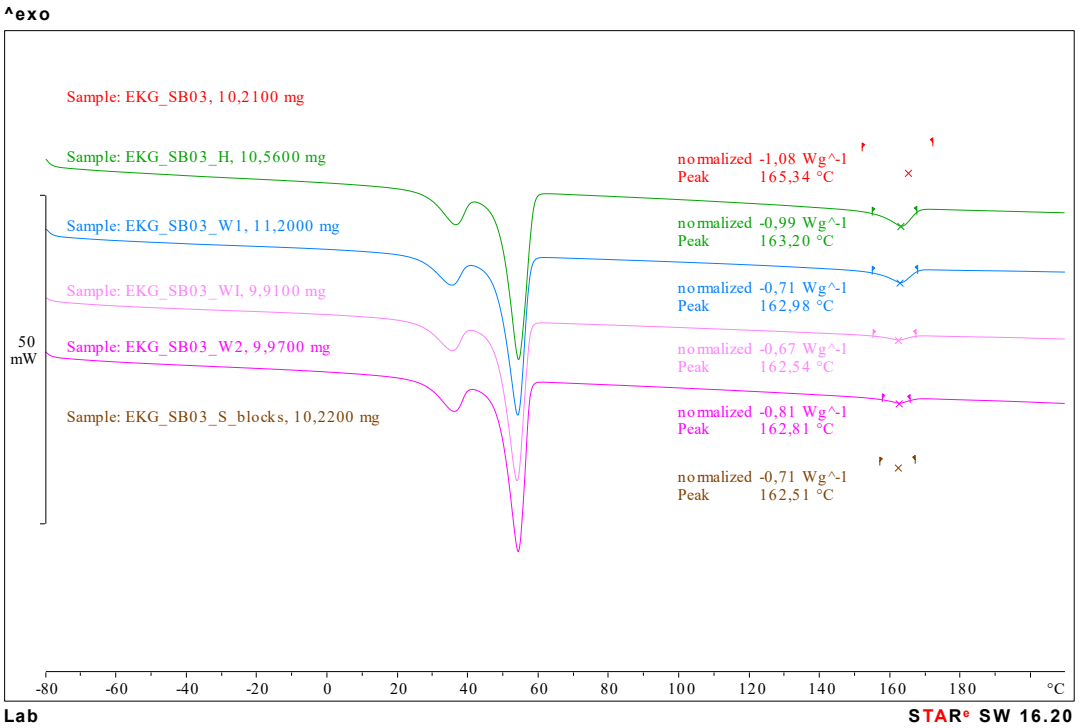

Figure 4.29 DSC second heating curve for latex (red) and the material collected from the reactor wall (other colors).

Some samples presented an interesting difference in the peak related to the melting temperature of PVDF for the material collected from the hydrofoil, where two melting temperatures could be identified and the molecular weight analysis of the latex collected was showing only one peak. All the results obtained for this kind of investigation are presented in the Table 4.13.

Table 4.13 DSC results comparing the original produced latex and the material collected from the reactor's surfaces.

Sample	Mass (mg)	Tg (°C)	Tm (°C)	Tc (°C)	Cryst (%)
B155.135.35	11.68	-45.95	170.17	131.68	55.04
Hydrofoil	10.33	-	166.08 169.59	135.98	13.71
B155.135.11	10.23	-44.36	167.74	131.29	53.61
Hydrofoil	10.22	-	166.45 170.11	135.47	13.65

Sample	Mass (mg)	Tg (°C)	Tm (°C)	Tc (°C)	Cryst (%)
B150.153.11	9.85	-40.22	170.47	130.91	46.89
Hydrofoil	9.59	-	167.24 170.91	137.12	14.55
B150.153.00	10.35	-44.22	170.38	130.87	51.91
Shaft	10.26		170.21 166.42	134.27	52.37
W2	10.36		170.03	136.98	51.93
B125.153.11	10.23	-42.07	170.76	130.01	51.84
Shaft	10.9		170.33 166.01	136.56	18.65
Hydrofoil	10.21	-	170.39 166.23	135.83	13.81
22S150.068.11.115	10.19	-44.36	167.75	128.22	48.39
Hydrofoil	9.15	-	164.32	135.04	10.68
WI	9.86	-	164.50	133.51	1.31
W1	9.89	-	164.65	133.26	10.53
W2	10.46	-	164.50	133.85	2.91
22S150.031.05.95	10.21	-44.38	165.34	134.30	39.28
Hydrofoil	10.56	-	163.20	133.58	15.92
W1	11.2	-	162.98	132.44	11.35
WI	9.91	-	162.37	132.99	4.19
W2	9.97	-	162.64	133.86	4.69

It can be concluded that there is no difference in the thermal properties of the PVDF recovered as latex or as material attached to the reactor's surfaces.

4.3.3.2 Fouling Molecular Weight

For some of the presented semi-batch reactions, the material attached to the shaft and hydrofoil were collected and analyzed to compare its molecular weight to the molecular weight of the latex recovered after the reaction.

The results are presented in the Table 4.14 and the only reaction presenting a difference between the latex and the fouling is the reaction S150.080.11.120 where the fouling recover has a bimodal distribution and the average molecular weight is bigger than the one of the latex produced. It is worth to mention that the molecular weight results above 1000 kDa are the result of an extrapolation of the calibration data. From the results presented, it is not possible to assume that there is a specific tendency for fouling when the molecular weight is low or high.

Table 4.14 Weight average molecular weight.

	Overall		Peak 1		Peak 2	
Sample	**Mw (kDa)**	**PDI**	**Mw (kDa)**	**PDI**	**Mw (kDa)**	**PDI**
S075.153.11.180B	432	2.94	-	-	-	-
Shaft	436	2.75	-	-	-	-
S075.153.11.120	382	2.60	-	-	-	-
Shaft	380	2.53	-	-	-	-
Hydrofoil	352	2.92	-	-	-	-
S150.080.11.120	910	3.72	-	-	-	-
Shaft	2055	6.52	29278	1.20	1011	3.34
Hydrofoil	1819	7.76	30058	1.15	1063	6.53
S300.080.11.180A	1534	4.71	26225	1,19	1034	3.25
Shaft	2437	8.16	29865	1.19	1010	3.67
Hydrofoil	2017	5.91	28396	1.24	1092	3.28
S300.080.11.180B	2721	8.11	31267	1.20	1127	3.52
Shaft	3098	10.26	33181	1.20	1174	4.17
Hydrofoil	2155	6.54	28422	1.21	1142	3.82

4.4 Conclusions

According to the experimental results on fouling formation during PVDF emulsion polymerization, it is possible to assume that fouling can have several different causes and that it is difficult to isolate them when performing a reaction. The deposition of a material is heterogeneous and follows the flow pattern in the reactor. It was also observed that the fouling in the area of the reactor initially filled with water is different from the fouling created during the reaction due to the vortex at the water-air interface and splashing of liquid.

The effectiveness of the wax as anti-fouling agent was confirmed, as well as the use of electropolished surfaces, generating always the lowest density of deposition in all the cases analyzed. The mass of material deposited on the wall is not enough to generate a sensitive change on the overall heat exchange coefficient of the jacketed part of the reactor.

As expected, the increase of the surfactant concentration provides more stability to the latex, decreasing the amount of fouling produced. However, when the latex was destabilized during the polymerization, it was noticed that the fouling increased mainly in the reactor's internals.

While producing a latex with the same solids content but in different times, the fouling was the same, leading to the conclusion that the main influence on fouling is the solids content, not the duration of the reaction, even if the latexes had a very different molecular weight or different concentrations of CTA.

It was found that the rate of depressurization of the monomer after the end of the reaction has an impact in the fouling, and there is no difference in the thermal properties or the molecular weight between the PVDF produced (as the latex or that found on the reactor's surface as fouling), that can lead to an explanation for the deposition.

It seems that the keys to have a low deposition of PVDF during the emulsion polymerization is to work with enough surfactant to keep the latex stable, use electropolished surfaces for all the parts of the reactor and depressurize the reactor fast at the end of the reaction as shown in Table 4.15 and Table 4.16.

Table 4.15 Quantitative fouling and coagulation results for different factors analyzed.

Analysis	Volume of water (L)	Time (min)	TA (g/L)	CTA (g/L)	SC (wt%)	Npx10^{-19} (1/m3)	θ (%)	Mw (kDa)	PVDF lost as fouling (%)	PVDF lost as coagulum (%)
a	**2.2**	180	1.50	15.3	32	4.0	8.0	257	0.05	0
	1.6	180	1.50	15.3	39	4.6	6.4	415	0.14	0
b	1.6	180	**0.75**	15.3	35	2.6	4.2	401	0.16	6.5
	1.6	180	**1.50**	15.3	39	4.6	6.4	415	0.14	0
	1.6	180	**3.00**	15.3	37	7.0	11.8	452	0.03	0
c	1.6	**180**	0.75	15.3	35	2.6	4.2	401	0.16	6.5
	1.6	**120**	0.75	15.3	29	2.4	5.1	382	0.06	0
d	1.6	**180**	1.50	**15.3**	39	4.6	6.4	415	0.14	0
	1.6	**120**	1.50	**7.9**	38	4.7	6.6	910	0.12	0
e	1.6	180	3.00	**15.3**	37	7.0	11.8	452	0.03	0
	1.6	180	3.00	**7.8**	50	6.3	9.5	>1000	0.19	2.9
f	1.6	180	3.00	7.8	50	6.3	9.5	>1000	0.19	2.9
	1.6	180	3.00	7.8	46	6.5	9.9	>1000	0.34	2.4

Table 4.16 Qualitative results about fouling for PVDF latex.

Mechanism	Experiment	Factor	
Perikinetic	SS316 impellers in contact with pre-formed latex 20 wt%	Metals • SS316 / Aluminum • SS316 / non-galvanized steel	Passivation layer does not increase with time ↑ Fouling when 2 metals with different potentials are in contact
Orthokinetic	Batch reactions	Presence or absence of wax in the recipe	↓ Fouling in the presence of wax
	Batch and Semi-batch reactions	Surface treatment	↓ Fouling when using electropolished surfaces (↓ roughness)
	Semi-batch reactions	a) Mixing effect - Reaction volume (L): • 1.6 • 2.2	↑ Fouling when working with a better mixing (↑ SC and ↓ θ)
		b) Surfactant concentration (g/L): • 0.75 • 1.50 • 3.00	↓ Fouling when working with a higher surfactant concentration (↑ θ)
		c) Reaction time (min) (TA = 0.75 g/L): • 180 • 120	↑ Fouling with reaction time (↑ SC, ↓ θ)
		d) Reaction time (min) (TA = 1.50 g/L): • 180 (CTA = 15.3 g/L) • 120 (CTA = 7.8 g/L)	There is no influence of reaction time on fouling if the same solids content is obtained at the end
		e) Solids content (wt%) (TA = 3.00 g/L, time = 180 min): • 37 (CTA = 15.3 g/L) • 50 (CTA = 7.8 g/L)	↑ Fouling with solids content (↓ θ)
		f) Depressurization rate (bar/min): • 8 (at the end of the reaction) • 2 (to recover a sample by decompressing / compressing the reactor plus at the end of the reaction)	↑ Fouling when decreasing the depressurization rate

REFERENCES

[1] Plastic Market Size, Share & Trends Analysis Report by Product, by Application, by End-use, by Region, and Segment Forecasts, 2021-2028 2021:230. https://www.grandviewresearch.com/industry-analysis/global-plastics-market (accessed May 18, 2021).

[2] Jasinski F, Zetterlund PB, Braun AM, Chemtob A, Jasinski F, Zetterlund PB, et al. Photopolymerization in dispersed systems. Prog Polym Sci 2018;84:47–88.

[3] Cheng D, Ariafar S, Sheibat-Othman N, Pohn J, McKenna TFL. Particle Coagulation of Emulsion Polymers: A Review of Experimental and Modelling Studies. Polym Rev 2018;58:717–59. doi:10.1080/15583724.2017.1405979.

[4] Jeldres RI, Fawell PD, Florio BJ. Population balance modelling to describe the particle aggregation process: A review. Powder Technol 2018;326:190–207. doi:10.1016/j.powtec.2017.12.033.

[5] Sheibat-Othman N, Vale HM, Pohn JM, McKenna TFL. Is Modeling the PSD in Emulsion Polymerization a Finished Problem? An Overview. Macromol React Eng 2017;11:1–32. doi:10.1002/mren.201600059.

[6] Zhang J, Morris AJ, Martin EB, Kiparissides C. Estimation of impurity and fouling in batch polymerisation reactors through the application of neural networks. Comput Chem Eng 1999;23:301–14. doi:10.1016/S0098-1354(98)00275-0.

[7] Cardoso MN, Fisch AG. Mechanism of Fouling in Slurry Polymerization Reactors of Olefins. Ind Eng Chem Res 2016;55:9426–32. doi:10.1021/acs.iecr.6b02490.

[8] Urrutia J, Peña A, Asua JM. Reactor Fouling by Preformed Latexes. Macromol React Eng 2017;11:1–14. doi:10.1002/mren.201600043.

[9] Henry C, Minier JP, Lefèvre G. Towards a description of particulate fouling: From single particle deposition to clogging. Adv Colloid Interface Sci

2012;185–186:34–76. doi:10.1016/j.cis.2012.10.001.

[10] Kemmere MF, Meuldijk J, Drinkenburg AAH, German AL. Colloidal Stability of High-Solids Polystyrene and Polyvinyl Acetate Latices. J Appl Polym Sci 1999;74:1780–91.

[11] Henry C, Minier JP, Lefèvre G. Numerical study on the adhesion and reentrainment of nondeformable particles on surfaces: The role of surface roughness and electrostatic forces. Langmuir 2012;28:438–52. doi:10.1021/la203659q.

[12] Van de Ven TGM. The capture of colloidal particles on surfaces and in porous material: Basic principles. Colloids Surfaces A Physicochem Eng Asp 1998;138:207–16. doi:10.1016/S0927-7757(96)03956-8.

[13] Lowry V, El-Aasser MS, Vanderhoff JW, Klein A, Silebi CA. Kinetics of Agitation-Induced Coagulation of High-Solid Latexes. J Colloid Interface Sci 1986;112:521–9. doi:10.1016/0021-9797(86)90121-9.

[14] Thomas TR. Characterization of surface roughness. Precis Eng 1981;3:97–104. doi:10.1016/0141-6359(81)90043-X.

[15] Glass Lined Process Reactors 2017. https://worldindustrialreporter.com/glass-lined-process-reactors/ (accessed January 15, 2021).

[16] Euro Inox. Roughness measurements of stainless steel surfaces 2014:1–7. https://www.worldstainless.org/Files/issf/non-image-files/PDF/Euro_Inox/RoughnessMeasurement_EN.pdf.

[17] Watkinson AP. Chemical reaction fouling of organic fluids. Chem Eng Technol 1992;15:82–90. doi:10.1002/ceat.270150203.

[18] Gottschalk N, Kuschnerow JC, Föste H, Augustin W, Scholl S. Experimentelle untersuchung zur foulingneigung einer polymerdispersion auf modifizierten oberflächen. Chemie-Ingenieur-Technik 2015;87:600–8. doi:10.1002/cite.201400126.

[19] Hohlen A, Augustin W, Scholl S. Quantification of Polymer Fouling on Heat Transfer Surfaces During Synthesis. Macromol React Eng 2020;14.

doi:10.1002/mren.201900035.

[20] Urrutia J, Asua JM. Reactor Fouling in Emulsion Polymerization. Ind Eng Chem Res 2021. doi:10.1021/acs.iecr.1c00097.

[21] Vanderhoff JW. The Formation of Coagulum in Emulsion Polymerization. In: Basset DR, Hamielec AE, editors. Emuls. Polym. Emuls. Polym., Washington, D.C.: American Chemical Society; 1981, p. 199–208.

[22] McFadden DM, Wu RS-H. REDUCTION OF POLYMER FOULING ON REACTOR SURFACE IN A CONTINUOUS PROCESS FOR PREPARING POLYMERS. US6380324B1, 2002. doi:10.1038/incomms1464.

[23] Böttcher A, Petri J, Langhoff A, Scholl S, Augustin W, Hohlen A, et al. Fouling Pathways in Emulsion Polymerization Differentiated with a Quartz Crystal Microbalance (QCM) Integrated into the Reactor Wall. Macromol React Eng 2022;2100045:1–8. doi:10.1002/mren.202100045.

[24] Kleine W, Frey W, Däweritz A. METHOD OF INHIBITING POLYMER DEPOSITION ON REACTOR WALLS DURING FREE-RADICAL POLYMERIZATION. 4661569, 1987.

[25] Watanabe M, Usuki M, Ueno S. Method for preventing polymer scale deposition. 0458267B1, 1991.

[26] Shimizu T, Kaneko I, Watanabe M. METHOD OF PREVENTING POLYMER SCALE DEPOSITION. 5053466, 1991.

[27] Shimizu T, Kaneko I, Watanabe M. METHOD OF PREVENTING POLYMER SCALE DEPOSITION IN A POLYMERIZATION VESSEL. 5115051, 1992.

[28] Shimizu T, Watanabe M. PROCESS FOR PRODUCING POLYMER WHEREIN POLYMER SCALE DEPOSITION IS PREVENTED. 5442017, 1995.

[29] Usuki M, Kitamura H, Ueno S, Watanabe M, Yono M. PROCESS TO PREVENT POLYMER SCALE ADHESION USING AN AROMATIC COMPOUND AND A SALT OF POLYVINYLSULFURIC ACID. 5430113, 1995.

[30] Watanabe M, Shimizu T. PROCESS OF PRODUCING POLYMER USING A POLYMER SCALE DEPOSITION PREVENTIVE AGENT. 5723553, 1998.

[31] Polacco F. ANTI-FOULING AGENT FOR THE POLYMERIZATION OF OLEFINIC CHLORIDE MONOMERS. WO88/05055, 1988.

[32] Geddes KR. PROCESS FOR REDUCING REACTOR FOULING DURING POLYMERIZATION IN AN AQUEOUS MEDIUM. 4957982, 1990.

[33] Shimizu T, Ueno S, Kaneko I, Watanabe M. METHOD OF PREVENTIVE POLYMER DEPOSITION AND POLYMER SCALE PREVENTIVE AGENT. 5214112, 1993.

[34] Idelmann P, Palmqvist U, Münstedt H. ANTIFOULING COATING. WO97/49771, 1997.

[35] Watanabe M, Usuki M, Ueno S. METHOD OF PREVENTING POLYMER SCALE DEPOSITION AND POLYMER SCALE PREVENTIVE LIQUID USED THEREIN. 5147455, 1992.

[36] Shimizu T, Shigemitsu M. POLYMER SCALE PREVENTIVE AGENT, POLYMERIZATION VESSEL FOR PREVENTING POLYMER SCALE DEPOSITION, AND PROCESS OF PRODUCING POLYMER USING SAID VESSEL. 5378775, 1995.

[37] Shimizu T, Shigemitsu M. PROCESS TO PREVENT POLYMER SCALE ADHESION USING A TWO PART COATING. 5418302, 1995.

[38] Ueno S, Kaneko I, Watanabe M. METHOD OF PREVENTING POLYMER SCALE DEPOSITION. 5037904, 1991.

[39] Balwe T, Bauer J, Fendel K, Kurz D, Sabel A. PROCESS FOR SUSPENSION POLYMERIZATION OF VINYL CHLORIDE WITH LOW POLYMER DEPOSITION. 3817959, 1974.

[40] Wempe LK, Bauman BD. METHOD FOR REDUCING WALL FOULING IN VINYL CHLORIDE POLYMERIZATION. 4420591, 1983.

[41] Kitamura H, Ueno S, Watanabe M, Usuki M, Nakano T. POLYMER SCALE

PREVENTIVE AGENT FROM NAPHTHOQUINONE DYE. 5360857, 1994.

[42] Goetze U, Wole A, Nettesheim G, Balwe T, Bauer J, Fendel K, et al. PROCESS FOR SUSPENSION POLYMERIZATION OF VINYL HALIDES WITH LOW POLYMER DEPOSITION. 3923765, 1975.

[43] Collete C, Garnier C, Guenez D, Tembou Nzudie D. METHOD FOR PREVENTING REACTOR FOULING IN THE SYNTHESIS OF WATER SOLUBLE POLYMERS. WO96/18656, 1996.

[44] Fitzwater SJ, McFadden DM. Continuous process for preparing polymers. EP 1136505 A1, 2001.

[45] Buchelli A, Call ML, Brown AL, Bird A, Hearn S, Hannon J. Modeling Fouling Effects in LDPE Tubular Polymerization Reactors. 1. Fouling Thickness Determination. Ind Eng Chem Res 2005;44:1474–9. doi:10.1021/ie040157q.

[46] Buchelli A, Call ML, Brown AL, Bird A, Hearn S, Hannon J. Modeling Fouling Effects in LDPE Tubular Polymerization Reactors. 2. Heat Transfer, Computational Fluid Dynamics, and Phase Equilibria. Ind Eng Chem Res 2005;44:1480–92. doi:10.1021/ie040158i.

[47] Buchelli A, Call ML, Brown AL, Bird A, Hearn S, Hannon J. Modeling Fouling Effects in LDPE Tubular Polymerization Reactors. 3. Computational Fluid Dynamics Analysis of a Reacting Zone. Ind Eng Chem Res 2005;44:1493–501. doi:10.1021/ie040159a.

[48] Fries S, Castañeda-Zúñiga DM, Duchateau J, Neuteboom P, Porras CT, Busch M. Fouling in the High Pressure LDPE Process: Experimental and Computational Investigation Approach. Macromol Symp 2016;360:78–86. doi:10.1002/masy.201500112.

[49] Begall MJ, Krieger A, Recker S, Herbstritt F, Mhamdi A, Mitsos A. Reducing the Fouling Potential in a Continuous Polymerization Millireactor via Geometry Modification. Ind Eng Chem Res 2018;57:6080–7.

[50] Stainless Steel in Contact with Other Metallic Materials 2009.

[51] Stefanichen Monteiro I, Mendez Ecoscia AC, McKenna TFL. Investigation

of the Chain Transfer Agent Effect on the Polymerization of Vinylidene Fluoride. Ind Eng Chem Res 2019;58:20976–86. doi:10.1021/acs.iecr.9b02755.

[52] Bottino A, Capannelli G, Munari S, Turturro A. Solubility Parameters of Poly(vinylidene fluoride). J Polym Sci Part B Polym Phys 1988;26:785–94.

[53] Amin-Sanayei R, Olmstead C. Aqueous Process for Making Fluoropolymers. US20070270534A1, 2007.

[54] Hedhli L. Polymerization of Fluoropolymers Using Polycaprolactone. EP2274345B1, 2009.

[55] Durali M, Hedhli L. Method of Producing Fluoropolymers Using Acid-Functionalized Monomers. US9434837B2, 2016.

[56] Pugh RJ. Generation of bubbles and foams. Bubble Foam Chem., Cambridge University Press; 2016, p. 155–93. doi:10.1017/cbo9781316106938.006.

CHAPTER 5. MIXING EFFECTS DURING VDF POLYMERIZATION

5.1 Introduction

The complexity of the emulsion polymerization process is due to various phenomena occurring at different scales, like the ones occurring in particle size scale like the adsorption of surfactant and mass transfer (radicals, monomer, diffusion limitations); the ones in a mesoscale including interactions between particles as well as the influence of the particle distribution on the fluid rheology; and finally the events at the reactor scale such as the effect of mixing [1].

More particularly, the emulsion polymerization kinetics is dependent on the monomer concentration in the polymer particles. When a gas monomer is used, the mass transfer coefficient and the total area of monomer particles affect the transfer of monomer from the gas phase to polymer particles [2]. The mass transfer coefficient is directly influenced by the mixing process. The effect of agitation on the monomer conversion, polymer MW should be evaluated for different speeds or agitation set-up [2,3].

5.2 Literature Review

5.2.1 Mechanically Stirred Vessels

Mechanically stirred vessels are used in a variety of processes in the industry to homogenize single or multiple phases in terms of concentration of chemicals and temperature, which will help to produce a product with uniform properties [4]. A good mixing can increase profitability especially in applications where mass transfer is limiting the yield.

When studying the mixing in a vessel equipped with an impeller, there are three main components to be taken into consideration: the process design, the mechanical design of the impeller and the impeller power characteristics [5]. The process design comprises the fluid mechanics of the impellers (in agreement with the fluid regime required by the mixing process) and the scale-up similarities. The

mechanical design is related to the impellers, shaft and drive assembly and the impeller power characteristics takes into consideration the impeller speed and diameter, as well as the power consumption.

5.2.1.1 Impeller types

The flow pattern in the reactor must be chosen according to the application, and may involve gas-liquid, liquid-solid, miscible or immiscible liquids [5]. Some of the types of turbine impellers that will create different flow patterns and different levels of shearing are: axial flow, radial flow and hydrofoil. They are used in applications with low and medium liquid viscosity, suspension of solids, liquid-liquid emulsification and gas dispersion [4].

Axial Flow Impellers

Axial flow impellers move the fluid parallel to its axis of rotation [5]. They are used for blending, solids suspension, gas inducement, and heat transfer [4]. Propellers and the 45° pitched blade turbine (PBT) are examples of this type of impellers. As the PBT has components of flow velocity in axial and radial directions, it is considered as a mixed-flow impeller [4].

Radial Flow impellers

Radial flow impellers move the fluid along the impeller radius in different patterns [5]. The disc flat blade turbine, commonly called Rushton impeller, is an example of radial impeller. Radial impellers are more effective for gas-liquid and liquid-liquid dispersion and provide a higher shear and turbulence with lower pumping than the axial impellers.

Hydrofoil impellers

Hydrofoil (or high efficiency) impellers are axial flow impellers. They are designed for applications in which the axial flow is important but a low shear is desired [4]. The Lightin A315 and Prochem Maxflo are examples of hydrofoil impellers. These kind of impellers are effective for gas dispersion in viscous system, liquid blending and solids suspension. The hydrofoil impellers are able to pump a higher flow per unit power when compared to a PBT.

5.2.1.2 Characteristics of impellers

When talking about some of the characteristics of impellers, the pumping is related to the amount of material discharged by the impeller. Pumping is a function of impeller geometry, so each impeller has its pumping capacity and flow pattern.

As the impellers generate velocity gradients in the fluid, there will be shearing forces that are desired for the fluid intermixing, gas bubbles dispersion, and stretching / breaking liquid drops [4]. But at the same time, it can lead to coagulation and fouling as it increases the probability of collision among particles and between the particles the reactor surface, as observed in the previous chapters. So, a kind of compromise of mixing is required.

The difference in the velocity gradients in different parts of the reactor, is a function of the impeller blade pressure drop, agitation speed and viscosity and is function of the impeller type (axial or radial), diameter, and the use of multiple impellers. This makes difficult the determination of the distribution of shear in mechanically agitated reactors. Shear distributions can be obtained by computation fluid dynamics (CFD) [2,6,7].

A general overview of the pumping capacity, shearing and flow pattern for the different impellers mentioned previously is given in Table 5.1.

Table 5.1 Characteristics of axial and radial impellers.

<table>
<tr><th>Type</th><th>Pumping</th><th>Shearing</th><th colspan="2">Flow pattern</th></tr>
<tr><td>Axial</td><td colspan="2">Good balance between pumping and shearing</td><td rowspan="2">Flow pattern throughout the entire tank as a single stage</td><td>Small reverse loop underneath</td></tr>
<tr><td>Hydrofoil</td><td>High</td><td>Low</td><td>Streamlined discharge</td></tr>
<tr><td>Radial</td><td>Low</td><td>High</td><td colspan="2">Two circulating loops (above and below the impeller)</td></tr>
</table>

5.2.1.3 Reactors with multiple impellers

For tanks with high height / diameter ratio, multiple impellers are required to improve the circulation and narrow the distribution of shear and energy dissipation. When multiple impellers are used, it is important to tune the spacing between the impellers to ensure good pumping. If the spacing between impellers is lower than one impeller diameter, there will be interaction between them,

generating high shear [4,8]. Depending on the application, the flow of an axial impeller can be directed to the head (up-pumping) or to the bottom (down-pumping) of the reactor [9–11]. For gas dispersion applications, an efficient agitation set-up requires one up-pumping impeller at the bottom along with down-pumping impeller at the top. With this configuration, the radial flow impeller breaks and disperses the gas introduced from gas sparger, and the axial flow impeller circulates the gas-liquid flow [12]. There is also a minimal liquid level to keep on the top of the impeller. Indeed, to avoid splashing and vortex formation, the top impeller must not be located close to the liquid surface. In the cases the vortex created by the impeller rotation is two dimensional and causes swirling, baffles must be used to improve the mixing quality [4].

More information about the design of mechanically stirrer reactors can be found in the specialized literature as [4,5].

5.2.2 Gas-liquid mass transfer

When a contact between a gas and a liquid is important, it should be efficient and effective. The selection of the equipment to perform this operation must take into consideration some factors as [4]:

- Allowable pressure drop
- Relative flow rates of gas and liquid
- Mass transfer performance (dispersion size and turbulent mass transfer)
- Need to supply or remove heat
- Presence of solid particles
- Foaming behavior and phase separation
- Flow pattern requirements
- Rheological behavior in laminar and transitional flow regimes

During the operations of gas-liquid unbaffled stirred reactors, a vortex can be created depending on the agitation speed. Once this agitation is at the called critical impeller speed [13,14], the vortex reaches the impellers leading to the gas ingestion promoting a better gas dispersion. The vortex shape can be influenced

by the impeller geometry, speed and fluid viscosity [13,15–17]. This is an important factor to be considering during a reactor scale-up [16]. The ingestion of gas from the headspace by the vortex breakage is a way of increasing gas hold-up in a stirred vessel. But, the gas hold-up is also function of the bubble size and the degree of bubble recirculation [4]. Sparging the gas in the reactor will enhance the gas-liquid mass transfer since this increases the surface transfer area [18]. So, the used mixing system should allow both the incorporation of gas from the headspace of the reactor into the liquid as well as its uniform dispersion into the liquid phase.

In applications with multiphase reactions, the mass transfer from one phase into another is necessary. The mass is transferred from the phase with higher chemical potential to the one with the lower potential until equilibrium is reached [19]. The flux from the gas phase bubbles to the liquid is given by:

$$V_{\mathrm{L}} \frac{\mathrm{d}A_{\mathrm{l}}}{\mathrm{d}t} = k_{\mathrm{L}} a (A^{*} - A_{\mathrm{l}}) \tag{5.1}$$

where V_{L} is the volume of liquid in the reactor, A_{l} is the concentration of component A in the bulk liquid, t is the time, k_{L} is the liquid mass transfer coefficient, a is the gas-liquid interfacial area per unit of volume of the dispersion and A^{*} is the concentration of A in the liquid in equilibrium with the gas phase (here it will be assumed that it follows the Henry's law).

The determination of the mass transfer coefficient should be done based on the local bubble sizes and gas fractions, probably calculated by CFD [4] however, there are several measuring techniques for gas-liquid reactors [20,21], but one commonly used is the dynamic pressure method [10,11,21]. The dynamic pressure method consists in monitoring the pressure drop caused by the absorption of gas A in the liquid over time. The concentration of the gas A in the liquid is related to the pressure drop in the reactor as [21],

$$V_{\mathrm{L}} \frac{\mathrm{d}A_{\mathrm{l}}}{\mathrm{d}t} = -\frac{V_{\mathrm{g}}}{RT} \frac{\mathrm{d}P}{\mathrm{d}t} \tag{5.2}$$

where V_g is the volume of gas in the reactor, P is the pressure, R is the gas constant and T is the temperature.

After some mathematical manipulation of the previous equations, assuming that at time zero the pressure will be equal to P_b (registered before monomer addition), and that P_0 is the initial pressure, after adding the monomer (before starting the mass transfer) we have,

$$\ln\left[\frac{P_0 - P_b}{(1+C)(P(t) - P_b) - C(P_0 - P_b)}\right] = \left(1 + \frac{1}{C}\right) k_L a.t \qquad 5.3$$

$$C = \frac{P_f - P_b}{P_0 - P_f} = \frac{HV_g}{V_L RT}$$

where P is the pressure at a given time t, P_f is the final pressure obtained when equilibrium is reached after gas absorption and H is the Henry's law constant.

Rearranging the equation 5.3, the final equation to calculate the mass transfer coefficient will be [22],

$$\ln\left[\frac{P_0 - P_f}{P(t) - P_f}\right] = \left(\frac{P_0 - P_b}{P_f - P_b}\right) k_L a.t \qquad 5.4$$

So, by plotting $\ln\left[\frac{P_0 - P_f}{P(t) - P_f}\right]$ versus time, the value of $k_L a$ can be found by dividing the slope of the linear regression of the plotted curve by $\left(\frac{P_0 - P_b}{P_f - P_b}\right)$.

The obtained coefficient is valid for a specific impeller geometry (width and orientation of the blades) and position in the reactor, medium viscosity, and agitation speed. An increase in agitation speed increases the mass transfer coefficient due to the increased volumetric flow rate of ingested gas and the enhanced bubble breakup which increases their surface area [11,12,21,23]. The impeller distance to the liquid level, also affects the gas-liquid mass transfer [8,12,21]. This makes the determination of $k_L a$ a heavy task, as the level in the bed usually changes with time.

Chaudhari et al. [21] compared $k_{\mathrm{L}}a$ values for a dead-end reactor using different methods: dynamic physical absorption, catalytic hydrogenation of styrene and oxidation of sodium sulfite. From the results, it was possible to state that the different methods led to a similar mass transfer coefficient and that the mode of introduction of gas in the system also influences the coefficient. They found out that when a dip tube was used to introduced the gas, the $k_{\mathrm{L}}a$ values increased in 3 to 5 times, opposite to the results from Sardeing et al. [11] that reports the difference in the mass transfer coefficient, when gas is ingested by surface or sparger aeration, lower than 5 %.

An empirical correlation commonly used for $k_{\mathrm{L}}a$ calculation in a turbulent regime in a stirred vessel with a single impeller has the form [4],

$$k_{\mathrm{L}}a = \alpha \left(\frac{Po}{V}\right)^{\beta} v_{\mathrm{s}}^{\gamma} \qquad 5.5$$

where Po includes shaft power and gas buoyancy power and v_{s} is the gas superficial velocity. The constants α, β and γ are fitting parameters. This correlation is normally used for scale-up purposes but not for general prediction [4].

5.2.2.1 Studies regarding the Influence of Agitation in Emulsion Polymerization

As presented in the previous sections, the stirred reactor configuration and operational variables affect the mixing and mass transfer during gas-liquid operation, which will have consequences in a reaction that occurs in the liquid phase. As in emulsion polymerization there are more than one phase present, the following studies discuss the effects of agitation in this kind of systems, both including gas or liquid monomers.

Effect on the monomer droplet size and mass transfer

Evans et al. [24] studied the influence of stirring in batch emulsion polymerization of vinylidene chloride. The highest agitation speed tested gave a slower rate in the early stage of polymerization due to the increased area of liquefied monomer droplets that adsorbs surfactant. This increase in area reduces the effective

amount of surfactant that take part in nucleation and stabilization of the polymer particles. A similar trend was also observed by Weerts et al. and Omi et al. [25,26]. However, an increase in speed at the second stage of polymerization, enhanced the rate because in this stage the reaction is starved in monomer, and becomes diffusion controlled, so an increase in agitation increases the monomer transport from the droplets to the polymer particles.

Weerts et al. [25] reported the effects of mixing on the emulsion polymerization of butadiene. When the mixing does not provide enough turbulence in the system, there is a phase separation of the liquefied butadiene, so the mass and heat transfer are not optimal, leading to a low polymerization rate. The authors also observed that once the ratio monomer / water (M/W) increased, the turbine impeller is no longer providing sufficient agitation. In this case, a low pitch helical ribbon agitator was used, and gave the same performance conversion-time and particle number as the turbine impeller for a M/W equal to 5.

Roudsari et al. [6] used CFD to explore the effect of the agitator type, speed and baffles in the emulsion polymerization of MMA. In the model of the reactor, the mass transfer of monomer from the aqueous phase to the polymers affect nucleation and growth and the momentum balance determines its diffusion. The model was able to predict their previous results of conversion for the reactor with and without baffles and different agitation speeds (Roudsari et al. [27]). The lowest conversions observed when baffles were used were due to an accumulation of monomer phase near the tank wall, not observed in the absence of baffles. Replacing the PBT by a Rushton turbine increased the conversion and no reduction in conversion at high agitation rates was observed. At a low agitation speed as 100 rpm, the shear rate in the Rushton stirrer area led to the improvement of the mixing quality, collision of reactants, and diffusion of monomer to micelles, which resulted in a higher conversion in comparison with the PBT. Nevertheless, when an increase in speed to 250 rpm is done, the pumping action of PBT overcome the improved shearing of the Rushton impeller, resulting in a higher conversion for the PBT agitator.

Ecoscia et al. [22] studied the effects of mixing and reaction conditions on the initial rate of vinylidene fluoride emulsion polymerization. The increase in speed increases the polymerization rate for two the different set-up configurations, but

especially when using hydrofoil at the bottom, due to the improvement in mass transfer from monomer to the aqueous phase. This improvement in the mass transfer was also observed with the increase in molecular weight with the speed.

Effect of the emulsification of the initial charge

Omi et al. [26] studied the effect of agitation on the rate of polymerization of styrene. The results showed that when the pre-emulsion is sufficiently emulsified using a high speed mixer, the polymerization rate is independent of the agitation speed. In the cases the pre-emulsions were prepared with the reactor agitator, the nucleation period is the same, but the polymerization rate decreases when increasing the intensity of agitation, except in the cases there is a phase separation due to the poor mixing. As with the increase in agitation, the number of particles decreased, this may be due to an enhanced coagulation when increasing mixing, which decreases the polymerization rate.

Zubitur and Asua [2] studied the effect of agitation in semi-continuous emulsion polymerization of styrene and butyl acrylate (60/40) on conversion, number of particles and polymer molecular weight. When a pre-emulsified feed made with 300 rpm is used, high conversions can be achieved (even at low agitation speeds during the reaction), and there was no difference in the results of the speeds tested (100 and 150 rpm). This is a result already observed by Omi et al. [26] , because of the improved mass transfer by the total area of monomer particles. The reactions performed using pure monomer (with and without the presence of CTA) showed an increase in conversion when increasing the agitation speed during reaction from 70 to 150 rpm, but a further increase to 220 rpm did not improve the conversion. This means that above 150 rpm there is no mass transfer limitation and the kinetic is controlled by the chemical reaction, as there were no changes in the number of particles.

Optimal mixing to ensure mass transfer and avoid particle coagulation

Nomura et al. [28] observed the effects of stirring rate during emulsion polymerization of styrene. The presence of impurities in the nitrogen used during the reaction leads to an induction period that is extended when the agitation speed is increased. This happens due to the surface aeration by the nitrogen atmosphere and can be minimized using a float covering or a purified nitrogen.

In the presence of well purified nitrogen atmosphere, for all the agitation speeds tested, the polymerization rate during the nucleation period is independent of the agitation speed. After this period, the authors observed two different behaviors (similar to Omi et al. [26]): low polymerization rate at lower speeds due to the phase separation and a decrease in polymerization rate at higher speeds due to the coagulation of particles. The effect caused by the higher speeds is more pronounced for low surfactant concentration due to the lower availability of emulsifier already observed in the previous studies. The results led to the conclusion that there is an optimal range of agitation speed to perform the reaction (410 – 600 rpm) and interestingly between these two different speeds the polymerization proceeds by the same way, probably because above 410 rpm there is no more mass transfer limitation and below 600 rpm there is no shear caused coagulation.

Kiparissides et al. [29] studied the influence of operating conditions on continuous emulsion polymerization of vinyl acetate. They observed the decrease in the conversion with the increase in agitation speed. As already discussed by Nomura et al. [28] an increase in agitation generates a larger liquid-air interface, increasing the amount of impurity in the water, in this case oxygen. The oxygen will reduce the rate of radical generation and in addition. Also, the high stirring probably increased the coagulation, reducing the number of particles. Both effect lead to the decrease in the polymerization rate.

Bataille et al. [30] observed the effect of agitation on vinyl acetate batch emulsion polymerization. At low agitation speed there is a phase separation leading to a lower conversion, except when working with a surfactant concentration about 8 times its CMC. For the agitation speeds of 150 and 220 rpm the polymerization rate showed little influence of speed.

Kim et al. [31] investigated the agitation effect on the tetrafluoroethylene emulsion polymerization. The rate of polymerization was the same for the different speeds tested, except for the highest speed, that led to coagulation in the system, as confirmed by the decrease in the number of particles. This decreases the polymerization rate.

Oprea and Dodita [32] reported similar results, where during the nucleation stage there is no influence of the agitation speed, in the semi-continuous emulsion polymerization of styrene, a methacrylic ester, and aliphatic acrylic ester and a methacrylic acid. When the agitation speed is at 180 rpm, there was a significant coalescence of particles, and the reactions performed at 220 rpm generated a highly foamed product. The results pointed to the establishment of an optimal agitation speed that provides a good dispersion of monomers and avoiding coalescence and foaming.

Krishnan et al. [33] studied the effect of agitation in semi-batch emulsion copolymerization of n-butyl methacrylate and n-methylol acrylamide using impellers with different diameters. The particle size decreased (and their number increased) with a higher agitation, in this case a higher impeller diameter, due to the better emulsification of monomer. But, for the impeller diameters of 6 and 8 cm, coagulum was produced. With the progress of the reaction, the liquid level increased and the viscosity increased with the solids content. Consequently, for the smaller agitator, which provides a less vigorous agitation, a zone of poor mixing was observed leading to a decrease in the polymerization rate. For the BA emulsion polymerization, a pitched 4-blades turbine was used at 400 and 990 rpm, and it the polymerization rate increased with the speed because of the greater number of particles nucleated.

Roudsari et al. [27] studied the effect of reactor configuration and agitation speed during the emulsion polymerization of methyl methacrylate. When the agitation speed is low, there is a phase separation due to the poor mixing, leading to low polymerization rate. An increase in speed increases the polymerization rate until the speed of 250 rpm, because of the better emulsification, increasing the number of particles in the system. However, a further increase to 350 rpm resulted in a lower conversion profile because of the destabilization of latex, observed by the decrease in particle number and foaming formation. The use of baffles presented a negative impact in the polymerization rate, especially at 250 rpm, with a reduction of 9 % in the conversion.

Effect on gas incorporation

Scott et al. [18] studied semi-batch emulsion polymerization of ethylene-vinyl acetate. With the progress of the reaction, there was a decrease in the ethylene composition in the copolymer. This is caused by mass transfer limitations of the ethylene gas going to the particles due to the increase of viscosity, related to the increase in solids content. This decrease in the ethylene composition is less pronounced for the agitation speed of 400 rpm for the different agitator types, showing that at this speed the mass transfer limitation is overcome. At 200 rpm, the decrease in ethylene composition was less pronounced for the axial impeller compared to the radial impeller, due to its flow pattern providing an increase in the contact time of the emulsion with the gas in the headspace. This showed that the ethylene ingestion from the headspace is an important mechanism for the ethylene solubilization. Changing the sparger from a single-orifice to a porous diffuser also helped to improve the mass transfer of ethylene by the reduction of bubble diameter which increases the total area for mass transfer.

Table 5.2 presents some of the results of the studies about the influence of agitation in emulsion polymerization found in the literature.

Table 5.2 Results of the effect of agitation in emulsion polymerization found in the literature.

Reference	Monomer/Reaction	Reactor	Speed (rpm)	Results
Evans et al. (1961) [24]	Vinylidene chloride Batch	0.5 L round-bottomed with a Teflon stirring blade (d_I = 7.6 cm).	N = 106, 131, 388 and 756.	Nucleation stage: ↑N decreases Rp. semi-continuous stage: ↑ N increases Rp.
Weerts et al. (1961) [25]	Butadiene Batch	2.4 L with 4 baffle plates and twelve-bladed turbine impeller (d_I/d_r = 0.45).	N = 100, 150, 200, 250, 300, 400, 500, 750 and 1000.	↑ N decreases Rp. Low N: phase separation and low Rp. For ↑M/W a low pitch helical ribbon agitator gave the best results.
Omi et al. (1968) [26]	Styrene Batch	4 baffle plates and a paddle-type agitator.	N = 350, 700 and 1500. High speed mixer with N = 16000 rpm used for pre-emulsification.	↑ N decreases Rp (i.e. coagulation). Low N: phase separation, low Rp. Nucleation is independent of N.
Nomura et al. (1972) [28]	Styrene Batch	Reactor with a dished bottom, 4 baffle plates and a four-bladed turbine impeller (d_I/d_r = 0.5).	N = 200, 300, 410, 600, 800 and 1050.	↑ N decreases Rp (i.e. coagulation, more pronounced for low surfactant). Low N: phase separation, low Rp. Nucleation is independent of N. Optimal range of N (410 – 600 rpm) (good mass transfer, no coagulation).
Kiparissides et al. (1980) [29]	Vinyl acetate Batch	2 L reactor with a flat blade paddle stirrer and the cooling coil inside act as baffling.	N = 220, 320, 420 and 500.	↑ N decreases Rp
Bataille et al. (1990) [30]	Vinyl acetate Batch	1 L reactor with a teflon paddle (d_I = 6 cm).	N = 75, 150 and 220.	Low N: phase separation, low Rp.
Scott et al. (1994) [18]	Ethylene-vinyl acetate Semi-batch	2 L reactor with a sparger, two agitators (either radial or axial) and d_r = 10 cm.	N = 200 and 400.	↑ N overcome mass transfer limitations. Above a certain N, there is no difference in the results of axial or radial impellers. Low N: axial impellers gave the best results.
Kim et al. (1999) [31]	Tetrafluoroethylene Semi-batch	1 L reactor with dished bottom, an anchor-type agitator (d_I/d_r = 0.94) and a baffle plate.	N = 250, 350, 430, 500 and 750.	Rp constant for N = 250 to 500 rpm. Higher N decreases Rp (i.e. coagulation of particles).
Mendoza et al. (2000) [34]	Styrene Batch	0.75 L reactor with a four-paddle stirrer (lowest paddle is an anchor	N = 200, 275 and 350.	No influence of N on Rp. ↑ N decreases the Mw by improving mass transfer of CTA.

Reference	Monomer/Reaction	Reactor	Speed (rpm)	Results
		and the other three are 45° pitched paddles).		
Zubitur and Asua (2001) [2]	Styrene-butyl acrylate Semi-continuous	2 L reactor with an anchor stirrer (d_I/d_r =0.75).	N = 70, 100, 150 and 220.	↑ N increases Rp, increases the Mw in the absence of CTA, and decreases it in its presence.
Oprea and Dodita (2001) [32]	Styrene-methacrylic ester-aliphatic acrylic ester and a methacrylic acid Semi-continuous	2 L reactor with a stirrer.	N = 100, 140, 180 and 220.	Nucleation is independent of N. N = 180 rpm leads to coalescence. N = 220 rpm leads to foaming.
Krishnan et al. (2003) [33]	n-butyl methacrylate-N-methylol acrylamide Semi-batch	0.2 L reactor with dish-shaped bottom and 6 baffles. Rushton turbines (d_I/d_r = 0.33, 0.44 and 0.59) or a pitched 4-blades turbine (d_I/d_r = 0.33).	N = 400 Rushton. N = 400 and 990 (PBT).	↑ d or ↑ N increases Rp. For the same N, only the smallest impeller did not produce coagulum. Smallest impeller presented a zone of poor mixing, decreasing Rp.
Roudsari et al. (2015, 2016) [6,27]	Methyl methacrylate Batch	2 L flat bottomed reactor with a 45° pitched 6 blade impeller (d_I/d_r = 0.5) and the option of using baffles.	N = 20, 100, 250 and 350.	↑ N increases Rp. Low N: phase separation, low Rp High N: low Rp, coagulation and foaming. The use of baffles decreased Rp.
		Same reactor but also studying the use of a Rushton turbine (d_I/d_r = 0.5).		At 100 rpm Rushton gave the higher conversion, At 250 rpm, the PBT gave higher conversion.
Ecoscia et al. (2022) [22]	Vinylidene fluoride Batch	4 L with conical bottom, 4 pitched 6-blade impellers (d_I/d_r = 0.5), diptube and thermowell acting as baffle. One PBT at the bottom can be replaced by a hydrofoil A315 (d_I/d_r = 0.8).	N = 350, 450, 550, 600 and 650.	↑ N increases Rp and Mw, especially when using the hydrofoil.

d = impeller diameter, T = reactor diameter, M = monomer, W = water.

5.2.3 Mixing in Chemical Reaction

In multiphase reactions, there is an interaction between the mass transfer process and the reaction rate. In some cases, the limiting step is the mass transfer rate and in others it will be the kinetics of the reaction [4].

In the cases a single gaseous reactant A is passing as bubbles through an agitated liquid where the reaction will happen, a general mass balance of A in the continuous liquid is [4],

$$V\frac{\mathrm{d}A_\mathrm{l}}{\mathrm{d}t} = k_\mathrm{L}aV(A^* - A_\mathrm{l}) - rV - Q_\mathrm{L}A_\mathrm{l} \tag{5.6}$$

where r is the reaction rate per unit volume and Q_L is the exit flow rate of liquid phase (equal to zero in batch and semi-batch operations). One should note that the equilibrium concentration of A (A^*) is a thermodynamic property (such as Henry's law coefficient) affected only by pressure and temperature, not by fluid dynamics or mixing. The concentration of A in the liquid (A_l) is affected by the transport and reaction rate.

When the reaction rate is faster than the mass transfer, the reaction progress is affected and the conversion obtained will be dependent on the mixing in the reactor. This can lead to scale-up problems when comparing the mixing between a small and industrial scale reactors [4].

The competition between the reaction and mixing in a reactor is calculated by the dimensionless Damköhler number, which is the ratio between the transport and reaction time scales [35],

$$Da = \frac{\tau_\mathrm{M}}{\tau_\mathrm{R}} \tag{5.7}$$

where τ_M is the characteristic mixing time and τ_R is the reaction time. Estimations of the mixing and mass transfer rates can be made based in reactor configurations and combined with the estimation of the reaction rate can give an

approximation for the conditions under which the mixing is critical in a stirred reactor [4].

When the reaction rate is comparable to the mass transfer rate in the diffusion film between the gas-liquid interface, the interaction between the reaction and the diffusion must be taken into consideration. This is done calculating the dimensionless Hatta number [36], in example for a first order reaction,

$$Ha = \frac{\sqrt{k_r D_{\mathrm{A,l}}}}{k_{\mathrm{L}}} \qquad 5.8$$

where k_r is the reaction rate constant and $D_{\mathrm{A,l}}$ is the diffusion coefficient in the liquid phase. According to the calculated value of Hatta number, five different profiles of concentration in the liquid film are obtained, and more details can be found in the specialized literature [4,37].

In the literature, works dedicated to modelling of gas-liquid reactors consider that the gas concentration in the liquid phase is in equilibrium with the gas concentration, calculated from Henry's law [38–42] what can diverge from this condition depending on the mixing in the reactor.

Zubitur et al. [43] is one of the few works considering the impact of the mass transfer during a polymerization reaction. They studied the impact of the oxygen as impurity on inhibition during the seeded semi-batch emulsion polymerization of styrene / butadiene / acrylic acid. The simulated results showed that it was necessary to take into account the inhibition effect to have a reliable prediction of the emulsion polymerization in terms of solid contents and free styrene concentration.

In works not related to polymerization, normally the authors calculate the mass transfer from the gas to the liquid in the absence and in the presence of reaction, this enabled the calculation of the mass transfer enhancement factor. With the enhancement factor is possible to estimate the intrinsic reaction kinetic constant. This method is used in several works as Moreno et al. [44], Đeković-Šević et al. [45], Lu et al. [46] and Chiu et al. [47]. Unfortunately, the works did not compare the results when this method of enhancement is not used.

Lu et al. [48] proposed a fuzzy-logic-based modeling for High-Gravity Advanced Oxidation Process (HiGee-AOP) nitric oxide attenuation to solve the mismatch issue from theoretical model and the coupled effects of operating variables such as agitation speed. The model combines reaction kinetics, gas diffusion under high gravity and mass transfer theory to show the impact of agitation speed on the gas-liquid interfacial area, and consequently on the mass transfer. The authors compared the experimental data with theoretical model and their hybrid fuzzy model, showing that the prediction accuracy was improved.

5.3 Results

5.3.1 Mass Transfer Limitations in the Reactor

The stainless steel reactor used to perform the emulsion polymerizations presented in this work has a capacity for 4 liters (see chapter 2 for more information), but there is also a glass container with the same diameter and height, available to observe the mixing profile in the reactor. The only difference between them is that the glass container has a flat bottom and the reactor a conical one.

Tests were performed with the glass container, to study the mixing for different agitation speeds and volumes. This made possible to notice the loss of vortex with the increase of the liquid volume as shown in **Erreur ! Source du renvoi introuvable.**. Normally, the reactions were performed starting at 2.2 L water, reaching 2.6 L of latex when the solids content is 32 %.

The flow regime of the reactor was already studied by using computational fluid dynamics (CFD) for a latex with 15 wt% of solids content, and when the agitation speed is 100 rpm the flow is transitional [49]. The tests presented in this chapter were performed in a range of agitation speed that includes the agitation speed used for the batch (550 rpm) and semi-batch (400 rpm) reactions, so, it can be assumed that the regime is turbulent if we have a latex with 15 wt% solids in the reactor and if there is no coagulation.

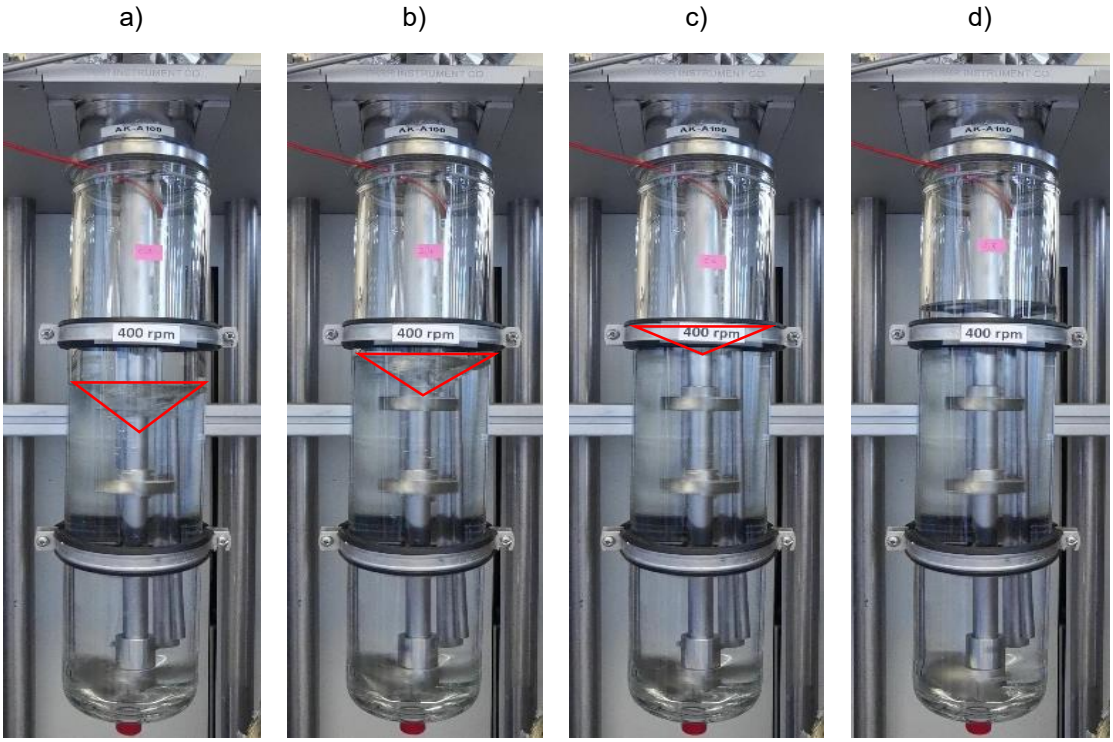

Figure 5.1 Vortex evolution for set-up 2 at 400 rpm and a) 2.2 L, b) 2.4 L, c) 2.6 L and d) 2.8 L of water.

The evolution of vortex height with the volume of water, is presented in Figure 5.2, for different agitation speeds. It is possible to notice that for the speed of 400 rpm, the vortex is lost at a volume of 2.8 L. This means that the useful volume of the reactor is 2.6 liters, because at this volume the liquid level is already touching the shaft's guide, reducing the quality of gas ingestion. This is the reason for the limit in solids content of 32 %wt. for a semi-batch reaction with reference recipe at 400 rpm because the final volume of latex is 2.6 L.

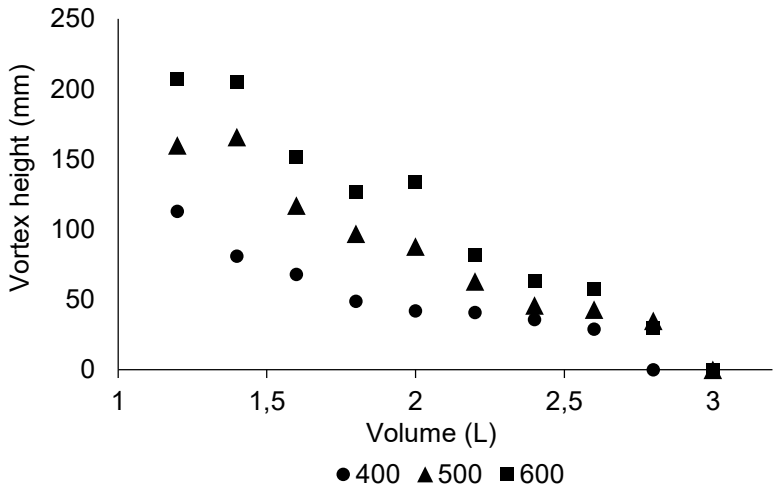

Figure 5.2 Vortex evolution for different volumes of water and agitation speeds for Set-up 2.

As presented in the literature [13,15–17], the vortex during gas-liquid mixing is important because it enables the ingestion of gas to the liquid, and consequently mass transfer to the particles, increasing the concentration of monomer available for the reaction. There are three possible actions to improve the reaction: work with higher speed, with a better organization of the distance between the impellers or a combination of both.

Increase in Speed

The effect of the speed could be noticed by comparing a reaction performed at different agitation speeds: 400 and 550 rpm. Figure 5.3 presents the polymerization rate and it can be seen that it was possible to obtain the double of the polymerization rate in 30 minutes when the speed was increased from 400 to 550 rpm. The increase of the polymerization rate with the speed is in agreement with the literature [2,11,12,21–24,27,33] and it is caused by the increased volumetric flow rate of ingested gas and increased turbulence which enhances bubble breakup, so increasing the surface area and consequently, the mass transfer.

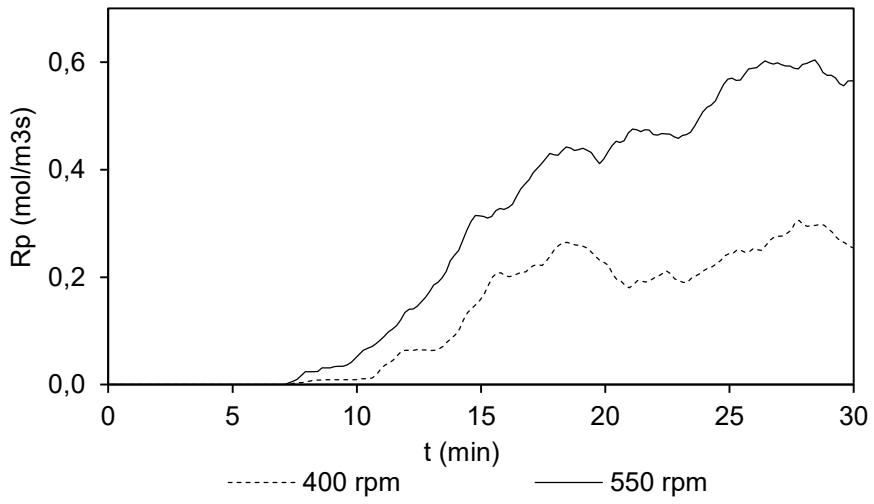

Figure 5.3 Polymerization rate progression for different speeds.

The increase in the vortex with the agitation speed is shown in Figure 5.4 for the same volume of liquid.

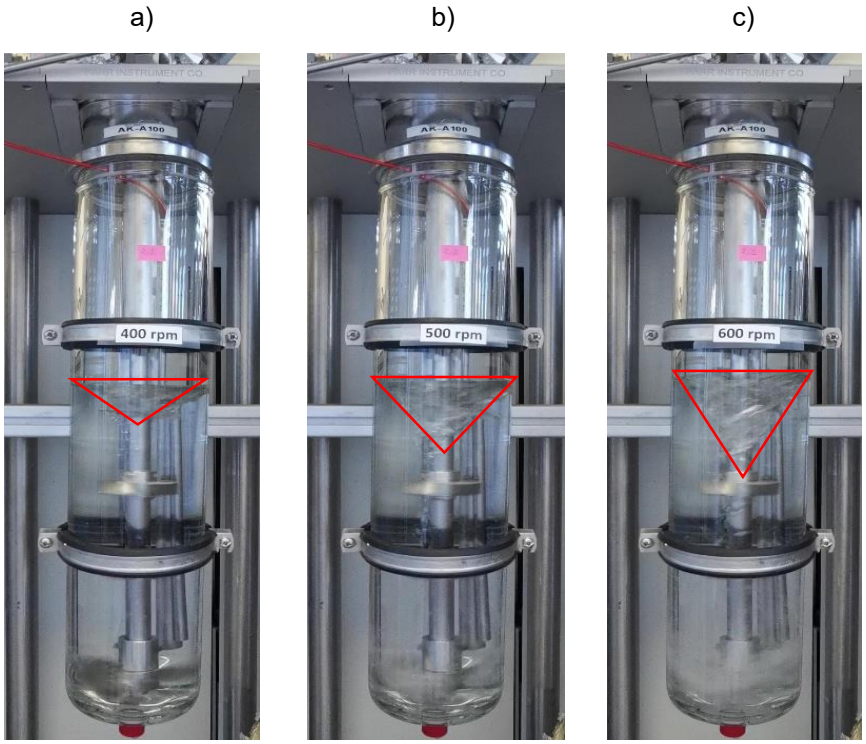

Figure 5.4 Vortex in set-up2 with 2.2 L of water for a) 400 rpm, b) 500 rpm and c) 600 rpm.

The increase in vortex with the agitation speed allows more gas to be ingested in the liquid, but this should be done carefully to avoid some thermal runaway due to the increase in the polymerization rate and at the same time, the increase in speed can increase the coagulation and fouling in the reactor, as observed by different authors [28,29,31–33].

Height of latex in the reactor with respect to the position of the impellers

A new reaction was performed with a lower amount of water in the recipe, keeping the concentration of chemicals as the reference recipe. Considering that with a total volume of 2.6 L it is still possible to have an acceptable vortex by the 4th impeller, this will be fixed as the total useful volume at the end of a reaction. It is possible to calculate the total amount of water to be used in the recipe to produce a latex with a solids content of 50 wt% and a latex volume of 2.6 L. The volume fraction of water in a latex with 50 wt% of solids is equal to 64.3 %, so the volume of water in 2.6 L of latex the recipe will be equal to 1.67 L. One should notice that, water is added as an initial charge and during the two-shot protocol to feed chemicals and to rinse the lines.

Figure 5.5 shows the polymerization rates of the reactions performed with 1.6 and 2.2 liters of initial water. It is possible to notice that when the polymerization is performed in the region with a better vortex, the rate of polymerization is improved, making it possible to increase the solids content from 32 to 39 wt% for the same polymerization time. As the hydrofoil impeller at the bottom has a high pumping capacity [22], it was expected that a lower volume of water would generate a better gas-liquid mass transfer.

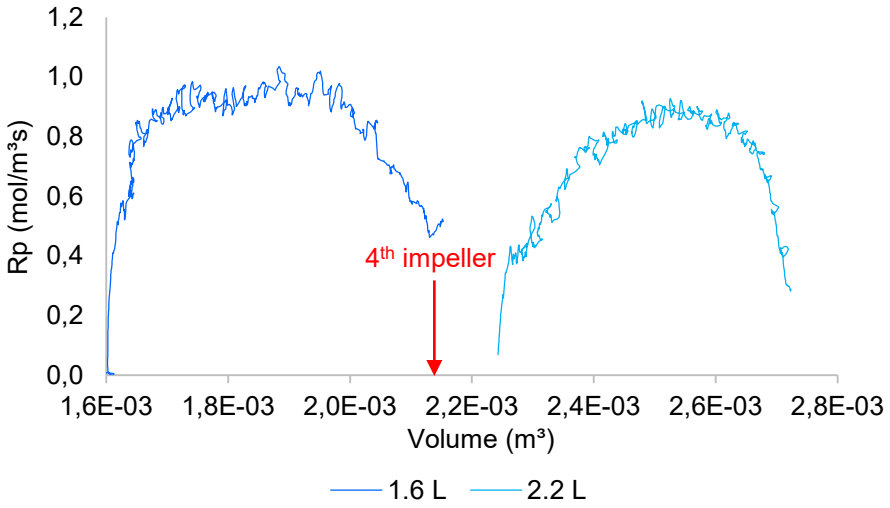

Figure 5.5 Semi-batch polymerization rate for reactions performed with reference recipe and different volumes of water with set-up 2 at 400 rpm.

For the two reactions, it is possible to notice the decrease in polymerization rate close to the end of the reaction. In both cases, this is caused because the liquid level is moving far from the last impeller which the liquid was in touch before.

The reaction performed with 1.6 L of water showed a tendency for the increase in polymerization rate when the liquid level started touching the fourth impeller. This is due to the fact that gas incorporation is enhanced when the impeller is close to the latex surface as shown in Figure 5.6.

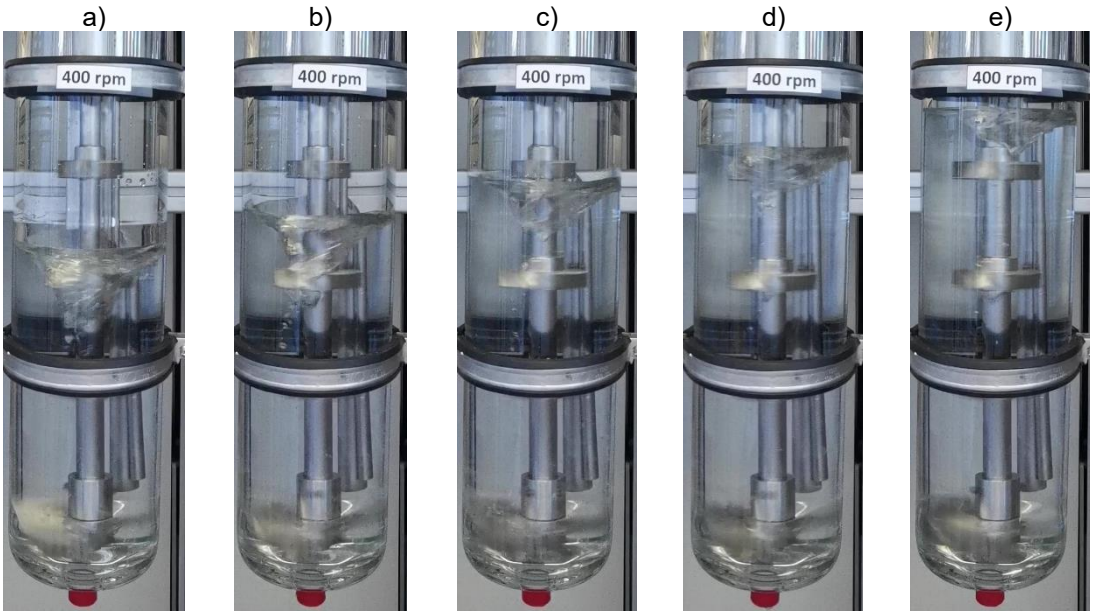

Figure 5.6 Vortex in set-up 2 at 400 rpm for a) 1.6 L, b) 1.8 L, c) 2.0 L, d) 2.2 L and e) 2.4 L.

The results from Table 5.3 show the improvement of the reaction by the increase in solids content for the same polymerization time and also the gain in mass transfer demonstrated by the increase in molecular weight of the polymer produced when reducing the height of the latex in the reactor, and working closer to the impellers.

Table 5.3 Results of semi-batch polymerizations performed with reference recipe and different volumes of water with set-up 2 at 400 rpm.

Water (L)	**2.2**	**1.6**
SC (%)	32.0	39.1
Dp (nm)	221	227
PdI	0.047	0.047
Npx10^{-19} (1/m^3)	3.9	4.6
θ (%)	8.0	6.4
Mw (kDa)	257	415
PDI	2.30	2.48

When continuing the reaction to a longer period, the reaction rate increases again as the latex reaches the fourth impeller which may create a vortex. For instance, Figure 5.7 shows a reaction performed with the double of surfactant compared to the reference recipe and approximately half the amount of CTA, and that discussed in Figure 5.5. It is possible to observe the decrease in the polymerization rate for the two reactions at the same volume of liquid and a

subsequent increase, that was not observed for the previous reaction because it was stopped at 120 minutes, and this one was left for 180 minutes.

Surprisingly, the same values of polymerization rate of the first plateau were recovered after the first decrease and recover of the polymerization rate, and then it is possible to observe again a decrease in the reaction rate. An estimation of the volumes in which the polymerization rate decreases are made based in the dotted lines. It is possible to say that the incorporation of gas decreases from 2.05 to 2.15 L and for volumes higher than 2.37 L, again an effect of poor zones of gas incorporation between two impellers [8].

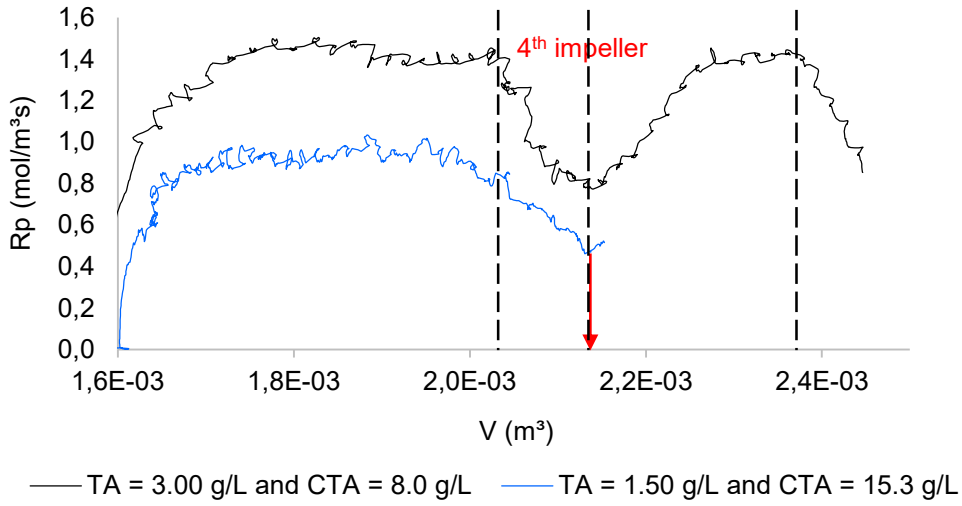

Figure 5.7 Semi-batch polymerization rates performed with different recipes and times for 1.6 L of water with set-up 2 at 400 rpm.

Increase in Speed and Decrease in Total Water Volume

When both changes are performed in the volume of water and agitation speed, the profile of polymerization rate is presented in Figure 5.8. Even if there are some differences in the recipe of the reaction performed at 550 rpm, it is possible to notice that the decrease in the reaction rate around 2.0 L was avoided.

Table 5.4 shows the results of the reactions when the total water volume is decreased and when the agitation speed is increased. Even if the reaction at 550 rpm was performed for only two hours, the solids content was higher than the reaction performed at 400 rpm and the same volume of water. Some discrepancies in the results can be due to the change in KPS used for the reaction at higher speed.

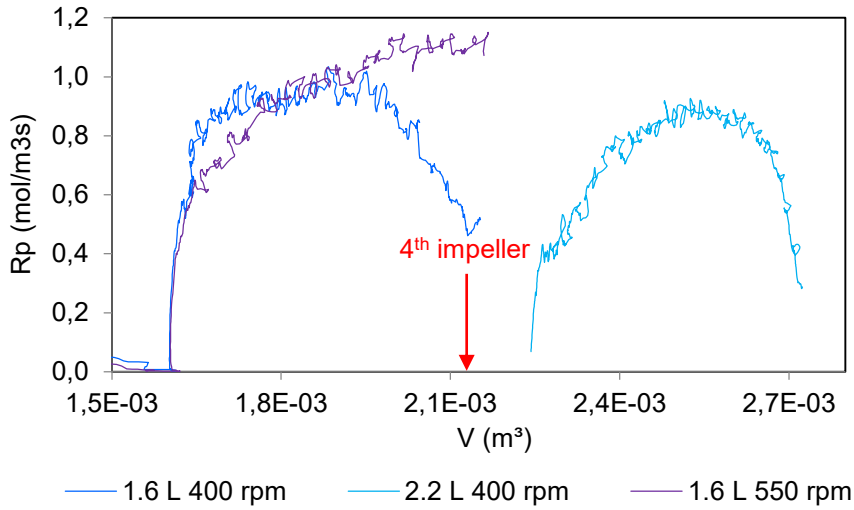

Figure 5.8 Semi-batch polymerization rates performed with similar recipes for 1.6 L and 2.2 L of water with set-up 2 at 400 and 550 rpm.

Table 5.4 Results of semi-batch polymerization rates performed with similar recipes for 1.6 L and 2.2 L of water with set-up 2 at 400 and 550 rpm.

Water (L)	**2.2**	**1.6**	
Speed (rpm)	400		550
Time (min)	180		120
Wax (g/L)	1.1		3.5
CTA (g/L)	15.3		13.5
SC (%)	32.0	39.1	34.6
Dp (nm)	221	227	221
PdI	0.047	0.047	0.022
Npx10^{-19} (1/m³)	3.9	4.6	4.3
θ (%)	8.0	6.4	7.0
Mw (kDa)	257	415	457
PDI	2.30	2.48	2.37

Based in all the information presented in this section, it can be said that under some conditions we may face gas-liquid mass transfer limitations in the reactor. In terms of productivity with solids content around 35 wt% it is better to run reactions with a total volume of water of 1.6 L at 550 rpm.

5.3.2 Improvements of the Agitation Set-Up

Based in the results of the previous section, it is possible to improve gas incorporation and mass transfer in the reactor rearranging the agitation set-up. As the 45° pitched 6-blade impellers can be moved on the shaft, it is possible to change its position and the hydrofoil A345 can also be inverted to have the A315

as in the Figure 5.9. When the hydrofoil is in the A345 configuration, it is called set-up 2 and when the hydrofoil is A315 it is called set-up 2D. The letter D was chosen because in this configuration the hydrofoil is in a down-pumping mode, improving the gas ingestion into the liquid. The improvement in gas ingestion when changing the pumping mode of an impeller was already explored in the literature [9–11]. But, to be considered an up-pumping impeller, the shaft should be turning counter clockwise [50]. If the reactor's shaft turns in clockwise sense (which is our case), the hydrofoil A345 is in a wrong configuration.

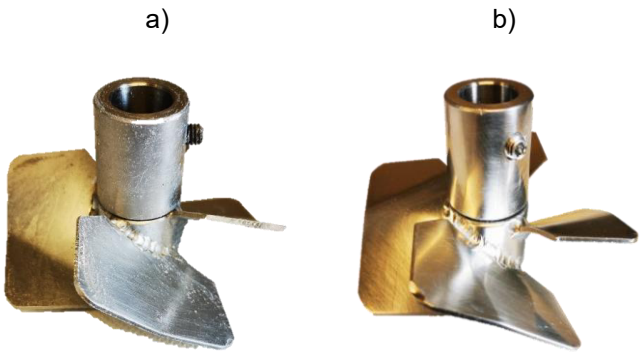

Figure 5.9 Hydrofoil in the a) A345 (set-up 2) and b) A315 (set-up 2D) configurations.

Initially the set-up 2 or 2D used in the experiments is composed by the hydrofoil in the bottom, with a 45° pitched 6-blade impeller placed 10 cm above it. The others two 6-blade impellers are spaced 8 cm from each other as shown in Figure 5.10. To try to avoid the decrease in the polymerization rate in the regions in which the impellers are not touching the liquid level, the 6-blade impellers that were initially spaced by 8 cm, now are 6 cm from each other, enabling the addition of a fifth impeller to the shaft, now called set-up 2/2D+.

As the gas incorporation is mainly related to the vortex generated on the top of the liquid, it is possible to conclude that the first three impellers from bottom to top, don't need to be moved. So, in a new configuration the 2nd and 3rd impellers are spaced 8 cm as in set-up 2/2D, but the 3rd and 4th impellers are spaced 6 cm and then the 4th to 5th impellers are spaced 5 cm (the minimum possible spacing before facing flow interaction problems [4,8]), this is called set-up 2/2D+new.

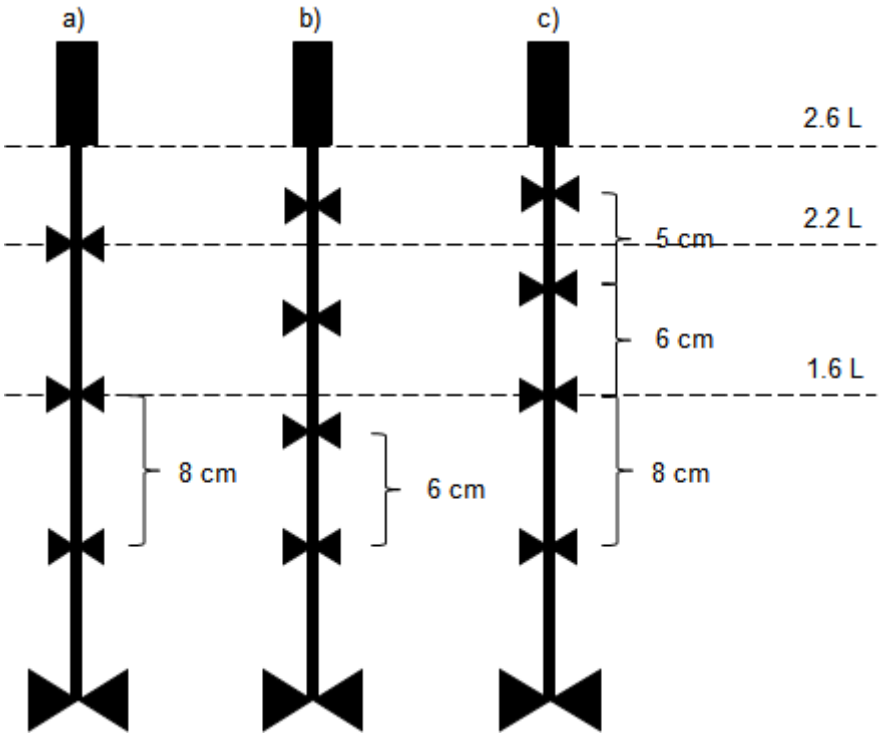

Figure 5.10 Different possible set-up configurations a) Set-up2, b) Set-up 2+ and c) Set-up 2+new. The dotted lines represent the volumes of liquid.

The polymerization rates of a semi-batch reaction with the reference recipe performed with set-up 2D and set-up 2D+new are shown in Figure 5.11. It is possible to observe that both reactions with different set-ups follow the same rate until 1.9 L of liquid and around 2.06 L the rate decreases for the set-up 2D because of the transition area between two impellers. This decrease in the rate is avoided with the set-up 2D+new because of the different distance between the 3rd and 4th impellers.

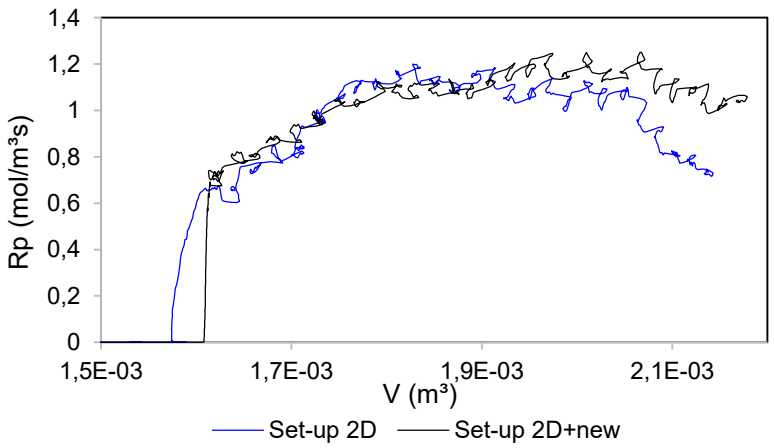

Figure 5.11 Semi-batch polymerization rates for reference recipe with different set-ups at 400/450 rpm. From 0<t<40 min N=400 rpm, 40<t<66 min N=450 rpm, 66 <t<92 min N=400 rpm and 92<t<118 min N=450 rpm.

The results of these two reactions are presented in Table 5.5. Avoiding the region in which we lose the quality of gas incorporation led to a slight increase in the solids content, as expected.

Table 5.5 Results of semi-batch polymerization rates for reference recipe with different set-ups at 400/450 rpm.

Set-up	2D	2D+new
SC (%)	37.7	39.1
Dp (nm)	235	238
PdI	0.038	0.025
Npx10^{-19} (1/m^3)	4.0	4.0
θ (%)	6.7	6.5
Mw (kDa)	417	443
PDI	2.14	3.10

Unfortunately, the results from set-up 2D+ are not available and the next section will show the differences caused by the hydrofoil in the A345 and A315 configurations.

5.3.3 Estimation of the Mass Transfer Coefficient

All the discussions up to now were based in visual observations of the mixing (vortex) in the reactor, so to have a quantitative result, mass transfer experiments were performed to calculate the mass transfer coefficient. The mass transfer experiments were based in the dynamic physical absorption method proposed by Chaudhari et al. [21] which consists in monitoring the pressure drop caused by the absorption of a gas A in a liquid over time as presented in the section **Erreur ! Source du renvoi introuvable.**.

The experiments were performed following these steps:

- The reactor is charged with a latex 10 wt% kindly provided by Arkema, and it is heated up until 83 °C at a low speed of 150 rpm to guarantee that we don’t have hot spots and also to avoid the coagulation.
- Once the desired temperature is reached, the reactor is left in equilibrium for 30 minutes.
- The agitation is turned off and the reactor is left again for 30 minutes.

- The reactor is charged with the monomer until the desired pressure is reached and the reactor is left for more 30 minutes to stabilize the temperature without mixing.
- The agitation is turned on at the desired speed and the pressure drop is followed for 30 minutes or until complete signal stabilization of the new pressure.

As already pointed by Ecoscia et al. [22] who studied the same reactor and set-up, the pressure drop in our system is reliable when performing the experiments below 40 bars, so the experiments were performed at 30 bars. The pressure is not supposed to affect the mass transfer coefficient estimation.

One example of the results obtained for an experiment performed with 2.5 L of latex 10 wt% in set-up 2 at 550 rpm is shown in Figure 5.12.

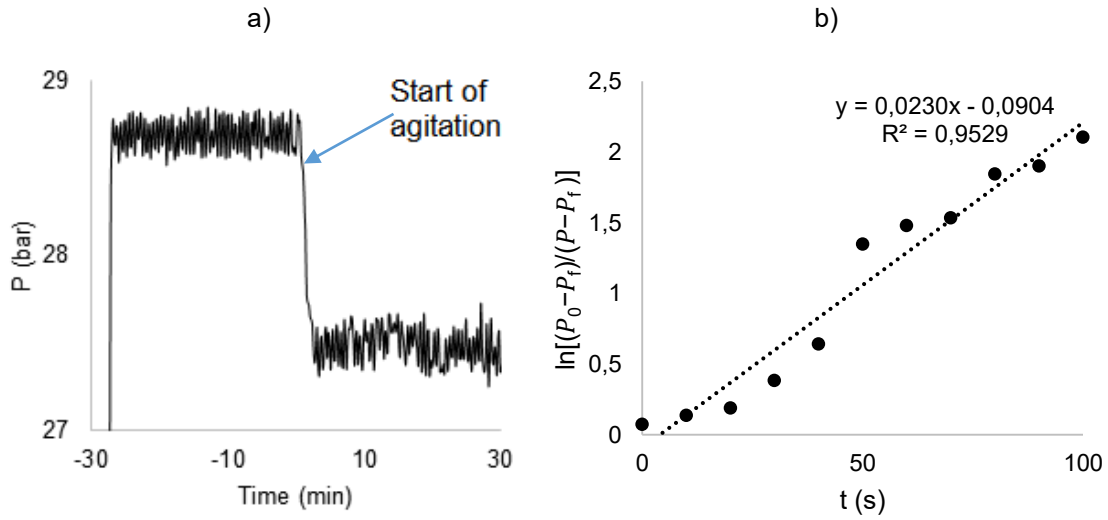

Figure 5.12 a) Pressure drop profile and b) data treatment for $k_{\mathrm{L}}a$ calculation.

The experiments were performed for the set-ups 2 and 2D and the results are presented in the Table 5.6, showing an average improvement of 20 % in the mass transfer coefficient when the set-up 2D is used.

Table 5.6 $k_L a$ results for Set-ups 2 and 2D for different volumes and speed.

V_L (L)	N (rpm)	$k_L a$ (min^{-1})	
		Set-up 2	Set-up 2D
2.0	400	0.610	0.727
	550	2.681	2.876
2.5	400	0.386	0.505
	550	1.320	1.705

Semi-batch polymerizations following the reference recipe were performed with different set-ups and speeds as presented in Figure 5.13. It is possible to observe that there is no difference in the reaction rate for the two set-ups tested when the speed is 550 rpm for the volume tested. There is an optimal speed in which the mass transfer limitations are no longer acting [2,18,28,30,32] and it seems that it is the case for 550 rpm with set-up 2 and set-up 2D.

As expected from the previous results, the polymerization rate is slower for a lower agitation speed, as the mass transfer coefficients are in average 75 % lower than the values found for 550 rpm. It is interesting to observe that during the nucleation period (0 to 40 min), the three curves are very similar, showing that the high capacity of the hydrofoil enables a good gas ingestion until the volume of 1.8 L.

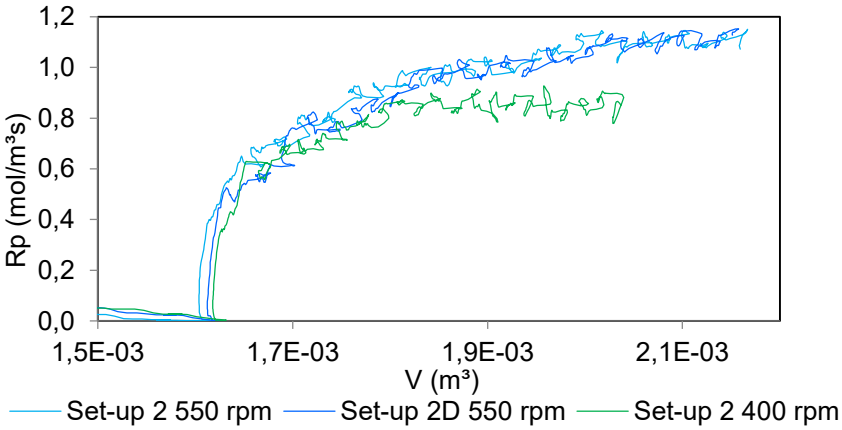

Figure 5.13 Semi-batch polymerization rates of reactions performed with different set-ups and speeds.

The results of these reactions are presented in Table 5.7. The effect of working with higher mass transfer coefficients is seen in the increase in solids content and

in the polymer molecular weight obtained, especially when comparing the reactions performed with the same set-up and different speeds.

Table 5.7 Semi-batch polymerizations performed with different set-ups and speeds.

Reaction	Set-up 2 400 rpm	Set-up 2 550 rpm	Set-up 2D 550 rpm
Time (min)		120	
SC (%)	29.4	34.6	35.8
Dp (nm)	208	221	225
PdI	0.012	0.021	0.007
Npx10^{-19} (1/m^3)	4.3	4.3	4.3
θ (%)	8.0	7.0	6.9
Mw (kDa)	398	457	485
PDI	2.51	2.37	2.50

These results were expected, and observed in the polymerization rate, so the next step is showing the effect of mass transfer during the polymerization with a model.

5.3.4 Emulsion Polymerization Model

5.3.4.1 Model development

The emulsion polymerization model is based on the works and reactions constants of Apostolo et al. [39] and Pladis et al. [51,52]. The model doesn't take into consideration the nucleation and coagulation of particles, modelling only the growth of particles.

The partial differential equations were discretized to become a set of ordinary differential equations using the Matlab software. The fitting parameters to the model are: the efficiency of radical's absorption, the desorption coefficient and the choice among several models for radical entry/exit.

The reaction scheme taken into consideration as well as the material balance equations are presented below.

Reaction Scheme

Initiator decomposition	$\mathrm{I} \xrightarrow{k_\mathrm{d}} 2\mathrm{R}^*$
Chain initiation reaction	$\mathrm{R}^* + \mathrm{M} \xrightarrow{k_\mathrm{i}} \mathrm{R}_1^*$
Chain propagation reaction	$\mathrm{R}_n^* + \mathrm{M} \xrightarrow{k_\mathrm{p}} \mathrm{R}_{n+1}^*$
Chain transfer to monomer reaction	$\mathrm{R}_n^* + \mathrm{M} \xrightarrow{k_\mathrm{fm}} \mathrm{R}_1^* + \mathrm{D}_n$
Chain transfer to CTA	$\mathrm{R}_n^* + \mathrm{CTA} \xrightarrow{k_\mathrm{fCTA}} \mathrm{R}_1^* + \mathrm{D}_n$
Termination by combination reaction	$\mathrm{R}_n^* + \mathrm{R}_m^* \xrightarrow{k_\mathrm{tc}} \mathrm{D}_{n+m}$

The material balances are given by the equations [53–55],

Component	**Equation**
Initiator	$\frac{\mathrm{d}[I]}{\mathrm{d}t} = -k_\mathrm{d}[\mathrm{I}]$
Oligomeric radicals in aqueous phase (length 1 to j_cr)	$\frac{\mathrm{d}[R^\bullet]_\mathrm{w}}{\mathrm{d}t} = 2f_\mathrm{I}k_\mathrm{d}[\mathrm{I}] - \frac{[R^\bullet]_\mathrm{w}}{N_A}\frac{V_\mathrm{e}}{V_\mathrm{w}}\int_0^\infty k_\mathrm{e}(v)f(v)\mathrm{d}v - k_\mathrm{tw}[R^\bullet]_\mathrm{w}^2 + \frac{1}{N_\mathrm{A}}\frac{V_\mathrm{e}}{V_\mathrm{w}}\int_0^\infty k_\mathrm{des}\bar{n}(v)f(v)\mathrm{d}v$
Monomer reaction rate in particles (mole/s/m^3 emulsion)	$R_\mathrm{p}^\mathrm{p} = \left(k_\mathrm{tm} + k_\mathrm{p}\right)\frac{[\mathrm{M}]_\mathrm{p}}{N_\mathrm{A}}\int_0^\infty \bar{n}(v)f(v)\mathrm{d}v$
Monomer reaction rate in water (mole/s/m^3 emulsion)	$R_\mathrm{p}^\mathrm{w} = \left(k_\mathrm{tm} + k_\mathrm{pw}\right)[\mathrm{M}]_\mathrm{w}[R^\bullet]_\mathrm{w}\frac{V_\mathrm{w}}{V_\mathrm{e}}$
Total reaction rate	$R_\mathrm{p} = R_\mathrm{p}^\mathrm{p} + R_\mathrm{p}^\mathrm{w}$
Volume of the swollen particle phase	$V_\mathrm{part} = V_\mathrm{p} + V_\mathrm{m}^\mathrm{p}$ $V_\mathrm{part} = V_\mathrm{p}\frac{1}{\left(1-[M]_\mathrm{p}\frac{M_\mathrm{w,m}}{\rho_\mathrm{m}}\right)}$
Volume of the unswollen polymer phase	$\frac{\mathrm{d}V_\mathrm{p}}{\mathrm{d}t} = \frac{M_\mathrm{w,m}}{\rho_\mathrm{p}}R_\mathrm{p}V_\mathrm{e}$
Volume of the emulsion (water, polymer and dissolved monomer)	$V_\mathrm{e} = V_\mathrm{part} + V_\mathrm{w} + V_\mathrm{m}^\mathrm{w}$ with $V_\mathrm{m}^\mathrm{w} = \frac{[M]_\mathrm{w}M_\mathrm{w,m}V_\mathrm{w}}{\rho_\mathrm{m}}$
number of particles in the reactor per unit volume.	$N_\mathrm{p} = \int_0^\infty f(r,t)\mathrm{d}r$

Radical entry into particles

Frequency of radical entry	$\rho = k_e[R^\bullet]_w$
Diffusion-controlled mechanism Smith and Ewart [53]	$k_e = 2\pi d_s N_A D_{w(i)} f_e$ f_e: efficiency of radical entrance

Radical exit/desorption from particles [56–59]

Radical desorption rate per particle	$R_{des} = k_{des}(r,t)\bar{n}(r,t)$
Smith and Ewart [53]	$k_{des} = \frac{ap'}{v} = \frac{6}{d}k_0$ $k_0 = k_{des0} + k_{des1}[CTA]_p$ $k_{des0} = 0.001$ s^{-1} $k_{des1} = 1.5 \times 10^{-5}$ m^3 mol^{-1} s^{-1}
Combining Friis & Nyhage [54] and Ugelstad & Hansen (1976) [55]	$P = \frac{k_0}{k_0 + k_p[M]_p}$ [54] $k_0 = \frac{12 D_p D_w}{d^2(mD_p + D_w)}$ [55] $k_{des} = P\left(k_{fM}[M]_p + k_{fCTA}[CTA]_p\right)$ $m = \frac{[M]_w^{eq}}{[M]_p^{eq}}$ Assuming $D_p = D_w$

Assuming equi-partitioning of CTA between particles and water.

Particle size distribution and particle growth

$\frac{\partial}{\partial t} f(v,t) = -\frac{\partial}{\partial v}[G(r,t)f(v,t)]$

$G(v,t)$ (m^3/s) of unswollen particles, $f(v,t)$ (part / m^3 of emulsion / m^3 of polymer)

$G(v,t) = \bar{n}(v)\frac{k_p[M]_p M_{w,m}}{N_A \rho_p}$

Average number of radicals per particle: pseudo-bulk model

$$\frac{\partial}{\partial t}\bar{n}(v,t) = \rho_{\mathrm{e}} - k_{\mathrm{des}}(v)\bar{n}(v,t) - 2c(v)\bar{n}(v,t)^2$$

$$c = \frac{k_{\mathrm{tp}}}{N_{\mathrm{A}}v}$$

$$\rho_{\mathrm{e}} = k_{\mathrm{e}}[R^{\bullet}]_{\mathrm{w}}$$

Concentration of monomer into particles and water

$$\frac{\mathrm{d}[M]_{\mathrm{p,am}}}{\mathrm{d}t} = k_{\mathrm{L}}a\left([M]^{\mathrm{eq}}_{\mathrm{p,am}} - [M]_{\mathrm{p,am}}\right) - \frac{V_{\mathrm{e}}}{V_{\mathrm{p}}}R^{\mathrm{p}}_{\mathrm{p}}$$

$$\frac{[M]_w}{[M]^{\mathrm{eq}}_{\mathrm{w}}} = \frac{[M]_{\mathrm{p,am}}}{[M]^{\mathrm{eq}}_{\mathrm{p}}}$$

$k_{\mathrm{L}}a$ values come from Table 5.6.

The concentration of monomer in the gas phase is:

$$[M]_{\mathrm{g}} = \frac{P_{\mathrm{m}}}{zRT}$$

From Henry's law

$$[M]^{\mathrm{eq}}_{\mathrm{p,am}} = H_{\mathrm{e,p}}P_{\mathrm{m}}$$

Table 5.8 Parameters used in the model.

Kinetic constant	Values
k_{d} (L/mol.s) [52]	$4.56\mathrm{x}10^{16}\exp\left(\frac{-16860}{T}\right)$
k_{p} (L/mol.s) [52]	$2.2\mathrm{x}10^{9}\exp\left(\frac{-4539}{T}\right)$
k_{tm} (L/mol.s) [52]	$1.2\mathrm{x}10^{11}\exp\left(\frac{-9020}{T}\right)$
k_{fCTA} (L/mol.s)	7×10^{2} m^3 mol^{-1} s^{-1}
k_{tw} (L/mol.s) [60]	$\left(\frac{k_{\mathrm{p}}}{0.14}\right)^2$
k_{tp} (L/mol.s) – analog to styrene	$0.05\ k_{\mathrm{tw}}$

Kinetic constant	Values
$H_{e,p}$: Henry coefficient (mol/Pa/m^3 am polymer)	3.1×10^{-4}
$[M]_w^{sat}$ [52] (mol/m³ at 74°C)	10^2 mole m^{-3}
D_w (m²/s)	1.5×10^{-9}
f	0.6

Initial condition of the model

As the model does not take into consideration the nucleation stage, normally seeded reactions are performed to generate the experimental results to be modelled. Unfortunately, we didn't succeed these kinds of experiments in our system. An alternative was taking the data from a reaction stopped at the nucleation period and use it as initial point to the model.

As shown in the previous section, even at different agitation speeds and set-ups, while performing the same recipe, the polymerization rate is virtually the same, so a reaction stopped at 40 minutes is our initial point and the polymerization rate profile is shown in Figure 5.14.

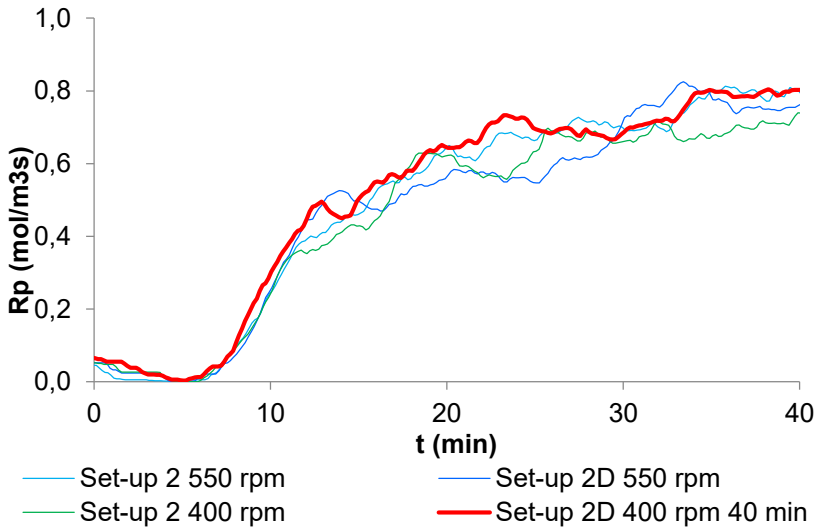

Figure 5.14 Polymerization rate for the first 40 minutes of semi-batch reactions performed with different set-ups and speeds.

The results of the reaction used as initial condition are presented in Table 5.9.

Table 5.9 Results of semi-batch polymerization stopped at 40 minutes.

Time (min)	**40**
SC (%)	9.9
Dp (nm)	170
PdI	0.01
Npx10^{-19} (1/m³)	2.3
θ (%)	16.8
Mw (kDa)	310
PDI	3.12

The reactions performed with different set-ups and agitation speeds presented in the previous section were simulated to check the robustness of the model.

5.3.4.2 Effect of mixing in the concentration of monomer in the amorphous polymer

To the best of our knowledge, in the works presented in the literature about modelling the emulsion polymerization of vinylidene fluoride, the effect of the mass transfer was never taken into consideration.

Figure 5.15 presents the results obtained with the model for the monomer concentration in the amorphous polymer particles. As already mentioned in the section 5.2.3, the equilibrium concentration of monomer calculated by Henry is only affected by pressure and temperature. If the models are not taking into consideration the mass transfer, it is assumed that the concentration of monomer in the polymer particles is at equilibrium, what is not true from our results.

It is possible to observe that the concentrations of monomer in the particles are below the equilibrium value, especially for the lowest agitation speed. An increase in speed increases this concentration, and as observed from the reaction results, the monomer concentration curves at 550 rpm and different set-ups are virtually the same. The results show that the use of a non-equilibrium model is essential when the agitation speed is low, because the results at 550 rpm are close to the Henry's law.

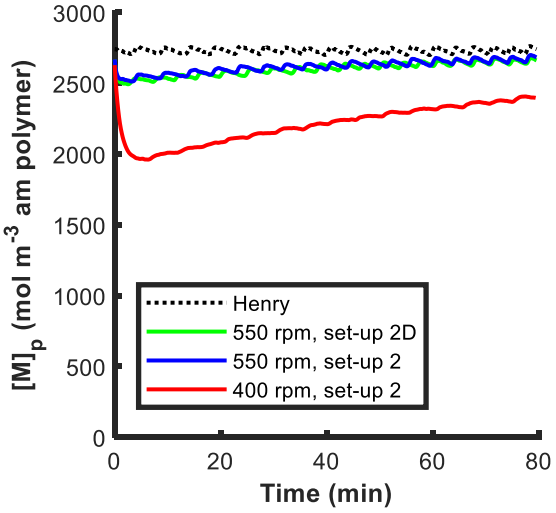

Figure 5.15 Monomer concentration in amorphous polymer.

5.3.4.3 Influence of different average number of radical models

The impact of different models for the radical desorption rates are tested using Smith & Ewart (1948) [53] and Friis & Nyhagen (1973) [54]/ Ugelstad & Hansen (1976) [55] models.

The reaction performed at 550 rpm with the set-up 2D is used to compare the models and the results are presented in Figure 5.16.

It is possible to observe the general improvement in the particle size distribution and polymerization rate when using the Friis & Nyhagen (1973) [54]/ Ugelstad & Hansen (1976) [55] model.

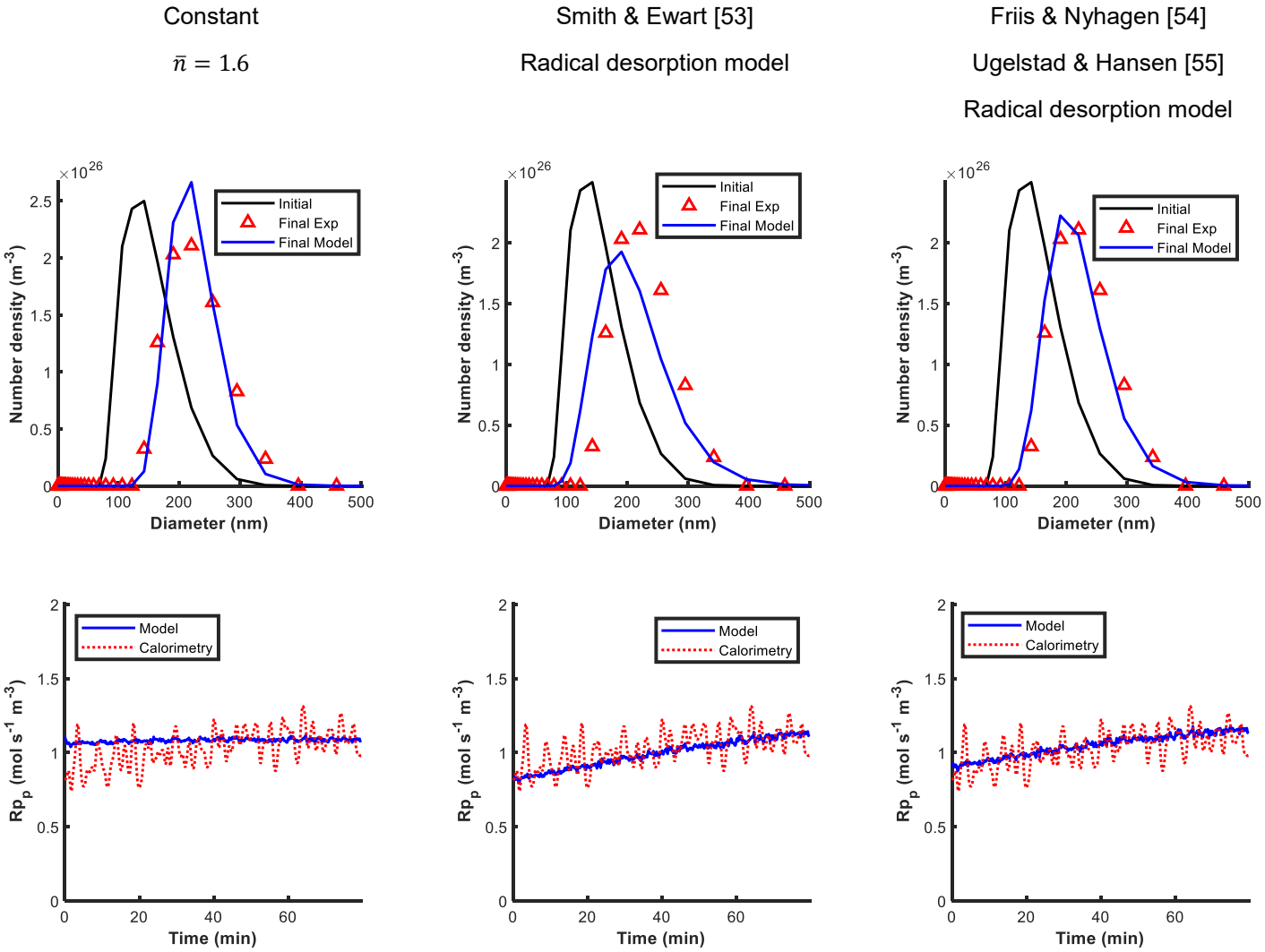

Figure 5.16 Influence of nbar in the model.

5.3.4.4 Prediction of the reaction rate by the model

Firstly, the results from monomer concentration in the amorphous polymer were shown, and now the polymerization rate curves are shown and compared to the experimental data obtained by calorimetry.

It can be seen in Figure 5.17 that the model fits the experimental data by calorimetry and that the polymerization rate of set-up 2D is slightly higher than the one performed with set-up 2. As the monomer concentration in particles is lower for the agitation speed of 400 rpm, it was expected that the polymerization rate follows this behavior, as the polymerization rate is function of the monomer concentration.

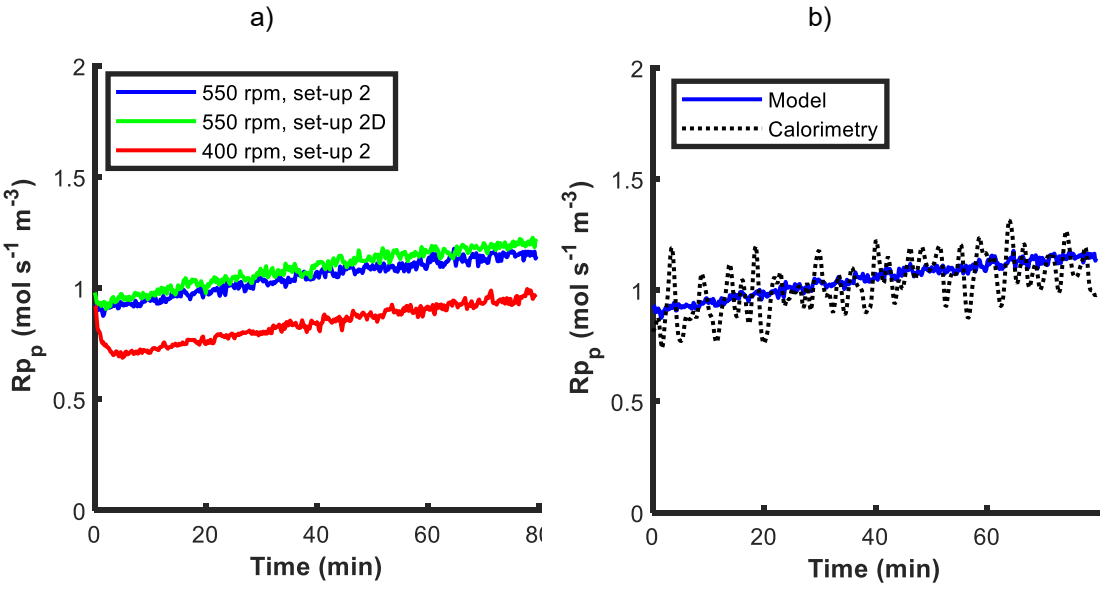

Figure 5.17 polymerization rate curves a) from the modelling and b) compared to the experimental results from calorimetry (Set-up 2D at 550 rpm)

5.3.4.5 Effect of mixing in the particle size distribution

Figure 5.18 shows the effect of mixing in the particle size distribution of reactions performed with different set-ups and speeds. We can observe that the model fits the experimental data, and as only the particle growth is modelled, different polymerization rates will have an impact on the final particle size distribution.

As the polymerization rate at 550 rpm was virtually independent on the set-up used, the final particle distribution is similar. At 400 rpm the polymerization rate is slower, not leading to same growth of particles, reflected by the slightly smaller particles obtained.

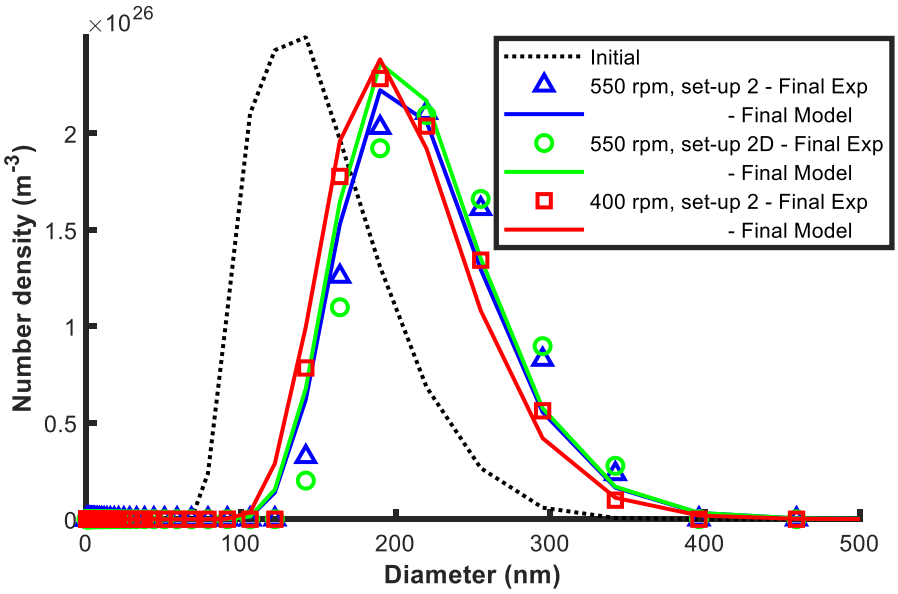

Figure 5.18 Initial and final particle size distributions.

5.3.4.6 Importance of a kLa model

The importance of a non-equilibrium model taking into account the mass transfer coefficient during the reaction is show in Figure 5.19 and Figure 5.20. It can be seen that when a model is considering that the monomer concentration in the polymer particles is in thermodynamic equilibrium, there is an overestimation of the polymerization rate. The higher polymerization rate will also lead to slightly bigger particle size distribution.

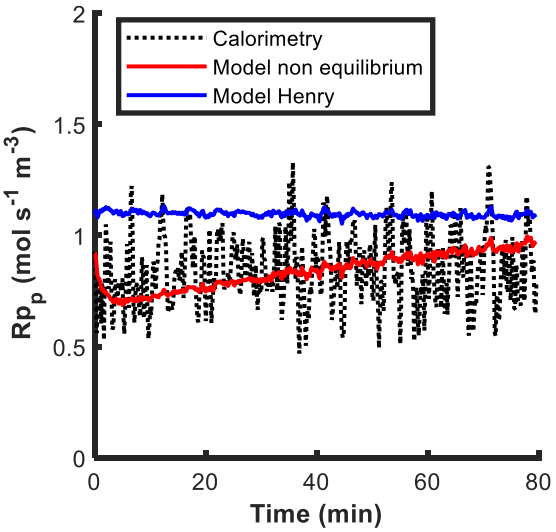

Figure 5.19 Polymerization rate of non-equilibrium and Henry models.

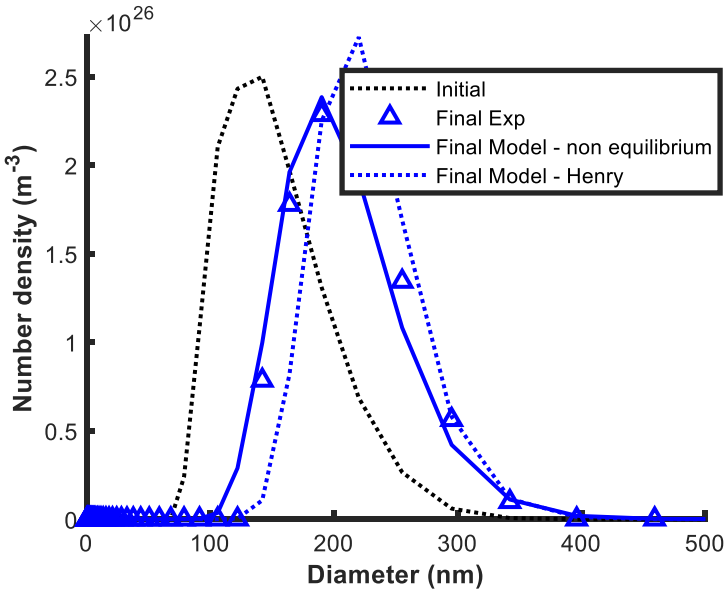

Figure 5.20 Initial and final particle size distributions for non-equilibrium and Henry models.

5.4 Conclusions

We were facing mass transfer limitations in the reactor due to a poor design, causing the loss of vortex when the liquid level touches the shaft guide at the volume of 2.6 L. This was limiting the solid contents produced to 32 % wt.

As there is no sparger to introduce the monomer in the reactor, the gas ingestion from the headspace is the only mechanism providing the gas-liquid mass transfer. From the observations performed using the glass reactor, the vortex height can be increased by working with low volumes of liquid and also with higher agitation speeds. These were the solutions found to overcome the reactor mass transfer limitations, giving great results showing the increase in polymerization rate and molecular weight of the final product. This improvement is caused by the increase in turbulence, gas hold-up and bubble breakup, increasing the total area available for mass transfer [2,11,12,21–24,27,33].

It was possible to identify the poor gas-liquid mass transfer zones of the reactor when working with set-up 2/2D at the volumes of 2.05 to 2.15 L and for volumes higher than 2.37 L. A proposed solution was the modification in the agitation set-

up by changing the spacing between impellers, together with the addition of a fifth PBT impeller in the shaft. As reported in the literature [8], the spacing modification was enough to avoid the decrease in polymerization rate for the region between 2.0 and 2.1 L tested.

It is worth to mention that there are also different factors during the emulsion polymerization that can lead to a decrease in the polymerization rate, as the increase in viscosity related to the increase in solid contents [18,33] or the coagulation of particles [28,29,31–33].

When studying the impact of using the hydrofoil as A345 or A315, on the mass transfer coefficient, it was found out that when the hydrofoil is providing a down-pumping flow (A315), the mass transfer was increased in 20 % when compared to the A345 configuration. This is logical as a down-pumping mode would help increasing the gas ingestion from the headspace [9–11].

It was observed that during the nucleation period of the reaction, the polymerization curves are virtually the same, no matter the agitation set-up or speed. At the stable stage the polymerization rate increases with the speed, but it seems that 550 rpm is the optimal speed to overcome the mass transfer limitations because the results are independent of the agitation set-up.

As novelty compared to the vinylidene fluoride modelling studies, a model considering the influence of the mass transfer in the monomer concentration (non-equilibrium) in the polymer particles was adapted from the works of Apostolo et al. [39] and Pladis et al. [51,52]. The model is not taking into consideration the nucleation and coagulation. It is simply modelling the particle growth.

The model provides a good fitting of the experimental data and it can be noticed that when a model is considering that the monomer concentration in the polymer particles is in thermodynamic equilibrium, there is an overestimation of the polymerization rate. The results also show that this non-equilibrium model is essential to represent the effect of low agitation speeds in the reactions.

NOTATION

a	Gas-liquid interfacial area per unit of volume of reactor, m²/m³
A_{l}	Concentration of A in the bulk liquid, mol/m³
A^*	Concentration of A in the liquid in equilibrium with the gas phase, mol/m³
c	Pseudo first order rate coefficient for termination in particles, s^{-1}
[CTA]	CTA concentration, mol m^{-3}
D_{p}	Diffusion coefficient of monomer (or oligoradicals) in the polymer particle, m^2 s^{-1}
D_{w}	Diffusion coefficient of monomer (or oligoradicals) in the aqueous phase, m^2 s^{-1}
$f(r)$	Number of particles density, part dm^{-1} m^{-3}
f_{e}	Radical entry efficiency
f_{I}	Initiation efficiency
H	Henry's law constant, Pa.m³/mol
[I]	Initiator concentration, mol m^{-3}
j_{cr}	Critical DP for particle formation by homogeneous nucleation for radicals generated by the initiator
k_0	Rate of diffusion of a monomeric radical out of a particle, s^{-1}
k_{d}	Rate coefficient for initiator decomposition, s^{-1}
k_{des}	Radical desorption rate coefficient, s^{-1}
k_{e}	Rate coefficient for entry of initiator-derived radicals into particles, m^3 mol^{-1} s^{-1}
k_{L}	Liquid film mass transfer coefficient, m/s
k_{p}	Rate coefficient for propagation in the polymer particles, m^3 $mol^{-1}s^{-1}$
k_{pw}	Rate coefficient for propagation in the aqueous phase, m^3 mol^{-1} s^{-1}
k_{tp}	Rate coefficient for radical termination in the polymer particles, m^3 mol^{-1} s^{-1}
k_{tm}	Rate coefficient for radical transfer to monomer, m^3 mol^{-1} s^{-1}
k_{tw}	Rate coefficient for radical termination in the aqueous phase, m^3 mol^{-1} s^{-1}
m	Partition coefficient of radicals between the polymer particles and the aqueous phase, usually approximated by $m = [\mathrm{M}]_{\mathrm{p}}/[\mathrm{M}]_{\mathrm{w}}$,

$[\mathrm{M}]_{\mathrm{p}}$	Concentration of monomer in the polymer particles, mol m^{-3}
$[\mathrm{M}]_{\mathrm{w}}$	Concentration of monomer in the aqueous phase, mol m^{-3}
$M_{\mathrm{w,m}}$	Molecular weight of monomer, kg mol^{-1}
$\bar{n}(r)$	Average number of radicals per particles of size r
N_{p}	Number of particles per unit volume, part m^{-3}
N_{A}	Avogadro's number, mol^{-1}
P	Pressure, Pa
P_{b}	Pressure of the baseline, Pa
P_{f}	Final pressure of equilibrium, Pa
P_0	Pressure at time zero, Pa
p, p'	Undetermined constants, adjustable parameters
Q_L	Flow rate of liquid phase, m^3/s
r	Reaction rate, mol/m^3s
r	Particle radius, m
R	Gas constant, $Pa.m^3/mol.K$
R_{p}	Total monomer propagation rate, mol m^{-3} s^{-1}
$R_{\mathrm{p}}^{\mathrm{p}}$	Monomer propagation rate in the polymer particles, mol m^{-3} s^{-1}
$R_{\mathrm{p}}^{\mathrm{w}}$	Monomer propagation rate in the aqueous phase, mol m^{-3} s^{-1}
$[R^{\bullet}]_{\mathrm{w}}$	Total concentration of oligomeric radicals in the aqueous phase, mol m^{-3}
t	Time, s
T	Temperature, K
V_{g}	Volume of gas in the reactor, m^3
V_{L}	Volume of liquid in the reactor, m^3
V_j	Volume of phase j ($j = \mathrm{e},\ m,\ \mathrm{part},\ \mathrm{pol}, \mathrm{w} - \mathrm{emulsion},\ \mathrm{monomer},\ \mathrm{particles},\ \mathrm{polymer}, \mathrm{water}$) ($m^3$)

Greek

ρ_j	Density of phase j ($j = m, \mathrm{w},\ \mathrm{pol} - \mathrm{monomer}, \mathrm{water},\ \mathrm{polymer}$) (kg m^{-3})
v_s	Gas superficial velocity, m/s

v	Volume of a particle, m³
ϕ	Gas volume fraction

REFERENCES

[1] Alexopoulos AH, Pladis P, Kiparissides C. Nonhomogeneous mixing population balance model for the prediction of particle size distribution in large scale emulsion polymerization reactors. Ind Eng Chem Res 2013;52:12285–96. doi:10.1021/ie303500k.

[2] Zubitur M, Asua JM. Agitation effects in the semicontinuous emulsion polymerization of styrene and butyl acrylate. J Appl Polym Sci 2001;80:841–51. doi:10.1002/1097-4628(20010509)80:6<841::AID-APP1162>3.0.CO;2-4.

[3] Xu CZ, Wang JJ, Gu XP, Feng LF. CFD modeling of styrene polymerization in a CSTR. Chem Eng Res Des 2017;125:46–56. doi:10.1016/j.cherd.2017.06.028.

[4] Paul EL, Atiemo-Obeng VA, Kresta SM, editors. Handbook of Industrial Mixing: Science and Practice. New Jersey: John Wiley & Sons, Ltd; 2004.

[5] Oldshue JY. Fluid mixing technology. New York: McGraw-Hill Inc.; 1983.

[6] Roudsari SF, Dhib R, Ein-Mozaffari F. Using a Novel CFD Model to Assess the Effect of Mixing Parameters on Emulsion Polymerization. Macromol React Eng 2016;10:108–22. doi:10.1002/mren.201500019.

[7] Aryafar S, Sheibat-Othman N, McKenna TFL. Coupling of CFD Simulations and Population Balance Modeling to Predict Brownian Coagulation in an Emulsion Polymerization Reactor. Macromol React Eng 2017;11:1–17. doi:10.1002/mren.201600054.

[8] Hari-Prajitno D, Mishra VP, Takenaka K, Bujalski W, Nienow AW, McKemmie J. Gas-Liquid Mixing Studies with Multiple Up- and Down-Pumping Hydrofoil Impellers: Power Characteristics and Mixing Time. Can J Chem Eng 1998;76:1056–68.

[9] Aubin J, Le Sauze N, Bertrand J, Fletcher DF, Xuereb C. PIV measurements of flow in an aerated tank stirred by a down- and an up-pumping axial flow impeller. Exp Therm Fluid Sci 2004;28:447–56.

[10] Moucha T, Linek V, Prokopová E. Gas hold-up, mixing time and gas-liquid volumetric mass transfer coefficient of various multiple-impeller configurations: Rushton turbine, pitched blade and techmix impeller and their combinations. Chem Eng Sci 2003;58:1839–46.

[11] Sardeing R, Aubin J, Xuereb C. Gas-Liquid Mass Transfer. A Comparison of Down- and Up-pumping Axial Flow Impellers with Radial Impellers. Trans IChemE Part A 2004;82:1589–96.

[12] Zhang J, Gao Z, Cai Y, Cai Z, Yang J, Bao Y. Mass transfer in gas-liquid stirred reactor with various triple-impeller combinations. Chinese J Chem Eng 2016;24:703–10.

[13] Busciglio A, Caputo G, Scargiali F. Free-surface shape in unbaffled stirred vessels: Experimental study via digital image analysis. Chem Eng Sci 2013;104:868–80. doi:10.1016/j.ces.2013.10.019.

[14] Scargiali F, Tamburini A, Caputo G, Micale G. On the assessment of power consumption and critical impeller speed in vortexing unbaffled stirred tanks. Chem Eng Res Des 2017;123:99–110. doi:10.1016/j.cherd.2017.04.035.

[15] Busciglio A, Grisafi F, Scargiali F, Brucato A. Mixing dynamics in uncovered unbaffled stirred tanks. Chem Eng J 2014;254:210–9. doi:10.1016/j.cej.2014.05.084.

[16] Busciglio A, Scargiali F, Grisafi F, Brucato A. Oscillation dynamics of free vortex surface in uncovered unbaffled stirred vessels. Chem Eng J 2016;285:477–86. doi:10.1016/j.cej.2015.10.015.

[17] Prakash B, Bhatelia T, Wadnerkar D, Shah MT, Pareek VK, Utikar RP. Vortex shape and gas-liquid hydrodynamics in unbaffled stirred tank. Can J Chem Eng 2019;97:1913–20. doi:10.1002/cjce.23433.

[18] Scott PJ, Penlidis A, Rempel GL. Reactor Emulsion Design Considerations for Gas-Liquid Emulsion Polymerizations: the Ethylene-Vinyl Acetate Example. Chem Eng S 1994;49:1573–83.

[19] Kashid MN, Renken A, Kiwi-Minsker L. Gas-liquid and liquid-liquid mass transfer in microstructured reactors. Chem Eng Sci 2011;66:3876–97.

doi:10.1016/j.ces.2011.05.015.

[20] Boyer C, Duquenne A, Wild G. Measuring techniques in gas-liquid and gas-liquid-solid reactors 2002;57:3185–215.

[21] Chaudhari R V., Gholap R V., Emig G, Hofmann H. Gas-liquid mass transfer in “dead-end” autoclave reactors. Can J Chem Eng 1987;65:744–51. doi:10.1002/cjce.5450650506.

[22] Ecoscia ACM, Sheibat-Othman N, McKenna TFL. Emulsion polymerization of vinylidene fluoride: Effects of mixing and reaction conditions on the initial rate of polymerization. Can J Chem Eng 2022;100:654–65. doi:10.1002/cjce.24145.

[23] Conway K, Kyle A, Rielly CD. Gas-liquid-solid operation of a vortex-ingesting stirred tank reactor. Chem Eng Res Des 2002;80:839–45. doi:10.1205/026387602321143372.

[24] Evans CP, Hay PM, Marker L, Murray RW, Sweeting O. Mechanism of Emulsion Polymerization of Vinylidene Chloride. III. Effects of Stirring Rate on Kinetics. J Appl Polym Sci 1961;V:39–47.

[25] Weerts PA, M van der LQOS JL, German AL. Emulsion polymerization of butadiene. 3. Kinetic effects of stirring conditions and monomer/water ratio K. Makromol Chem 1993;192:1993–2008.

[26] Omi S, Shirashi Y, Sato H, Kubota H. The effect of agitation on the rate of emulsion polymerization of styrene. J Chem Eng Japan 1969;2:64–70.

[27] Roudsari SF, Dhib R, Ein-Mozaffari F. Mixing Effect on Emulsion Polymerization in a Batch Reactor. Polym Eng Sci 2015:945–56. doi:10.1002/pen.

[28] Nomura M, Harada M, Eguchi W, Nagata S. Effect of stirring on the emulsion polymerization of styrene. J Appl Polym Sci 1972;16:835–47. doi:10.1002/app.1972.070160403.

[29] Kiparissides C, MacGregor JF, Hamielec AE. Continuous Emulsion Polymerization of Vinyl Acetate. Part I: Experimental Studies. Can J Chem Eng 1980;58:48–55.

[30] Bataille P, Dalpé JF, Dubuc F, Lamoureux L. The Effect of Agitation on the Conversion of Vinyl Acetate Emulsion Polymerization. J Appl Polym Sci 1990;39:1815–20.

[31] Kim CU, Lee JM, Ihm SK. Emulsion polymerization of tetrafluoroethylene: effects of reaction conditions on the polymerization rate and polymer molecular weight. J Appl Polym Sci 1999;73:777–93. doi:10.1002/(SICI)1097-4628(19990801)73:5<777::AID-APP18>3.0.CO;2-C.

[32] Oprea S, Dodita T. Influence of agitation during emulsion polymerization of acrylic-styrene latexes on end product properties. Prog Org Coatings 2001;42:194–201.

[33] Krishnan S, Klein A, El-Aasser MS, Sudol ED. Agitation Effects in Emulsion Copolymerization of n-Butyl Methacrylate and N-Methylol Acrylamide. Polym React Eng 2003;11:335–57.

[34] Mendoza J, De La Cal JC, Asua JM. Kinetics of the styrene emulsion polymerization using n-dodecyl mercaptan as chain-transfer agent. J Polym Sci Part A Polym Chem 2000;38:4490–505. doi:10.1002/1099-0518(20001215)38:24<4490::aid-pola180>3.3.co;2-2.

[35] Damköhler G. Einflüsse der Strömung, Diffusion und des Wärmeüberganges auf die Leistung von Reaktionsöfen: I. Allgemeine Gesichtspunkte für die Übertragung eines chemischen Prozesses aus dem Kleinen ins Große. Phys Chemie 1936;42:846–62.

[36] Hatta S. Technological Reports of Tôhoku University. 1932.

[37] Vinu R. Gas–Liquid and Gas–Liquid–Solid Reactors. 2017. doi:10.1016/b978-0-08-101096-9.00004-2.

[38] Vale HM, Mckenna TF. Particle Formation in Vinyl Chloride Emulsion Polymerization: Reaction Modeling. Ind Eng Chem Res 2009;48:5193–210. doi:10.1021/ie801406n.

[39] Apostolo M, Arcella V, Storti G, Morbidelli M. Kinetics of the Emulsion Polymerization of Vinylidene Fluoride and Hexafluoropropylene.

Macromolecules 1999;32:989–1003. doi:10.1021/ma980683r.

[40] Urrea-Quintero J-H, Ochoa S, Hernández H. A reduced-order multiscale model of a free-radical semibatch emulsion polymerization process. Comput Chem Eng 2019;127:11–24.

[41] Urrea-Quintero J-H, Marino M, Hernández H, Ochoa S. Multiscale modeling of a free-radical emulsion polymerization process: Numerical approximation by the Finite Element Method. Comput Chem Eng 2020;140:106974.

[42] Banetta L, Storti G, Hoggard G, Simpson G, Zaccone A. Predictive model of polymer reaction kinetics and coagulation behavior in seeded emulsion co-and ter-polymerizations. Polym Chem 2020;11:6599–615. doi:10.1039/d0py01138j.

[43] Zubitur M, Ben Amor S, Bauer C, Amram B, Agnely M, Leiza JR, et al. Multimonomer emulsion copolymerization in presence of inhibitors. Chem Eng J 2004;98:183–98. doi:10.1016/S1385-8947(03)00185-2.

[44] Moreno VC, Ledoux A, Estel L, Derrouiche S, Denieul MP. Valorisation of CO2 with epoxides: Influence of gas/liquid mass transfer on reaction kinetics. Chem Eng Sci 2017;170:77–90. doi:10.1016/j.ces.2017.01.050.

[45] Đeković-Šević M, Bošković-Vragolović N, Garić-Grulović R, Pejanović S. Experimental study on the ozone absorption accompanied by instantaneous chemical reaction. Chem Eng Commun 2018;205:571–80. doi:10.1080/00986445.2017.1399125.

[46] Lu C, Chen M, Luo X, Liang Z. The Effects of Mass Transfer on the Determination of Gas-Liquid Reaction Kinetics in a Stirred Cell Reactor: In the Case of CO2 Absorption by Aqueous Alkanolamine Solution. Energy and Fuels 2019. doi:10.1021/acs.energyfuels.9b02986.

[47] Chiu CY, Chang CY, Huang WH, Lee SJ, Yu YH, Liou HT, et al. A refined model for ozone mass transfer in a semibatch stirred vessel. Ozone Sci Eng 1997;19:439–56. doi:10.1080/01919512.1997.10382870.

[48] Lu Z, Sun Y, Liu S, Qian Z, Chen H, Wu S, et al. Fuzzy-Logic-Based

Modeling and Control for HiGee-AOP Nitric Oxide Attenuation with a Complex Gas-Liquid Mass-Transfer-Reaction Process. Ind Eng Chem Res 2022;61:3428–38. doi:10.1021/acs.iecr.1c04835.

[49] Ariafar S. Scale-up of Emulsion Polymerization Process: Impact of changing characteristic times. Université Claude Bernard Lyon 1, 2016.

[50] Nienow AW, Bujalski W. The versatility of up-pumping hydrofoil agitators. Trans IChemE 2004;82:1073–81.

[51] Pladis P, Alexopoulos AH, Bousquet J, Kiparissides C. Modelling of vinylidene fluoride emulsion polymerization. Comput Aided Chem Eng 2005;20:319–24. doi:10.1016/S1570-7946(05)80175-0.

[52] Pladis P, Alexopoulos AH, Kiparissides C. Mathematical Modeling and Simulation of Vinylidene Fluoride Emulsion Polymerization. Ind Eng Chem Res 2014;53:7352–64. doi:10.1021/ie403548m.

[53] Smith W V., Ewart RH. Kinetics of Emulsion Polymerization. J Chem Phys 1948;16:592–9. doi:10.1002/app.1965.070090410.

[54] Friis N, Nyhagen L. A kinetic study of the emulsion polymerization of vinyl acetate. J Appl Polym Sci 1973;17:2311–27. doi:10.1002/app.1973.070170802.

[55] Ugelstad J, Hansen FK. Kinetics and Mechanism of Emulsion Polymerization. Rubber Chem Technol 1976;50:536–640.

[56] Asua JM, editor. Polymeric Dispersions : Principles and Applications. 1st ed. Springer Science+Business Media Dordrecht; 1997.

[57] Asua JM, editor. Polymer Reaction Engineering. 1st Ed. Oxford: Blackwell; 2007.

[58] Gilbert RG. Emulsion Polymerization. A Mechanistic Approach. London: Academic Press Limited; 1995.

[59] Coen EM, Gilbert RG, Morrison BR, Leube H, Peach S. Modelling particle size distributions and secondary particle formation in emulsion polymerisation. Polymer (Guildf) 1998;39:7099–112. doi:10.1016/S0032-

3861(98)00255-9.

[60] Ameduri B. From Vinylidene Fluoride (VDF) to the Applications of VDF-Containing Polymers and Copolymers: Recent Developments and Future Trends. Chem Rev 2009;109:6632–86. doi:10.1002/chin.201017230.

CONCLUSIONS & PERSPECTIVES

The scope of this thesis was the comprehension of latex stability and the mechanisms leading to coagulation and fouling, to minimize these unwanted materials and keep the VDF emulsion polymerization as clean as waste free as possible.

The study of coagulation and fouling during polymerization reaction makes it challenging because there are some factors that cannot be kept constant during the reactions and the absence of a sampling tool due to the high pressure, enables only the study of the final point of the reactions.

The investigations were based in the concentrations of surfactant, chain transfer agent, reaction time and solid contents. Table 1 and Table 2 summarize the main observations related to the coagulation and fouling according to the factors studied.

As expected, a higher concentration of surfactant leads to a higher surface coverage of the polymer particles, and a higher stability against coagulation and fouling. At the times some coagulation and deposits were created during the reaction, the total amount of out of specification material is decreased with the highest concentration of surfactant. Additionally, the cleanest condition of the reactor at the end of a polymerization without coagulation was obtained with the highest concentration of surfactant.

The effect of surfactant against the coagulation was also confirmed in the orthokinetic tests performed in the Mastersizer and in the rheometer. Up to our knowledge, the use of Mastersizer is an innovative way of monitoring the coagulation in real time. It is possible to obtain the rate of disappearance of the first family of particles and the results were reproducible. Future works must include the acquisition of data in the equipment for a longer period of time, to observe if a complete coagulation of the first family of particles will happen, as we observed that the rate of creation of coagulum decreases.

The effect of shearing in coagulation was observed with the experiments performed in the reactor, Mastersizer and rheometer. An increase on shearing or time leads to an increase in coagulation as expected. This a sensitive point during the production of PVDF, as with the progress of the reaction, the solids content increases, increasing the probability of particle collision and coagulation.

Therefore, probably with the progress of reaction it would be interesting to decrease the agitation speed, or even rethink the impellers related to the shearing provided.

A point that must still be studied is the coagulation in the reactor in the absence of reaction but in the presence of monomer. The tests for latex coagulation in the absence of reaction were performed with a low solids content latex and times way lower than reaction times. Sometimes a latex with the double of solids content was produced during reactions after more time under shearing than the tests performed, without generating the coagulation.

No matter the destabilization mechanism of the latex, the second family of particles was always detected in the range of 5 to 300 μm without the presence of intermediary sizes of particles. This may be due to the timescale of the coagulation that is so fast that during the measurements with laser diffraction it was not possible to detect. At the same time, from the use of ultrasound with Mastersizer, it seems that the second family of particles are aggregates and the shearing limits the biggest size found.

During the polymerization reactions the coagulation and fouling were studied at the same time. The deposition of a material is heterogeneous and follows the flow pattern in the reactor. The vortex / splashing in the liquid surface creates the polymer rings found on the reactor wall. From the results it can be said that the use of wax and electropolished surfaces are effective against fouling, so, future studies can investigate the use of different roughness of materials in the reactor's internals.

Interestingly it was shown that the solids content is the main factor on fouling creation and not the duration of the reaction, even if the latexes had a very different molecular weight or different concentrations of CTA.

While performing the studies, it was observed that there were mass transfer limitations on the reactor due to a poor design, causing the loss of vortex when the liquid level touches the shaft guide at the volume of 2.6 L. This was limiting the solids content produced to 32 % wt. The solutions proposed to work in a better mixing area enabled the increase in solids content, in some cases reaching 50 %wt. depending on the recipe and reaction time. This made also possible the

observation of coagulation during polymerization, which was not observed before for reactions producing the solids content around 30 %wt.

There are also limitations related to poor mixing zones when the liquid level is between two impellers, but this can be solved adding more impellers and changing the distance between them, which led to the new configuration of the agitation set-up. An additional improvement to reactor design should be the gas introduction by a sparger, as with the actual configuration, the monomer is introduced in the headspace of the reactor.

The new agitation set-up proposed initially with the hydrofoil pumping down improved the mass transfer in the reactor in 20 % when compared to the original set-up. As the mass transfer coefficient is also dependent on the impellers position, the next studies should acquire more data for different volumes of liquid in the reactor.

From the results comparing different agitation set-ups and speeds, a polymerization model for growth of particles was adapted to include the mass transfer limitations and up to our knowledge this was not done before in the literature for the emulsion polymerization of VDF.

The model provides a good fitting of the experimental data and it can be noticed that when a model is considering that the monomer concentration in the polymer particles is in thermodynamic equilibrium, there is an overestimation of the polymerization rate. The results also show that this non-equilibrium model is essential to represent the effect of low agitation speeds in the reactions. Future improvements in the model must consider the nucleation period and the coagulation of particles.

The last point is study if reactors with similar mass transfer coefficients can lead to similar polymerization rates, what can be useful for scale up purposes.

CONCLUSIONS ET PERSPECTIVES

L’objectif de cette thèse était la compréhension de la stabilité du latex et des mécanismes menant à la coagulation et à l'encrassement, afin de minimiser ces matériaux indésirables et de garder la polymérisation en émulsion VDF aussi propre et sans déchets que possible.

L'étude de la coagulation et de l'encrassement pendant la réaction de polymérisation est un défi car certains facteurs ne peuvent pas être maintenus constants pendant les réactions et l'absence d'un outil d'échantillonnage en raison de la haute pression, ne permet que l'étude du point final des réactions.

Les études étaient basées sur les concentrations de tensioactif, d'agent de transfert de chaîne, de temps de réaction et de teneur en solides. Le Tableau 1 et le Tableau 2 résument les principales observations relatives à la coagulation et à l'encrassement en fonction des facteurs étudiés.

Comme prévu, une concentration plus élevée de surfactant conduit à une plus grande couverture de surface des particules de polymère, et une plus grande stabilité contre la coagulation et l'encrassement. Au moment où une certaine coagulation et des dépôts ont été créés pendant la réaction, la quantité totale de matériau hors spécifications est diminuée avec la concentration la plus élevée d'agent de surface. De plus, l'état le plus propre du réacteur à la fin d'une polymérisation sans coagulation a été obtenu avec la plus haute concentration d'agent de surface.

L'effet du tensioactif contre la coagulation a également été confirmé dans les tests orthocinétiques réalisés dans le Mastersizer et dans le rhéomètre. A notre connaissance, l'utilisation du Mastersizer est un moyen innovant de suivre la coagulation en temps réel. Il est possible d'obtenir la vitesse de disparition de la première famille de particules et les résultats sont reproductibles. Les travaux futurs doivent inclure l'acquisition de données dans l'équipement pour une plus longue période de temps, afin d'observer si une coagulation complète de la première famille de particules se produira, car nous avons observé que le taux de création de coagulum diminue.

L'effet du cisaillement dans la coagulation a été observé avec les expériences réalisées dans le réacteur, le Mastersizer et le rhéomètre. Une augmentation du cisaillement ou du temps conduit à une augmentation de la coagulation comme prévu. Il s'agit d'un point sensible lors de la production de PVDF, car avec la progression de la réaction, le taux de solides augmente, ce qui accroît la probabilité de collision des particules et de coagulation. Par conséquent, il serait probablement intéressant de diminuer la vitesse d'agitation au fur et à mesure de la progression de la réaction, voire de repenser les turbines en fonction du cisaillement fourni.

Un point qui doit encore être étudié est la coagulation dans le réacteur en l'absence de réaction mais en présence de monomère. Les essais de coagulation du latex en l'absence de réaction ont été réalisés avec un latex à faible teneur en solides et des temps bien inférieurs aux temps de réaction. Parfois un latex avec le double de la teneur en solides a été produit pendant les réactions après un temps de cisaillement plus long que les tests effectués, sans générer la coagulation.

Quel que soit le mécanisme de déstabilisation du latex, la deuxième famille de particules a toujours été détectée dans la gamme de 5 à 300 µm sans la présence de particules de tailles intermédiaires. Cela peut être dû à l'échelle de temps de la coagulation qui est si rapide qu'elle n'a pas pu être détectée lors des mesures par diffraction laser. En même temps, d'après l'utilisation des ultrasons avec le Mastersizer, il semble que la deuxième famille de particules soit des agrégats et que le cisaillement limite la plus grande taille trouvée.

Pendant les réactions de polymérisation, la coagulation et l'encrassement ont été étudiés en même temps. Le dépôt d'un matériau est hétérogène et suit le schéma d'écoulement dans le réacteur. Le tourbillon/éclaboussure à la surface du liquide crée les anneaux de polymère que l'on trouve sur la paroi du réacteur. D'après les résultats, on peut dire que l'utilisation de cire et de surfaces électropolies est efficace contre l'encrassement. Ainsi, les études futures pourront examiner l'utilisation de matériaux de rugosité différente dans les internes du réacteur.

Il est intéressant de noter que le taux de solides est le principal facteur de création d'encrassement et non la durée de la réaction, même si les latex ont une masse moléculaire très différentes ou des concentrations différentes de CTA.

Lors de la réalisation des études, il a été observé qu'il y avait des limitations de transfert de masse sur le réacteur en raison d'une mauvaise conception, provoquant la perte de vortex lorsque le niveau de liquide touche le guide d'arbre au volume de 2,6 L. Cela limitait les contenus solides produits à 32 % en poids. Les solutions proposées pour travailler dans une meilleure zone de mélange ont permis d'augmenter la teneur en solides, atteignant dans certains cas 50 % en poids selon la recette et le temps de réaction. Cela a également permis d'observer la coagulation pendant la polymérisation, ce qui n'avait pas été observé auparavant pour les réactions produisant une teneur en solides d'environ 30 % en poids.

Il y a également des limitations liées aux mauvaises zones de mélange lorsque le niveau de liquide se trouve entre deux hélices, mais cela peut être résolu en ajoutant plus d'hélices et en modifiant la distance entre elles, ce qui a conduit à la nouvelle configuration de l'installation d'agitation. Une amélioration supplémentaire de la conception du réacteur devrait être l'introduction de gaz par un sparger, car dans la configuration actuelle, le monomère est introduit dans l'espace de tête du réacteur.

La nouvelle configuration d'agitation proposée initialement avec le pompage vers le bas de l'hydrofoil a amélioré le transfert de masse dans le réacteur de 20 % par rapport à la configuration originale. Comme le coefficient de transfert de masse dépend également de la position des hélices, les prochaines études devraient acquérir plus de données pour différents volumes de liquide dans le réacteur.

A partir des résultats de la comparaison des différents réglages et vitesses d'agitation, un modèle de polymérisation pour la croissance des particules a été adapté pour inclure les limitations du transfert de masse et, à notre connaissance, cela n'avait pas été fait auparavant dans la littérature pour la polymérisation en émulsion du VDF.

Le modèle fournit un bon ajustement des données expérimentales et on peut remarquer que lorsqu'un modèle considère que la concentration de monomère dans les particules de polymère est en équilibre thermodynamique, il y a une surestimation de la vitesse de polymérisation. Les résultats montrent également que ce modèle de non-équilibre est essentiel pour représenter l'effet des faibles vitesses d'agitation dans les réactions. Les améliorations futures du modèle doivent prendre en compte la période de nucléation et la coagulation des particules.

Le dernier point est l'étude si les réacteurs avec des coefficients de transfert de masse similaires peuvent conduire à des taux de polymérisation similaires, ce qui peut être utile à des fins de mise à l'échelle.